

Prediction of Fibre Waviness in a Thermosetting Composite Panel With Ply Drop-off's

by

Makoena Raymond Botete



*Thesis presented in partial fulfilment of the requirements for
the degree of Master of Engineering (Mechanical) in the
Faculty of Engineering at Stellenbosch University*

Supervisor: Prof. G. Venter

April 2019

Declaration

By submitting this thesis electronically, I declare that the entirety of the work contained therein is my own, original work, that I am the sole author thereof (save to the extent explicitly otherwise stated), that reproduction and publication thereof by Stellenbosch University will not infringe any third party rights and that I have not previously in its entirety or in part submitted it for obtaining any qualification.

Date: April, 2019

Copyright © 2019 Stellenbosch University
All rights reserved.



UNIVERSITEIT • STELLENBOSCH • UNIVERSITY
jou kennisvenoot • your knowledge partner

Plagiaatverklaring / Plagiarism Declaration

- 1 Plagiaat is die oorneem en gebruik van die idees, materiaal en ander intellektuele eiendom van ander persone asof dit jou eie werk is.
Plagiarism is the use of ideas, material and other intellectual property of another's work and to present it as my own.
- 2 Ek erken dat die pleeg van plagiaat 'n strafbare oortreding is aangesien dit 'n vorm van diefstal is.
I agree that plagiarism is a punishable offence because it constitutes theft.
- 3 Ek verstaan ook dat direkte vertalings plagiaat is.
I also understand that direct translations are plagiarism.
- 4 Dienooreenkomstig is alle aanhalings en bydraes vanuit enige bron (ingesluit die internet) volledig verwys (erken). Ek erken dat die woordelike aanhaal van teks sonder aanhalingstekens (selfs al word die bron volledig erken) plagiaat is.
Accordingly all quotations and contributions from any source whatsoever (including the internet) have been cited fully. I understand that the reproduction of text without quotation marks (even when the source is cited) is plagiarism.
- 5 Ek verklaar dat die werk in hierdie skryfstuk vervat, behalwe waar anders aangedui, my eie oorspronklike werk is en dat ek dit nie vantevore in die geheel of gedeeltelik ingehandig het vir bepunting in hierdie module/werkstuk of 'n ander module/werkstuk nie.
I declare that the work contained in this assignment, except where otherwise stated, is my original work and that I have not previously (in its entirety or in part) submitted it for grading in this module/assignment or another module/assignment.

16557891	
Studentenommer / Student number	Handtekening / Signature
MR Botete	April 2019
Voorletters en van / Initials and surname	Datum / Date

Abstract

Prediction of Fibre Waviness in a Thermosetting Composite Panel With Ply Drop-off's

M.R. Botete

*Department of Mechanical and Mechatronic Engineering,
University of Stellenbosch,
Private Bag X1, Matieland 7602, South Africa.*

Thesis: MEng Mechanical

April 2019

Production of high-quality composite structures is a challenging process. This is because of a large number of defects that may occur during the curing process. Thermal deformations such as fibre waviness are the most critical, since they can lead to a total scrap of the component if not accounted for in the design. The aim of this project was to predict the formation of fibre waviness defects in a thermosetting composite panel that comprises ply drop-offs. This composite panel was constructed from 24 unidirectional plies (IM7/977-2 carbon epoxy tape) and cured in the autoclave with a tool made from Invar material. The predictions were accomplished by performing cure simulations using a newly developed Ansys Composite Cure Simulation (ACCS) analytical tool-kit. The simulation results showed that the composite panel goes through material evolutions throughout the curing process that leads to the development of stresses and strains. The alternation of transverse strains (between high and low values) and shear strains (between negative and positive values) when plies are in compression in their fibre direction was shown to result in the formation of fibre waviness defects when the resin viscosity is at its minimum. The fibre waviness defects were predicted to occur at the drop-off stations on the bag side of the composite panel and validated by practical observations after manufacturing. Using this fibre waviness mechanism, the effect of various parameters were investigated to understand the main drivers of fibre waviness defects. Stagger length and the cure-pressure had an effect on the formation of fibre waviness, while parameters such as drop-off sequence, pressure ramp-up rate and the heat-up rate did not show any effect.

Uittreksel

Voorspelling van Formasie van Vesel-Golwing in 'n Termiese-Set Saamgestelde Paneel met Interne Lagies wat Ophou

M.R. Botete

*Department Meganies en Megatronies Ingenieurswese,
Universiteit van Stellenbosch,
Private Bag X1, Matieland 7602, South Africa.*

Tesis: MIng Meganies

April 2019

Die produksie van saamgestelde strukture van hoë-kwaliteit is 'n uitdagende proses. Dit is as gevolg van moontlike defekte wat kan ontstaan gedurende die verhardingsproses. Termiese deformasies soos vesel-golwing is die mees kritiese tipe defek, omdat hierdie soort defek kan lei tot 'n totale afskryf van die vervaardigde komponent indien dit nie in ag geneem is tydens die ontwerpfasie nie. Die doel van hierdie projek was om die formasie van vesel-golwing in 'n termiese-set saamgestelde paneel waarvan die lagies binne die paneel ophou ("ply drop-offs") te voorspel. Hierdie saamgestelde paneel bestaan uit 24 eenrigting lagies (IM7/977-2 koolstof epoksie in band vorm), en word gekuur in 'n outoklaaf met 'n werkstuk wat van Invar vervaardig is. Die voorspellings is bereik deur kursimulasies uit te voer met die nuut ontwikkelde "Ansys Composite Cure Simulation (ACCS)" sagteware. Die resultate van die simulasies toon dat die saamgestelde paneel se materiaal 'n evolusie proses gaan tydens die kuurproses, wat lei tot die ontwikkeling van spanning en vervorming in die paneel. Die afwisseling van dwars-vervormings (tussen hoë en lae waardes) en skuif-vervormings (tussen negatiewe en positiewe waardes) wanneer 'n lagie in kompressie is in die veselrigting, het aangedui dat vesel-golwing defekte plaasvind wanneer die epoksie viskositeit by 'n minimum is. Die vesel-golwing defekte is voorspel om plaas te vind in die areas waar die interne lagies ophou aan die sak-kant van die saamgestelde paneel, en is verder bevestig met praktiese waarnemings na vervaardiging. Met die gebruik van hierdie golwingvormingsmeganisme is die effek van verskeie parameters ondersoek om

die hoof-drywers van vesel-golwing defekte te verstaan. Ophou volgorde lengte (stagger length) en die verhardingsdruk het die formasie van vesel-golwing beïnvloed, terwyl parameters soos die volgorde waarin die lagies opgelê word, die druktoeneemtempo en die opwarmingstempo nie enige invloed getoon het nie.

Acknowledgements

I would like to express my sincere gratitude to the following people and organisations:

- Prof. Gerhard Venter for taking me as his student, the support and guidance he gave me throughout the project
- Stefan, Danie and Robert from Denel Aero-structures division for their experience, guidance and support
- Franz and Waltraud Muller for the financial backing and support
- Family and friends for the unconditional support and prayers

Contents

Declaration	i
Abstract	iii
Uittreksel	iv
Acknowledgements	vi
Contents	vii
List of Figures	x
List of Tables	xiii
Nomenclature	xiv
1 Introduction	1
1.1 Background	1
1.2 Objectives	2
1.3 Thesis Overview	3
2 Literature Review	4
2.1 Curing of Thermosetting Composites	4
2.2 Cure-induced Stresses and Strains	6
2.2.1 Chemical origin	7
2.2.2 Thermal origin	7
2.2.3 Tool-part interactions origin	8
2.3 Defects During Composite Production	8
2.3.1 Fibre waviness defects	8
2.3.2 Mechanisms behind fibre waviness formation	9
2.4 Cure Process Simulation	10
2.5 Ply Drop-off in Composite Structures	12
2.6 FE Formulation of Composites With Ply Drop-off	13
2.7 Summary	14

3	Finite Element Modelling	15
3.1	Panel Layout	15
3.2	FE Models	17
3.2.1	Composite panel model	17
3.2.2	Tool model	18
3.2.3	Panel-tool assembly model	19
3.3	Conclusion	19
4	FE Model Preparations	20
4.1	Simulation Procedure	20
4.2	Material Properties	22
4.2.1	Composite panel material	23
4.2.2	Tool material	26
4.2.3	Contact properties	26
4.3	Loads and Boundary Conditions	26
4.4	Conclusion	27
5	Simulation Results and Validation	28
5.1	Cure Process Results	28
5.2	Development of Cure-induced Stresses	30
5.3	Development of Cure-induced Strains	31
5.4	Cure-strain Distribution	33
5.4.1	Bag side (ply 24: -45° fibre direction)	33
5.4.2	Tool side (ply 1: -45° fibre direction)	35
5.5	Fibre Waviness Predictions	37
5.6	Experimental Validation	40
5.7	Conclusion	42
6	Parametric Study	43
6.1	Ply Drop-off Effects	43
6.1.1	Drop-off sequence	44
6.1.2	Stagger length	45
6.2	Cure Cycle Effects	47
6.2.1	Cure-pressure	47
6.2.2	Pressure ramp-up rate	51
6.2.3	Heat-up rate	53
6.3	Tool Material	57
6.4	Conclusion	60
7	Conclusion and Recommendations	62
7.1	Conclusion	62
7.2	Recommendations	65
	List of References	66

<i>CONTENTS</i>	ix
Appendices	70
Appendix A Material Properties	A2
A.1 IM7/977-2	A2
A.2 CYCOM 977-2 epoxy resin	A3
A.3 Invar	A3
Appendix B Ply Strain Distributions	B1
B.1 Ply 2	B1
B.2 Ply 3 (Dropped)	B2
B.3 Ply 4 (Dropped)	B3
B.4 Ply 5	B4
B.5 Ply 6	B5
B.6 Ply 7	B6
B.7 Ply 8 (Dropped)	B7
B.8 Ply 9 (Dropped)	B8
B.9 Ply 10	B9
B.10 Ply 11	B10
B.11 Ply 12	B11
B.12 Ply 13	B12
B.13 Ply 14	B13
B.14 Ply 15	B14
B.15 Ply 16	B15
B.16 Ply 17 (Dropped)	B16
B.17 Ply 18	B17
B.18 Ply 19	B18
B.19 Ply 20	B19
B.20 Ply 21 (Dropped)	B20
B.21 Ply 22 (Dropped)	B21
B.22 Ply 23	B22

List of Figures

Figure 2.1:	Stages of thermosetting resin cure process	5
Figure 2.2:	Temperature vs. degree of cure plot	6
Figure 2.3:	Types of fibre waviness defects	9
Figure 2.4:	Stages of thermosetting resin cure process	12
Figure 3.1:	Geometrical layout and ply lay-up of the composite panel	16
Figure 3.2:	Panel Mesh showing resin pocket elements	18
Figure 3.3:	Geometrical layout and mesh of the tool	18
Figure 3.4:	Tool and composite panel assembly FE model	19
Figure 4.1:	Full cure simulation procedure	21
Figure 4.2:	Cure properties for performing cure simulation	22
Figure 4.3:	Cure kinetic equations fitting to experimental data	23
Figure 4.4:	Fit of the rheology model to the viscosity profile	25
Figure 4.5:	Cure cycle for manufacturing composite panel	27
Figure 5.1:	Composite panel material evolutions	29
Figure 5.2:	Degree of cure distributions at gelation	30
Figure 5.3:	Maximum cure-induced Von-Mises stresses	31
Figure 5.4:	In-plane cure-induced strain development	32
Figure 5.5:	ε_1 strain distribution in ply 24	34
Figure 5.6:	ε_2 strain distribution in ply 24	34
Figure 5.7:	ε_{12} strain distribution in ply 24	35
Figure 5.8:	ε_1 strain distribution in ply 1	36
Figure 5.9:	ε_2 strain distribution in ply 1	36
Figure 5.10:	ε_{12} strain distribution in ply 1	37
Figure 5.11:	Locations analysed for fibre waviness defects	38
Figure 5.12:	Strain variations in ply 24 along the panel length	39
Figure 5.13:	Strain variations in ply 1 along the panel length	39
Figure 5.14:	Practical locations of fibre waviness defects	40
Figure 5.15:	Practical fibre waviness defects: drop-off station 2	41
Figure 5.16:	Practical fibre waviness defects: drop-off station 2	42
Figure 6.1:	Drop-off sequence	44
Figure 6.2:	Effect of drop-off sequence on ε_1	44

LIST OF FIGURES

xi

Figure 6.3: Effect of drop-off sequence on ε_2	45
Figure 6.4: Effect of drop-off sequence on ε_{12}	45
Figure 6.5: Effect of drop-off stagger length on ε_1	46
Figure 6.6: Effect of drop-off stagger length on ε_2	46
Figure 6.7: Effect of drop-off stagger length on ε_{12}	47
Figure 6.8: Effect of cure pressure on the development of ε_1	48
Figure 6.9: Effect of cure pressure on the development of ε_2	48
Figure 6.10: Effect of cure pressure on the development of ε_{12}	49
Figure 6.11: Effect of cure pressure on ε_1	49
Figure 6.12: Effect of cure pressure on ε_2	50
Figure 6.13: Effect of cure pressure on ε_{12}	50
Figure 6.14: Effect of pressure ramp-up rate on the development of ε_1	51
Figure 6.15: Effect of pressure ramp-up rate on the development of ε_2	51
Figure 6.16: Effect of pressure ramp-up rate on the development of ε_{12}	52
Figure 6.17: Effect of pressure ramp-up rate on ε_1	52
Figure 6.18: Effect of pressure ramp-up rate on ε_2	53
Figure 6.19: Effect of pressure ramp-up rate on ε_{12}	53
Figure 6.20: Effect of heat-up rate on material transition times	54
Figure 6.21: Effect of heat-up rate on the development of ε_1	54
Figure 6.22: Effect of heat-up rate on the development of ε_2	55
Figure 6.23: Effect of heat-up rate on the development of ε_{12}	56
Figure 6.24: Effect of heat-up rate on ε_1	56
Figure 6.25: Effect of heat-up rate on ε_2	57
Figure 6.26: Effect of heat-up rate on ε_{12}	57
Figure 6.27: Effect of tool material on the development of ε_1	58
Figure 6.28: Effect of tool material on the development of ε_2	58
Figure 6.29: Effect of tool material on the development of ε_{12}	59
Figure 6.30: Effect of tool material on ε_1	59
Figure 6.31: Effect of tool material on ε_2	60
Figure 6.32: Effect of tool material on ε_{12}	60
Figure B.1: Strain distributions in ply 2	B1
Figure B.2: Strains in ply 2 along ply length at various locations	B2
Figure B.3: Strain distributions in ply 3	B2
Figure B.4: Strains in ply 3 along ply length at various locations	B3
Figure B.5: Strain distributions in ply 4	B3
Figure B.6: Strains in ply 4 along ply length at various locations	B4
Figure B.7: Strain distributions in ply 5	B4
Figure B.8: Strains in ply 5 along ply length at various locations	B5
Figure B.9: Strain distributions in ply 6	B5
Figure B.10: Strains in ply 6 along ply length at various locations	B6
Figure B.11: Strain distributions in ply 7	B6
Figure B.12: Strains in ply 7 along ply length at various locations	B7
Figure B.13: Strain distributions in ply 8	B7

LIST OF FIGURES

xii

Figure B.14: Strains in ply 8 along ply length at various locations . . .	B8
Figure B.15: Strain distributions in ply 9	B8
Figure B.16: Strains in ply 9 along ply length at various locations . . .	B9
Figure B.17: Strain distributions in ply 10	B9
Figure B.18: Strains in ply 10 along ply length at various locations . .	B10
Figure B.19: Strain distributions in ply 11	B10
Figure B.20: Strains in ply 11 along ply length at various locations . .	B11
Figure B.21: Strain distributions in ply 12	B11
Figure B.22: Strains in ply 12 along ply length at various locations . .	B12
Figure B.23: Strain distributions in ply 13	B12
Figure B.24: Strains in ply 13 along ply length at various locations . .	B13
Figure B.25: Strain distributions in ply 14	B13
Figure B.26: Strains in ply 14 along ply length at various locations . .	B14
Figure B.27: Strain distributions in ply 15	B14
Figure B.28: Strains in ply 15 along ply length at various locations . .	B15
Figure B.29: Strain distributions in ply 16	B15
Figure B.30: Strains in ply 16 along ply length at various locations . .	B16
Figure B.31: Strain distributions in ply 17	B16
Figure B.32: Strains in ply 17 along ply length at various locations . .	B17
Figure B.33: Strain distributions in ply 18	B17
Figure B.34: Strains in ply 18 along ply length at various locations . .	B18
Figure B.35: Strain distributions in ply 19	B18
Figure B.36: Strains in ply 19 along ply length at various locations . .	B19
Figure B.37: Strain distributions in ply 20	B19
Figure B.38: Strains in ply 20 along ply length at various locations . .	B20
Figure B.39: Strain distributions in ply 21	B20
Figure B.40: Strains in ply 21 along ply length at various locations . .	B21
Figure B.41: Strain distributions in ply 22	B21
Figure B.42: Strains in ply 22 along ply length at various locations . .	B22
Figure B.43: Strain distributions in ply 23	B22
Figure B.44: Strains in ply 23 along ply length at various locations . .	B23

List of Tables

Table 3.1: Locations of first ply drop and ply fibre orientations colour scheme.	16
Table 4.1: IM7/997-2 prepreg and pure resin cure properties	24
Table A.1: Mechanical properties of IM7/977-2 composite (Cytec, 2012; Ahmed <i>et al.</i> , 2012; Joven <i>et al.</i> , 2012; Tavakol <i>et al.</i> , 2013).	A2
Table A.2: Mechanical properties of pure CYCOM 977-2 epoxy resin (Tabiei and Chen, 1999; Cytec, 2012; Joven <i>et al.</i> , 2012). . .	A3
Table A.3: Mechanical properties of Invar (AZoM, 2001).	A3

Nomenclature

Alphabetic Symbols

A	Cure kinetic equation pre-exponential factor	$[\text{s}^{-1}]$
AC_0	Initial degree of cure	$[-]$
AC_T	Temperature dependent degree of cure	$[-]$
B_i	Rheology model constants, $i = 1, 2$	$[-]$
C	Diffusion coefficient,	$[-]$
D_L	Diffusion limitation factor,	$[-]$
E_a	Apparent activation energy for cure reaction	$[\text{J}]$
E_u	Activation energy for viscosity	$[\text{J}]$
H_R	Heat of reaction	$[\text{J}]$
K_i	Arrhenius rate constant, $i = 1, 2$	$[-]$
m	Reaction constant	$[-]$
n	Reaction order	$[-]$
R	Universal gas constant	$[\text{J}/\text{mol} \cdot \text{K}]$
T	Temperature	$[\text{°C}]$
T_g	Glass transition temperature	$[\text{°C}]$
v_f	Fibre volume fraction	$[-]$

Greek Symbols

α	Degree of cure	$[-]$
α_g	Degree of cure at gelation	$[-]$
ε	Strain	$[-]$
λ	Fitting coefficient for glass transition temperature	$[-]$
μ	Viscosity	$[\text{Pa} \cdot \text{s}]$
μ_∞	Infinite viscosity	$[\text{Pa} \cdot \text{s}]$
ρ	Density	$[\text{kg}/\text{m}^3]$

Chapter 1

Introduction

1.1 Background

Composite materials have become popular over the past few decades. This is because composites offer many advantages over traditional materials due to their high strength and stiffness to weight ratios. Their applications are more popular in the aerospace and automotive industries where manufacturers are more concerned with weight reductions. This can be seen by the transition from metallic to composite materials, in both structural and non-structural applications, which is taking place in these industries.

Among the variety of composite materials, thermosetting composites such as epoxy-based resin systems are one of the most popular classes of composite materials. This is because thermosetting resin offers application diversity, ease of processing and handling, and outstanding mechanical properties. The desirable properties of thermosetting composites such as epoxy-resin composites include high strength, low creep, excellent corrosion resistance, low shrinkage after curing, high impact resistance and high fracture toughness (Sabzevari, 2010). However, the production of high-quality composite structures offers many challenges due to a large number of defects possible during the production process. There are approximately 130 possible defects that have been identified, from which thermal deformation defects such as fibre waviness, ply wrinkling, spring-in, etc. are the most critical (Potter, 2009). This is because thermal deformation defects greatly affect the mechanical properties of the structure and can lead to a total scrap of the component if they are not fully accounted for in the design.

To overcome such drawbacks, current designers typically rely on a trial-and-error approach to predict and control process-induced thermal deformations. This approach only gives reasonable results for relatively simple components. However, complex components require sophisticated numerical models to fully

capture the interactions between various geometric features. Furthermore, sophisticated numerical models are difficult to develop without effective analytical tools that can perform an in-depth simulation of the cure process (Johnston, 1997; ANSYS, 2017).

In the present study, a newly developed Ansys Composite Cure Simulation (ACCS) tool-kit is used to predict the formation of fibre waviness defects in a composite panel made of unidirectional carbon fibre reinforced epoxy prepregs with some plies terminated (ply drop-off) at various locations. Ply drop-off introduces discontinuities in the structure that leads to stress concentrations under loading, and high process-induced stresses might cause fibre waviness defects.

1.2 Objectives

The objectives of the project are as follows:

1. Simulate the curing process of the composite panel using the ACCS tool-kit to study and understand the mechanisms behind fibre waviness formation. The mechanisms must be formulated in terms of the stresses/strains obtained from the cure simulations.
2. Investigate the effect of various parameters (cure process, geometric and material) on the formation of fibre waviness defects. This is to help understand the main drivers behind fibre waviness formation and how it can be controlled.

The composite panel has already been designed by a partner-aerospace company for a specific purpose. Therefore, appropriate Finite Element (FE) models will be developed for performing cure simulations using the ACCS tool-kit. The results of the cure simulations will be verified by experimental results to ensure proper predictions.

To accomplish the objectives, the following steps were followed:

- Became familiar with the curing process of thermosetting composites and cure simulation procedures.
- Became familiar with the use of Ansys FE software and the ACCS tool-kit.
- Obtain all necessary material properties to perform cure simulation using the ACCS tool-kit.
- Develop all necessary FE models and perform cure simulations.
- Verify cure simulation results and initial predictions.

- Formulate the mechanism behind the fibre waviness formation.
- Apply the mechanism to study the effect of various parameters on fibre waviness formation.

1.3 Thesis Overview

This thesis is composed of six chapters laid out as follows:

- Chapter 1 introduces the project where a brief background and the objectives are discussed.
- Chapter 2 presents the literature review, which is the basis for the subsequent chapters. The literature review explains the curing process of thermosetting composite, and the background theory for performing cure simulations using the ACCS tool-kit. Other aspects such as fibre waviness and ply drop-off are also explained in detail in this chapter.
- Chapter 3 focuses on developing all necessary FE models for simulations.
- Chapter 4 focuses on the procedure of performing cure simulations using the ACCS tool-kit for fibre waviness predictions. Material properties, curing conditions and general assumptions are also presented in this chapter.
- Chapter 5 focuses on studying the mechanism behind the fibre waviness formation. The results of the cure simulations are analysed and validated, together with the predictions of fibre waviness defects.
- Chapter 6 focus on investigating the drivers of fibre waviness defects. The study on the effect of various geometric and manufacturing parameters is presented.
- Chapter 7 gives concluding remarks and recommendations for future studies.

Chapter 2

Literature Review

This chapter aims to provide a better understanding of the curing process of thermosetting composites, the development of the cure induced stresses/strains, defects that occur as a result of curing (i.e. mainly focusing on fibre waviness defects), as well as previous research conducted on mechanisms behind fibre waviness formation. The discussion will be followed by various ways in which cure simulations have been approached, mainly focusing on the functionality of a newly developed ACCS analytical tool-kit. The concept of ply drop-off in composite structures will also be discussed at the end.

2.1 Curing of Thermosetting Composites

During the curing process of thermosetting composites, the resin goes through cross-linking reactions that lead to changes in material properties and volumetric shrinkages (LMAT, 2016). Generally, curing of the thermosetting resin occurs in four stages known as A, B, C and D-stage, see Figure 2.1. The A-stage is when the resin is composed of only monomers (i.e. uncured resin) and has the ability to flow and impregnate a bundle of fibres. As the curing process begins, monomers start to form molecular chains by means of strong covalent bonds resulting in a partially cured and vitrified state with higher viscosity, i.e. stage B. Prepregs are basically at the advanced level of this stage for easy handling purposes (Niu, 1999). Stage C is gelation, which is when the molecular chains start cross-linking among themselves forming an infinite three-dimensional network. Stage D is the final stage when the resin is fully cured, no longer soluble nor fusible and has turned into a glassy solid. Generally, the autoclave/oven curing starts at stage B (i.e. with prepregs) under elevated temperature and pressure conditions (Niu, 1999; Sabzevari, 2010).

In other words, the curing process of thermosetting resin involves the transformation of a low molecular weight liquid into a high molecular weight amorphous solid by means of chemical reactions. Two major transitions can be identified

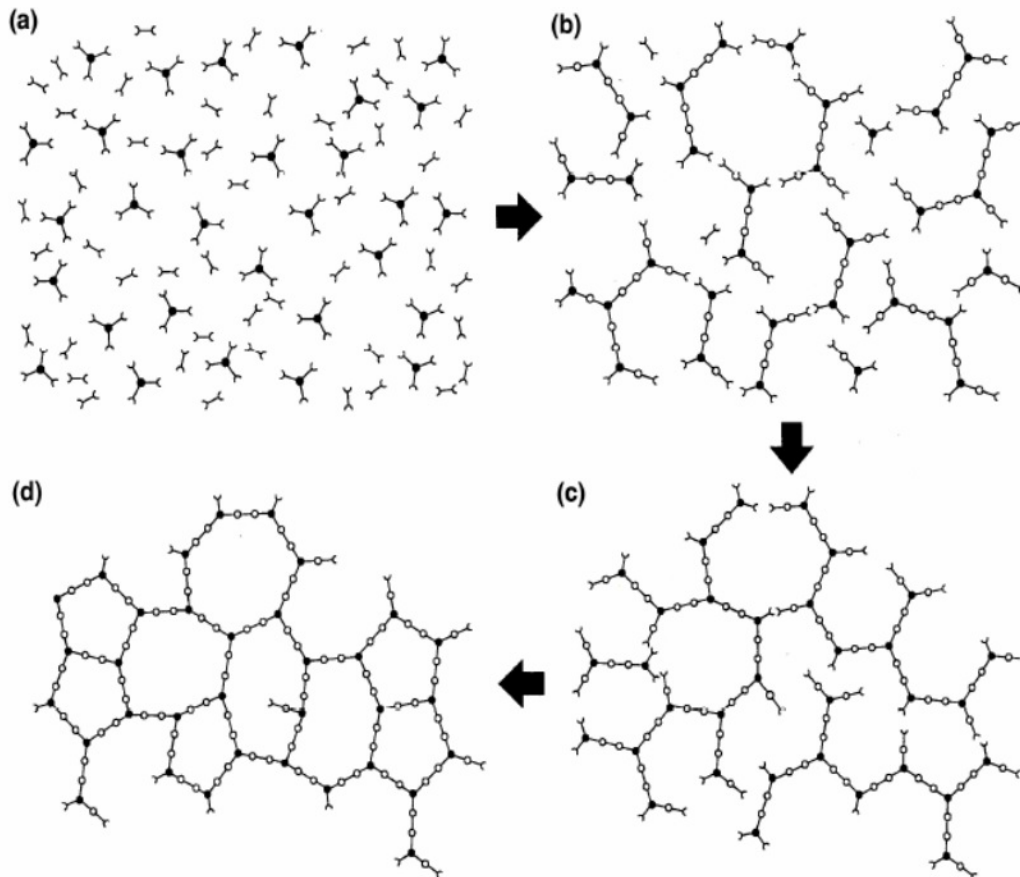


Figure 2.1: Stages of thermosetting resin cure process, (a) Stage A: unreacted monomers, (b) Stage B: the onset of the linear molecular chains extension and branching to gel point (prepreg), (c) Stage C - gelation: incipient formation of infinite 3D cross-linked network, (d) Stage D: fully cured thermosetting structure (Sabzevari, 2010; LMAT, 2016).

during this material transformation of viscous liquid into a glassy solid, i.e. gelation and vitrification (Sabzevari, 2010; LMAT, 2016). Gelation is the incipient formation of the gel from the branched molecules. Gelation is identified by an abrupt and irreversible transition from a viscous liquid into a rubbery (an elastic gel) state. Furthermore, the resin loses its ability to flow and the viscosity becomes very large during this transition (Sun, 2002; Sabzevari, 2010). Vitrification is defined as the formation of a glassy solid from the rubbery state due to an increase in the glass transition temperature to above the isothermal cure temperature as a result of cure reactions. Unlike gelation, vitrification is reversed by heating the material above its glass transition temperature. It is also important to note that chemical reactions change from being controlled by kinetic mechanisms into diffusion mechanisms at vitrification (Sabzevari, 2010).

Generally, these transitions separate the material into four states, i.e. ungelled glassy (preg state), liquid, rubbery and glassy (solid state). Figure 2.2 shows the conditions for these material states on a temperature vs. degree of cure graph. Gelation occurs when the degree of cure reach a certain value X_g and vitrification occurs when the temperature of the cured part crosses the glass transition temperature T_g line. Note that the glass transition temperature changes with the degree of cure as shown by the graph. The red arrowed lines indicate the material transition width since the transitions does not occur instantly.

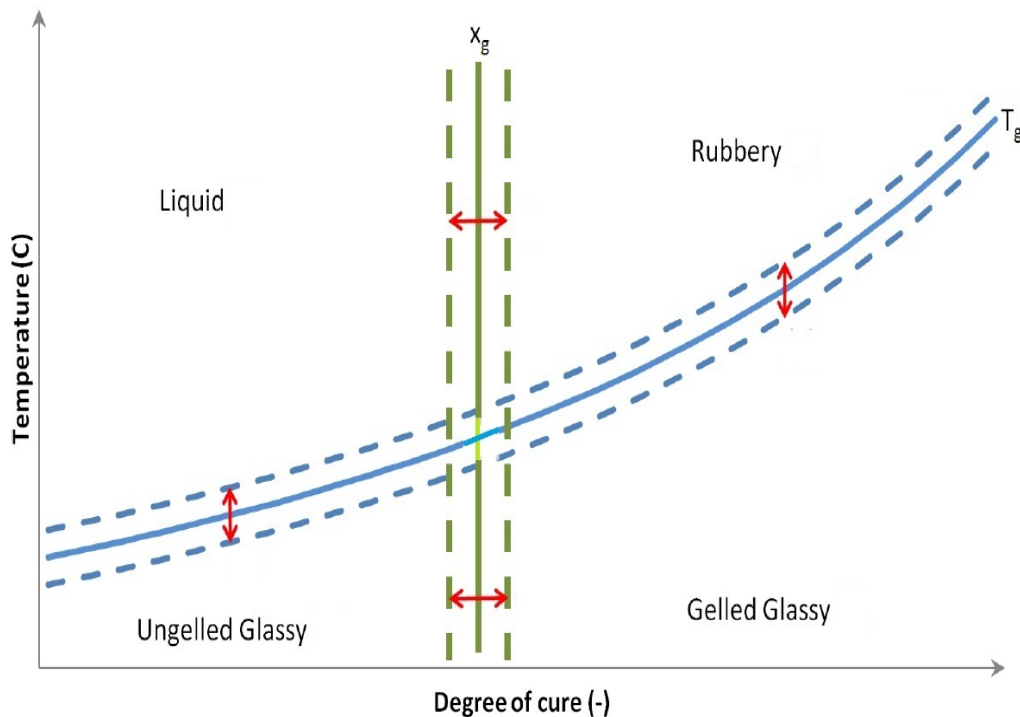


Figure 2.2: Plot of temperature vs. degree of cure, highlighting material states (LMAT, 2016).

2.2 Cure-induced Stresses and Strains

As mentioned in section 2.1, the thermosetting resin gradually undergoes polymerization at the curing temperature and becomes bonded to the fibres during the curing process. As this happens, the resin experiences volumetric changes while the fibres remain volumetrically stable. This mismatch, together with the thermal loads from the curing temperature, induces stresses within the cured laminate. When these stresses get locked in the laminate, cure residual stresses

develop which might cause distortions, cracks, or even a pre-stressed component after curing. Considerable efforts have been taken to study these cure-induced stresses and strains in composites. For instance, Mulle *et al.* (2009) revealed that cure-induced strains occur right from the start of the curing process by using the Fibre Bragg Grating (FBG) sensor to assess the cure-induced residual strains through the thickness of carbon-epoxy laminates.

The cure-induced stresses are noticed at the different levels of composite structures. At the micromechanics level, the mismatch in thermal expansion coefficients between the fibre and the resin results in stresses at the fibre-matrix interface. For instance, the resin tends to shrink more than the fibres due to the cross-linking reactions and the high compressive strength of the fibres (Niu, 1999; Mulle *et al.*, 2009). Other factors include the difference in fibre-resin elastic and viscoelastic properties, fibre architecture and fibre stiffness (Zobeiry *et al.*, 2016).

At the macromechanics level, the difference in fibre orientations between the plies impose constraints and subsequently causing cure-induced stresses within the plies. For example, the overall shrinkage within a unidirectional ply is higher along the transverse direction than that along the fibre direction (Niu, 1999). At the component level, the mismatch between the tool-part thermal expansion coefficient and the friction at the tool-part interface also results in additional cure-induced stresses.

Various factors have been found to contribute to the formation of cure-induced stresses. This factors can be categorised into three groups i.e. chemical origin, thermal origin and tool-part interaction origin.

2.2.1 Chemical origin

During curing, the thermosetting resin experiences volumetric shrinkages as a result of cross-linking reactions. This phenomenon is also known as chemical contraction or withdrawal (Li and Lee, 1998). As this happens, the reinforcement fibres oppose these chemical contractions due to their high compression stiffness; thus, they end up experiencing mechanical stresses (Schulz *et al.*, 2005; Guo *et al.*, 2007; Mulle *et al.*, 2009).

2.2.2 Thermal origin

Curing of composite laminates occurs at relatively high temperatures. As the temperature is being raised to or dropped from the cure temperature, differential thermal expansions occurs in the resin and fibres due to the mismatch in thermal expansion coefficients; thus resulting in cure induced stresses. In its liquid

phase, the resin has a low modulus, hence, negligible thermal stresses develop during the heat-up phase (Kravchenko *et al.*, 2016). Therefore, this results in low stresses developing in the heat-up phase. High compressive stresses are noticed during the cool-down phase because the resin has completely bonded with the fibres that have a higher modulus (Guo *et al.*, 2007; Mulle *et al.*, 2009).

2.2.3 Tool-part interactions origin

The differential thermo-elastic behaviour between the tool and laminates also results in cure-induced stresses. It has been found that, under the action of pressure and vacuum, shear stresses are generated at the tool-part interface during the curing process (Mulle *et al.*, 2009; Joven, 2013). These stresses exist during various phases of the curing process and can be transferred to all plies in the laminate (Kugler and Moon, 2002; Guo *et al.*, 2007; Potter, 2009).

2.3 Defects During Composite Production

Due to the existence of stresses and deformations (chemical shrinkages) during the curing process, defects are a big possibility when manufacturing composite structures. Defects can also result from inconsistencies in the laminate. Potter (2009), conducted a review study on the sources of variability and defects that exist in composite structures manufactured by autoclave curing and resin transfer moulding (RTM) process. During their study, they were able to identify approximately 130 defects possible during the manufacturing of composite structures. From this large number of defects, thermal deformations such as fibre waviness, spring-in, etc. were found to be the most critical since they can lead to a total scrap of the part if they are not accounted for in the design. This section discusses fibre waviness defects and mechanisms leading to their formation.

2.3.1 Fibre waviness defects

Fibre waviness results when fibres buckle and deviate from the mean direction of the laminate, forming a sinusoidal pattern (Kugler and Moon, 2002). The buckling can be in the plane of the laminate as in-plane waviness or through the thickness as out-of-plane waviness/ply wrinkling, see Figure 2.3. Fibre waviness defects significantly compromise the compressive strength of the structure (Piggott, 1995; Karami and Garnich, 2005).

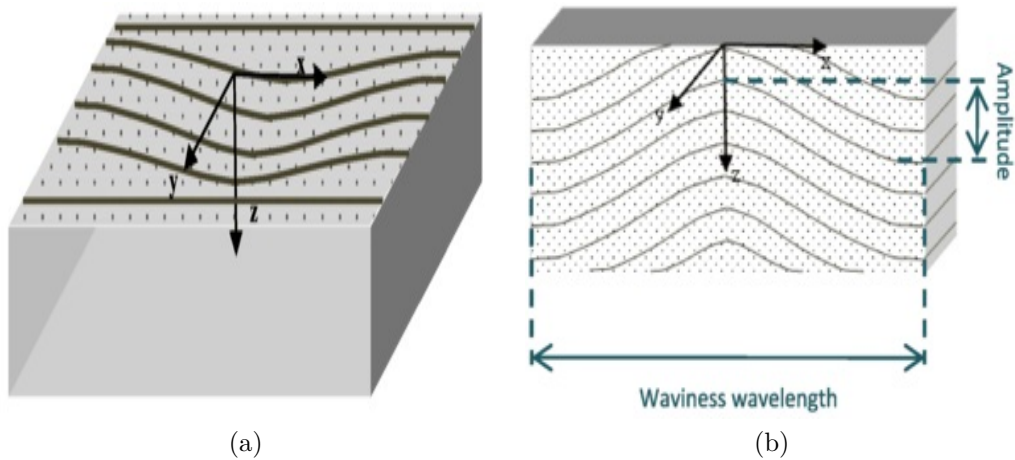


Figure 2.3: Types of fibre waviness defects: (a) in-plane fibre waviness, (b) ply wrinkling (out-of-plane fibre waviness); (Pain and Drinkwater, 2013).

2.3.2 Mechanisms behind fibre waviness formation

There have been a limited number of investigations on fibre waviness formation in terms of numerical modelling (Qu, 2010; Hallett *et al.*, 2016). However, two main mechanisms (in terms of stresses) that lead to fibre deformations have been identified. The first mechanism assumes that fibre deformations occur when the fibres experience axial compressive loading while the matrix is unable to provide sufficient transverse support (Parlevliet *et al.*, 2007). In support of this mechanism, Qu (2010) studied the buckling of fibres in a viscous medium due to axial compressive load, through practical experimentation. In their study, they concluded that the buckling of fibres is affected by the axial compressive loading and the transverse viscous forces. They also showed that fibre waviness can be identified by the alternation of high and low transverse stress regions.

The second mechanism predicts that fibre deformations are initiated by large shear stresses that result from a shear lag at the tool-part interface and away from the free edges (Kugler and Moon, 2002). In support of this mechanism, Lightfoot *et al.* (2013), developed a mechanism for fibre wrinkling due to shear stresses and verified it experimentally on a U-shaped channel. In their study, they also observed that fibre misalignment of about 50° results from this mechanism. Hallett *et al.* (2016) further confirmed the shear stresses as the drivers for fibre wrinkling through experimental study and numerical modelling.

2.4 Cure Process Simulation

The importance of cure-induced stresses and deformations during the curing of thermosetting composites has led many recent studies to focus on the cure simulations (Zobeiry *et al.*, 2016). Most of these studies have led to the development and implementation of various numerical models and simulation approaches for understanding the behaviour of thermosetting composites during the cure process (Ruiz and Trochu, 2005; Kravchenko *et al.*, 2016; Zhang *et al.*, 2016). This section focuses on the use of a newly developed ACCS analytical tool-kit to perform cure simulations.

The ACCS tool-kit is based on the theory that during the curing process, the thermosetting resin experiences changes in material properties (ANSYS, 2017). The material state during the curing process is assessed using a curing property defined as the degree of cure, α . The degree of cure is a measure of cure progress of a partially cured system with respect to the fully cured network (Sabzevari, 2010). The behaviour and material properties of composites during the curing process can be modelled and predicted using α and its time derivative, i.e. the reaction rate ($d\alpha/dt$). Several numerical models called cure kinetic equations have been developed which relate this rate of reaction to some function of cure time, temperature and degree of cure (Sun, 2002; Sabzevari, 2010). A general expression for these models has the form of equation 2.1, in which $K(T)$ is a function of cure temperature only and, defined by equation 2.2, known as the Arrhenius rate constant, and $f(\alpha)$ is called the conversion function that describes the shape of the heat flow curve reflecting the type of reaction.

$$\frac{d\alpha}{dt} = K(T)f(\alpha) \quad (2.1)$$

$$K(T) = Ae^{\frac{-E_a}{RT}} \quad (2.2)$$

In equation 2.2, A is called the pre-exponential factor, $R = 8.314 \text{ J/mol} \cdot \text{K}$ (universal gas constant), E_a is the apparent activation energy of the cure reaction and T is the temperature in Kelvin. A and E_a are obtained through fitting the experimental data from differential scanning calorimetry (DSC). The ACCS tool-kit has three cure kinetic models implemented to predict the behaviour and material properties of composites during cure simulations, i.e. the n^{th} order kinetic equation, the Autocatalytic kinetic equation and the Kamal-Sourour kinetic equation.

The n^{th} cure kinetic model predicts the maximum reaction at the beginning of the curing process without accounting for the autocatalysis which is a common phenomenon during cure of the epoxy resin systems (Liang and Chandrashekhara, 2006; Sabzevari, 2010). The general form of the conversion

function of the n^{th} cure kinetic model is shown in equation 2.3 where n is the reaction order obtained through the fitting to experimental data.

$$f(\alpha) = (1 - \alpha)^n \quad (2.3)$$

The Autocatalytic cure kinetic model accounts for the autocatalysis; however, it assumes that the initial reaction rate is zero and the maximum reaction occurs in the intermediate stage of cure at about 0.3-0.4 degree of cure (Sabzevari, 2010). The general form of the conversion function of the Autocatalytic model is shown in equation 2.4 where n and m are the reaction order and constant respectively, also obtained through the fitting to experimental data.

$$f(\alpha) = \alpha^m(1 - \alpha)^n \quad (2.4)$$

The Kamal-Sourour kinetic model takes account of both effects of the autocatalysis and where the initial reaction rate is not zero. Therefore, its general form is the combination of the n^{th} order and Autocatalytic models, see equation 2.5. This model is known to fit experimental data well, however, it does not satisfy conditions where cure reactions terminate before complete curing (degree of cure = 1), is achieved (Ruiz and Trochu, 2005).

$$\frac{d\alpha}{dt} = (K_1 + K_2\alpha^m)(1 - \alpha)^n \quad (2.5)$$

As mentioned in Section 2.1, the chemical reactions change from kinetically controlled into diffusion controlled. The diffusion limitation factor, equation 2.6, has also been implemented in the ACCS tool-kit to account for this effect, where C , AC_0 and AC_T are the diffusion coefficient, initial degree of cure and temperature dependent degree of cure respectively.

$$D_L = 1 + e^{C(\alpha - (AC_0 + AC_T T))} \quad (2.6)$$

The cure simulations in ACCS tool-kit occurs in two steps. The first step is the thermo-chemical analysis where the above mentioned cure kinetic models, together with the diffusion limitation factor are used to compute the instantaneous heat (\dot{q}) generated during the curing process. This is accomplished by a thermo-chemical model shown in equation 2.7, where H_R , ρ and v_f are the heat of reaction, density and fibre volume fraction of the composite respectively. The temperature distributions in the composite are then evaluated using Fourier's heat conduction theory.

$$\dot{q} = \frac{H_R \rho (1 - v_f)}{\alpha^\infty} \frac{d\alpha}{dt} D_L \quad (2.7)$$

The second step is the thermo-mechanical analysis where the viscoelastic effects are taken into account to compute the development of cure-induced stresses and strains. Although the exact models implemented in the ACCS tool-kit could not be found in the literature, various viscoelastic models have been

developed for computing cure-induced stresses of composite materials (Guo *et al.*, 2007; Zhang *et al.*, 2016; Ding *et al.*, 2017; Li *et al.*, 2018).

Material states are determined by both levels of degree of cure and glass transition temperature mentioned in Section 2.1. The ACCS tool-kit calculates the glass transition temperature using the constitutive equation 2.8, where T_g^0 and T_g^∞ are initial and final glass transition temperature respectively, and λ as the fitting coefficient.

$$T_g = T_g^0 + \lambda \alpha \frac{T_g^\infty - T_g^0}{1 - (1 - \lambda)\alpha} \quad (2.8)$$

2.5 Ply Drop-off in Composite Structures

Ply drop-off is a phenomenon in which plies are terminated at various locations to form tapered components. A typical component that contains ply drop-off has three sections, i.e. thick, tapered and thin sections, see Figure 2.4. Plies can also be grouped into three sets i.e. core, dropped and top belt plies (Vidyashankar and Krishna Murty, 2001). The core plies form the base of the laminate and are usually on the tool side. Dropped plies are cut at certain locations and the distance between successive cuts is called the stagger length. The top belt plies cover the dropped plies and get bend from the thick to the thin sections. The gap left by the top belt at the bend usually gets filled with resin during the curing process and this area is named the resin pocket.

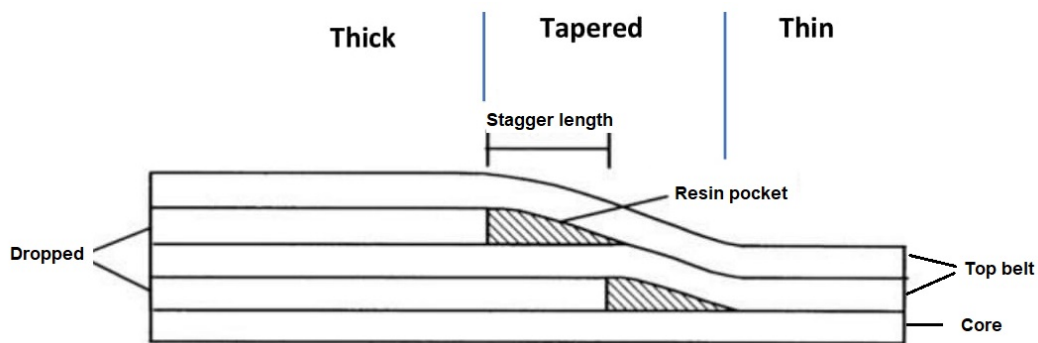


Figure 2.4: Typical structure of ply drop-off (Mukherjee and Varughese, 2001).

Numerous studies have been conducted on ply drop-off in composite materials. These studies found that ply drop-off introduces discontinuities in the laminate which results in stress concentrations during loading (Mukherjee and Varughese, 2001; Dhurvey and Mittal, 2012). Although no study was found that focused on curing composites with ply drop-offs, many studies have formulated design guidelines for composites with ply drop-offs (Mukherjee and Varughese, 2001).

2.6 FE Formulation of Composites With Ply Drop-off

The use of the Finite Element method in the analysis of laminated composite panels is very popular. Conventional FE modelling typically condenses the 3-D model which is accurate but computationally expensive, into a 2-D model by assuming that the variations of strain along the thickness of the laminate are a function of the strain at the reference plane. The 2-D model accurately predicts the in-plane displacements but the out-of-plane stresses are lost in the condensation. Therefore, the global stiffness properties of the laminate are found by superimposing/integrating the reduced transformed stiffness of each lamina over the entire thickness of the laminate. However, the modelling of tapered laminates (those with ply drop-off) is not that easy.

When modelling ply drop-offs, the stagger distance is very small which provides nodal lines along the drop-off locations thus generating very small elements. This means a fine mesh is required for accurate modelling of the drop-off which often results in the problem becoming computationally intractable (Mukherjee and Varughese, 2001). This has led many researchers into studying various ways of formulating FE models of composite laminates with ply drop-offs (Pian and Tong, 1969; Vizzini, 1995; Mukherjee and Varughese, 2001). The FE formulations used mostly follow two main approaches, i.e. the displacement-based FE approach or the hybrid stress FE approach.

The displacement-based FE approach assumes continuous displacements over the entire domain. This approach is the most popular and are implemented in commercial FE software packages such as Ansys. The main disadvantage of the displacement-based FE approach is that it can not satisfy the displacement continuity as a result of discontinuity in material properties as is the case of ply drop-off in tapered laminates. Therefore, the displacement-based approaches are generally good for providing qualitative and trend informations on the responses of structures under loading. To overcome this difficulty of the displacement-based approach when applied to the ply drop-off problem, hybrid stress based approaches were developed. The hybrid stress based approaches assume equilibrium of stress fields within the elements which enhance the stress accuracy and also uses the assumed boundary displacements in terms of nodal values such that they satisfy the inter-element continuity (Pian and Tong, 1969). More information on these two approaches is available in a review study conducted by He *et al.* (2000).

2.7 Summary

The background theory of the curing process of thermosetting composites has been presented. This theory indicated that during the curing process, thermosetting resin goes through cross-linking reactions that lead to material evolutions and volumetric shrinkages. These changes in turn, induce stresses in the laminate which might cause defects such as fibre waviness. Two types of fibre waviness i.e in-plane and out-of-plane waviness were discussed; however, this study focuses only on the in-plane fibre waviness. To study fibre waviness, cure simulations will be performed using a newly developed ACCS analytical tool-kit. The theory used by the tool-kit was briefly introduced and the constitutive models implemented for cure simulations were discussed. Using these models, the cure induced stresses and strains can be predicted which will enable the prediction of fibre waviness defects. Lastly, ply drop-off was discussed which is a source of stress concentrations in the laminate that might also lead to the formation of fibre waviness defects.

Chapter 3

Finite Element Modelling

The focus of this study was to predict the fibre waviness defect formation in a thermosetting composite panel which is cured in an autoclave. The predictions were achieved by performing cure simulations using the newly developed Ansys Composite Cure Simulation (ACCS) tool-kit. The composite panel comprises ply drop-offs which introduce structural complexities such as discontinuities that results in stress concentrations. The aim of this chapter is to discuss the geometrical layout of the composite panel and the corresponding finite element (FE) model. The FE model included both the composite panel and the tool since tools affects the behaviour of composites during the curing process.

3.1 Panel Layout

The composite panel used in this study was designed by an aerospace partner company as part of the spar-component for a commercial aeroplane's rear wing. This panel consists of 24 unidirectional plies in which some are terminated at various locations to create sections of different thickness. This termination of plies is called ply drop-off and the location where one or more plies are terminated is called the drop-off station as discussed in Chapter 2. Also remember that the panel is tapered at the drop-off station.

The geometrical layout and ply lay-up of the panel are shown in Figure 3.1. The panel has four drop-off stations (number 1 through 4) dividing the panel into five sections (named A through E) of different thickness. At each drop-off station, a stagger length of 5 mm is used which is the distance between two successive ply terminations. For instance, at drop-off station no. 1, there are four plies which are terminated at 5 mm intervals. The panel is 1007 mm long and 900 mm wide. Table 3.1 shows the ply fibre orientation colour scheme and the locations of the first ply drop for every drop-off station measured from the left end of the panel.

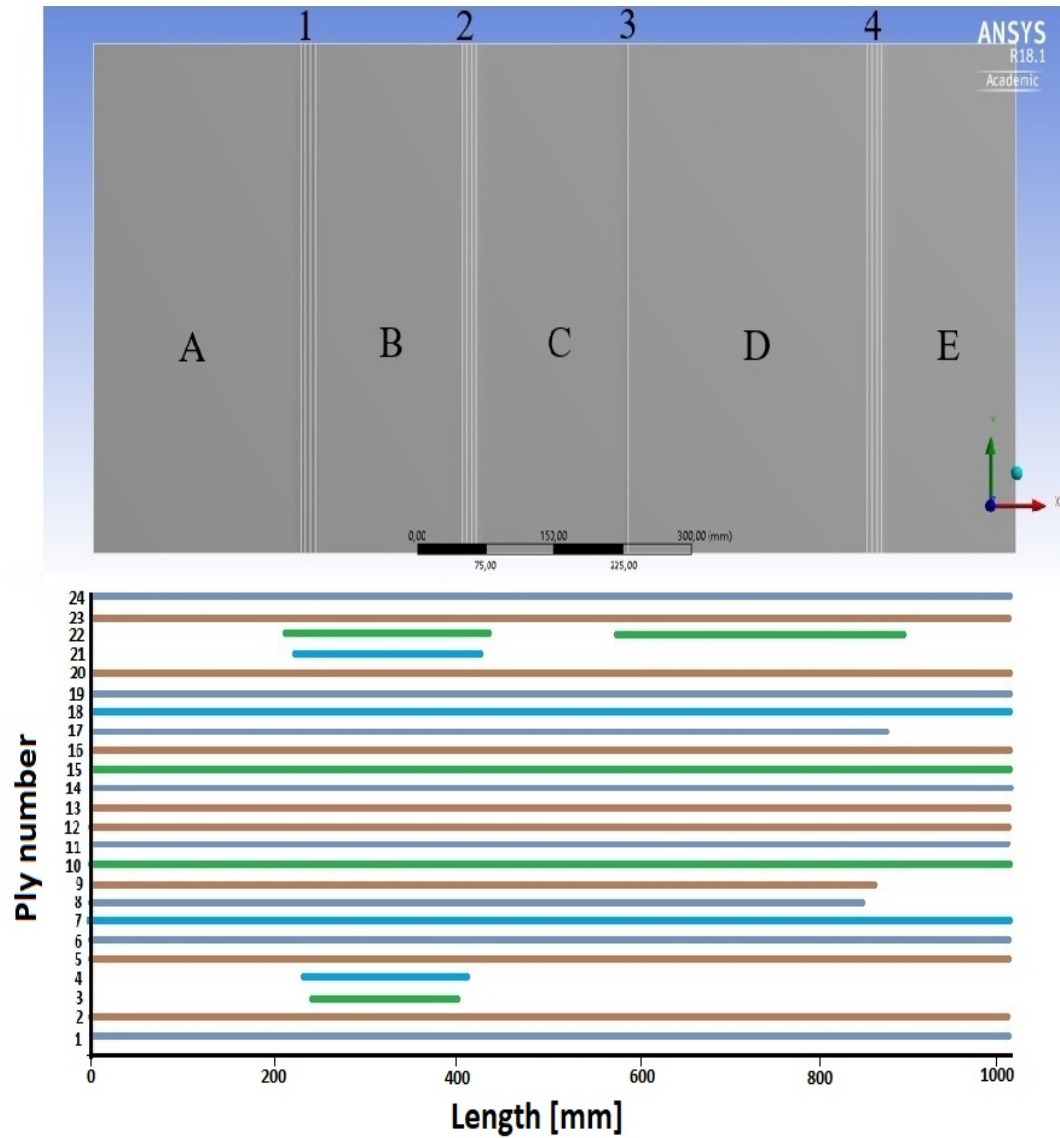


Figure 3.1: Geometrical layout and ply lay-up of the composite panel.

Table 3.1: Locations of first ply drop and ply fibre orientations colour scheme.

First ply drop locations			
227 mm	403 mm	584 mm	846 mm
Ply orientation colour scheme			
-45°	0°	45°	90°

3.2 FE Models

The composite panel is constructed by placing plies on a flat tool before being bagged and placed in a vacuum environment. Thus, both the composite panel and the tool were considered when developing the FE model. The composite panel and the tool were modelled separately and later assembled by defining contact conditions between them. This section discusses the procedures and assumptions followed to develop both models, and the final assembly model. All the modelling was done in Ansys.

3.2.1 Composite panel model

The composite panel was modelled using the Ansys Composite PrePost (ACP) tool-kit where the stacking sequence is defined on a meshed shell surface and then extruded into a layered solid model. During the extrusion, the Ansys SOLSH190 element was chosen which is a linear 3-D solid-shell element capable of modelling thin to moderately thick layered solid structures.

The composite panel also consists of ply drop-offs and as mentioned in Chapter 2, a triangular gap, i.e. resin pocket, is created by drop-off which gets filled with resin during the curing process. When modelling these resin pockets, the Ansys SOLID185 element which is the linear 3-D solid element equivalent to the Ansys SOLSH190 element capable of modelling thin to moderately thick solid structures was used. This is because the resin pocket elements are not layered and they are assigned properties of an isotropic material. Furthermore, these elements (SOLID185 and SOLSH190) were chosen because they have been tested and verified for performing cure simulations with the ACCS tool-kit (LMAT, 2016).

As stated, the mesh was generated on a shell surface before extruding into a solid model. A uniform mesh was used throughout the panel with a finer mesh (two elements per stagger length) at the drop-off stations due to stress concentrations induced by the dropping of plies. When extruding the elements into a solid model, one element was used per ply thickness due to the capabilities of the Ansys SOLSH190 elements. Figure 3.2 shows the mesh of the panel model with the zoomed region showing the resin pocket elements.

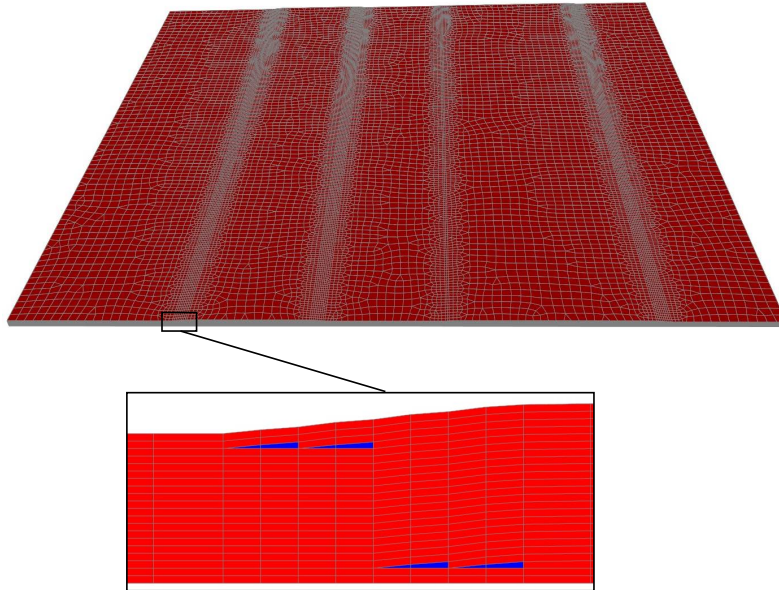


Figure 3.2: Mesh of the composite panel showing resin pocket elements (blue).

3.2.2 Tool model

The tool was assumed to be flat and 200 mm larger than the composite panel in all directions. It also has "dam" walls in the centre that serves as the frame into which plies are laid. To model the tool, Ansys SOLID185 elements was also used with a finer mesh on these "dam" walls due to stress concentrations at the corners, Figure 3.3.

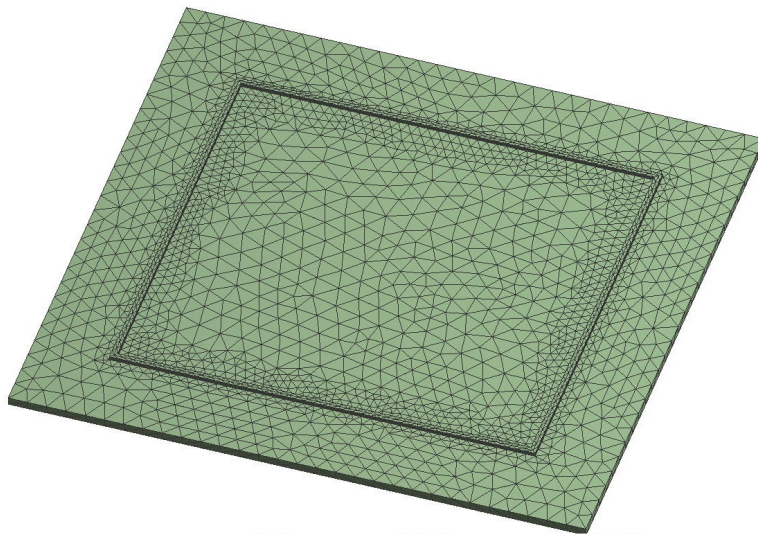


Figure 3.3: Geometrical layout and mesh of the tool.

3.2.3 Panel-tool assembly model

The assembled model of the composite panel and tool is shown in Figure 3.4. The contact between the panel and the tool was assumed to be frictional with an asymmetric behaviour since the composite panel is more flexible than the tool. This type of contact requires defining a friction coefficient, which depends on the type of release used and according to the study by Zeng and Raghavan (2010), continually changes with the changing conditions of the thermosetting composite during the curing process.

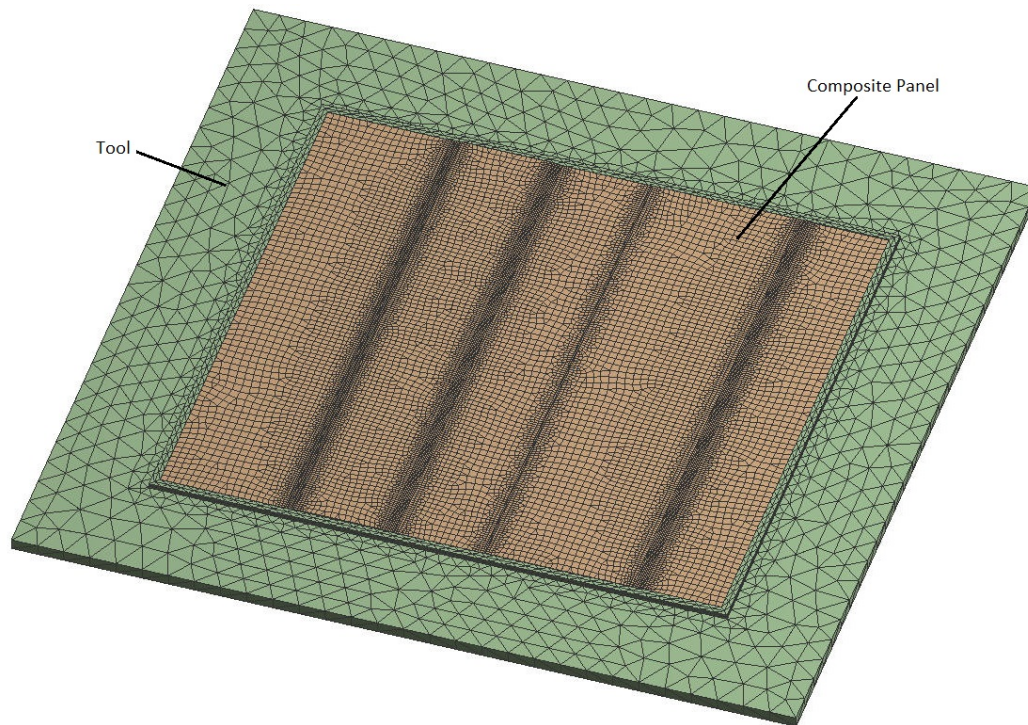


Figure 3.4: Tool and composite panel assembly FE model.

3.3 Conclusion

This chapter focused on developing the finite element models of the composite panel and tool. The two models were modelled separately and later assembled together by defining the contact conditions. A frictional contact was assumed since the tool has some roughness in practice. The friction coefficient will be defined in the succeeding chapter when defining material properties.

Chapter 4

FE Model Preparations

This chapter focus on preparing the FE model discussed in Chapter 3 for performing cure simulations using the ACCS tool-kit. First, the procedure of predicting fibre waviness by performing cure simulations with the ACCS tool-kit is discussed. Then the discussion of material properties, loads conditions and assumptions follow. The material properties used in this study were obtained from various studies in the literature. The load conditions were obtained from the aerospace partner company mentioned in Chapter 3 as per their design specifications.

4.1 Simulation Procedure

When performing cure simulations with the ACCS tool-kit, two simulation procedures can be followed, i.e. the full cure simulation procedure, or the fast cure simulation procedure (LMAT, 2016). The full cure simulation procedure starts by performing the transient thermal analysis to compute temporal thermal gradients followed by a static structural analysis for computing cure stresses and distortions. The fast simulation procedure assumes a uniform temperature distribution within the composite part; thus, only the static structural analysis is performed.

This study follows the full cure simulation procedure to fully capture the temporal material evolutions which highly depends on thermal histories (LMAT, 2016). Figure 4.1 shows the full cure simulation flowchart updated for fibre waviness predictions. The procedure starts by defining material and contact properties for the FE model discussed in Chapter 3. This is followed by a transient thermal analysis where the cure-temperature cycle is applied, and the ACCS tool-kit is used to compute thermal and material evolutions. The cure results (such as the degree of cure, glass transition temperature, viscosity and temperature gradients) are produced from this analysis.

Next, the temperature gradients are used as loads during the static structural analysis where the cure-pressure cycle is applied, and the ACCS tool-kit is used to compute cure-induced stresses and strains. These stresses and strains are then used to predict fibre waviness defects. The cure results can also be obtained from the static structural analysis.

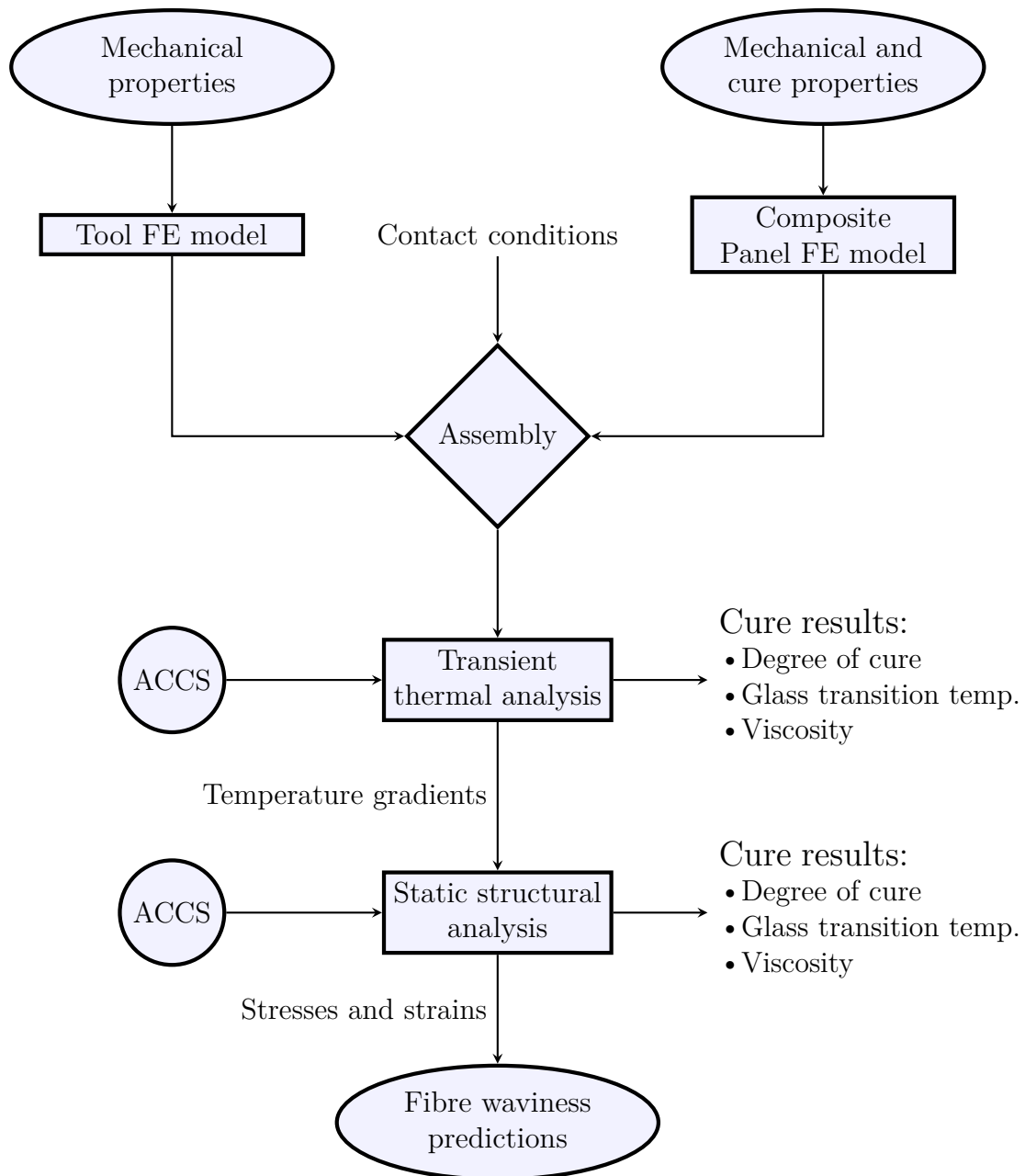


Figure 4.1: Full cure simulation procedure flow chart.

4.2 Material Properties

To perform cure simulations using the ACCS analytical tool-kit, the cure properties of the composite panel are required in addition to the mechanical (elastic and thermal) properties. The ACCS tool-kit evokes the Ansys solver with chemical cure and cure shrinkage sub-routines, for materials with defined cure properties during the analysis (LMAT, 2016). Figure 4.2 shows the list of cure properties, specific to the ACCS tool-kit, that can be added to the model to perform cure simulations. To activate the tool-kit for cure simulations, at least one of the cure kinetic equations (box 1) and all properties in boxes 2, 3 and 4 must be added to the model (LMAT, 2016). The rest of the properties can be added to improve the accuracy of the simulations. This section discusses the cure properties of the composite panel and tool materials.

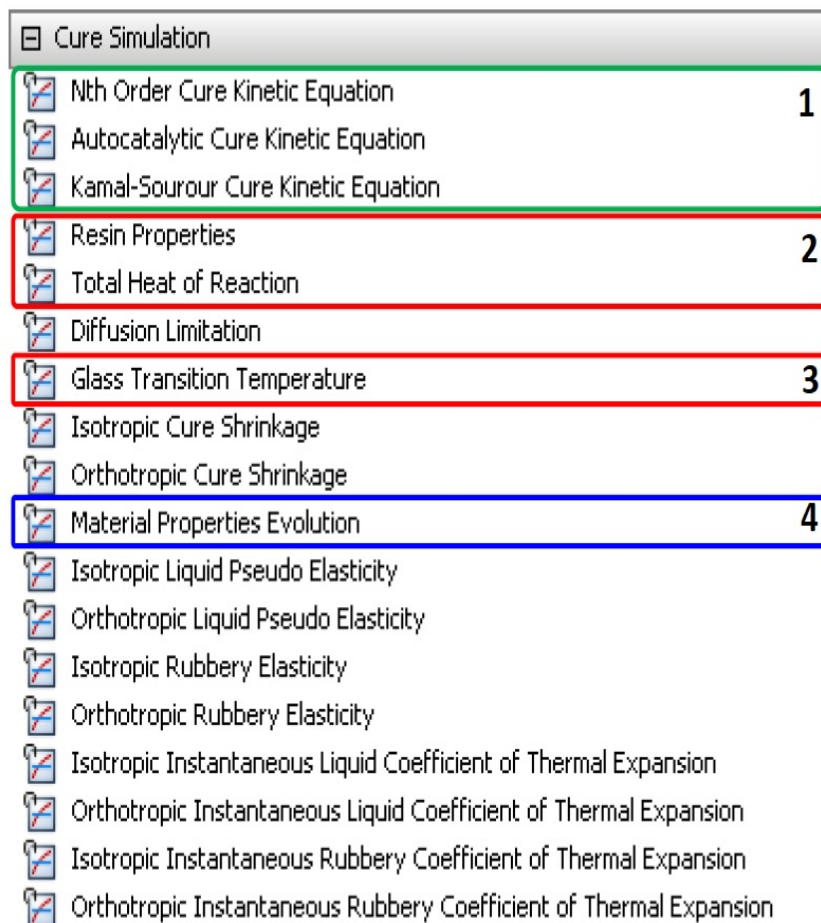


Figure 4.2: Cure properties needed to perform cure simulation with the ACCS tool-kit (LMAT, 2016).

4.2.1 Composite panel material

The composite panel used in this study was constructed from the IM7/977-2 prepreg. This material is a unidirectional tape consisting of CYCOM 977-2 which is a toughened-epoxy resin that is reinforced with IM7 carbon fibres. It is noted for its intermediate modulus (256 GPa class) suitable for the fabrication of large structures for aerospace applications (Cytec, 2012). As shown in Figure 4.2, defining the cure properties of this material include choosing the cure kinetic equation/model. In this study, the cure kinetic equation was chosen by fitting the experimental data obtained from Differential Scanning Calorimetry performed by Alavi-Soltani *et al.* (2012). The cure kinetic equations fitted were discussed in Chapter 2 and the Autocatalytic cure kinetic equation gave a better fit for the IM7/977-2 material, see Figure 4.3. Therefore the Autocatalytic cure kinetic equation was chosen. The parameters of the equation are shown in Table 4.1 together with the rest of the cure properties required for the activation of the ACCS tool-kit and additional properties to improve the accuracy of the simulation. The mechanical properties of this material were obtained from the various sources in the literature and are presented in Appendix A.

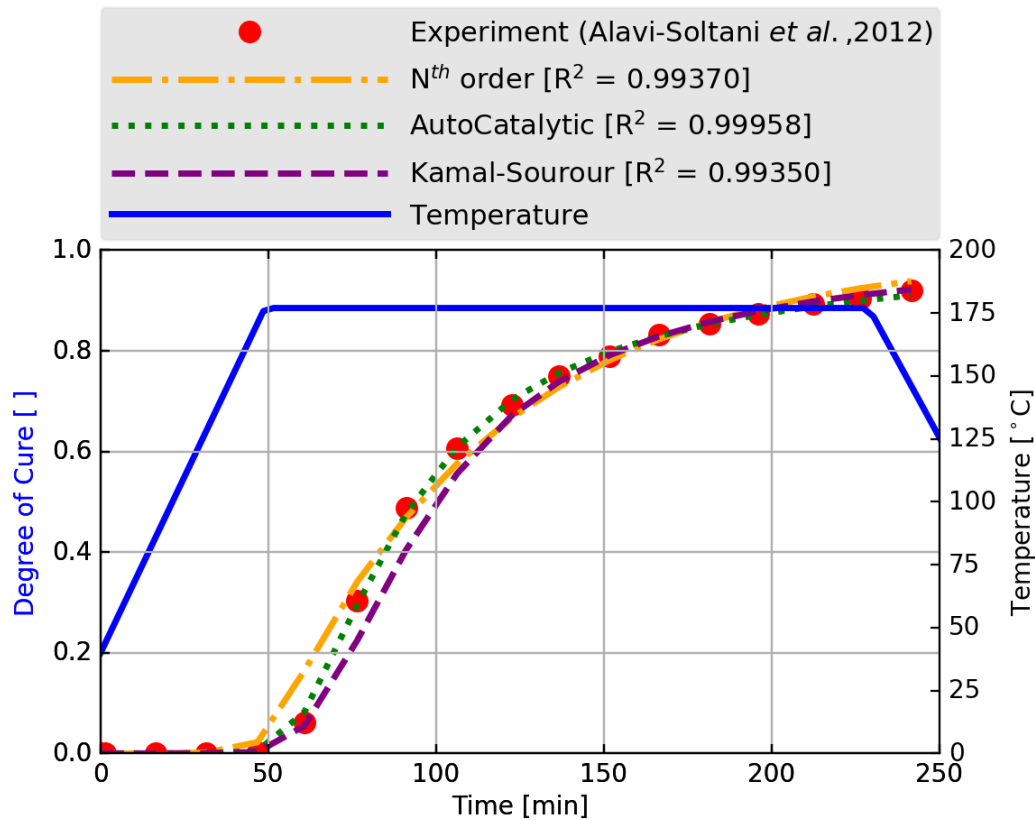


Figure 4.3: Cure kinetic equation fitting to experimental data.

Table 4.1: IM7/997-2 prepreg and pure resin cure properties.

Property	Value	Comment [reference]
Autocatalytic (Curve fitting results)		
A [s^{-1}]	63542	
E [J]	70830	
m power	0.1	
n power	1.5	
Resin Properties		
Fibre volume fraction	0.6	(Cytec, 2012)
Initial degree of cure	0.0001	
Maximum degree of cure	0.9999	
Gelation degree of cure	0.33	Prepreg (Sabzevari, 2010; Tavakol <i>et al.</i> , 2013)
	0.5	Pure resin (Tavakol <i>et al.</i> , 2013)
Total Heat of Reaction [J]	146400	Prepreg (Sabzevari, 2010)
	441000	Pure resin (Sabzevari, 2010)
Glass Transition Temperature		
Initial value [$^{\circ}C$]	2	Storage Temperature (Sabzevari, 2010)
Final value [$^{\circ}C$]	212	(Cytec, 2012)
λ	0.6	(Sabzevari, 2010)
Material Properties Evolution (Refer to Chapter 2)		
x_g smoothing width	0	Not known
T_g smoothing width	0	Not known
Orthotropic Cure Shrinkage		
$C1$ (Fibre direction)	0.42	(Joven <i>et al.</i> , 2012)
$C2$ (Transverse direction)	2.11	(Joven <i>et al.</i> , 2012)
$C3$ (Thickness direction)	4.82	(Joven <i>et al.</i> , 2012)

It is known that as the cure process proceeds, the molecular size and the cross-linking density increase, which in turn increase the viscosity of the resin system, thus decreasing resin mobility. On the other hand, the temperature has a large effect on the dynamics of the molecules and thus the viscosity (Liang and Chandrashekhara, 2006). Since fibres have low bending stiffness and are more likely to buckle when the resin is in a flowing state (low viscosity), the changes in resin viscosity need to be analysed to better understand when fibre waviness occurs.

Various empirical rheology models have been developed in the literature to describe the viscosity of thermosetting resin systems. This study uses the rheology model modified by Shanku *et al.* (1997) into a quadratic form, Equation 4.1, to account for the nonlinear relation between the logarithmic viscosity and degree of cure of epoxy systems, cited by Liang and Chandrashekhara (2006).

$$\mu = \mu_{\infty} \exp \left(\frac{E_u}{RT} + B_1 \alpha^2 + B_2 \alpha \right) \quad (4.1)$$

where E_u is the activation energy for viscosity, $R = 8.314 \text{ J/mol} \cdot \text{K}$ (universal gas constant) and, B_1 , B_2 and μ_{∞} are constants. To obtain these constants, the rheology model was fitted to the material's viscosity profile from the data sheet (Cytec, 2012), see Figure 4.4, and the following values were obtained: $E_u = 74441 \text{ J}$, $B_1 = 15$, $B_2 = 5$ and $\mu_{\infty} = 9.43\text{e-}10$.

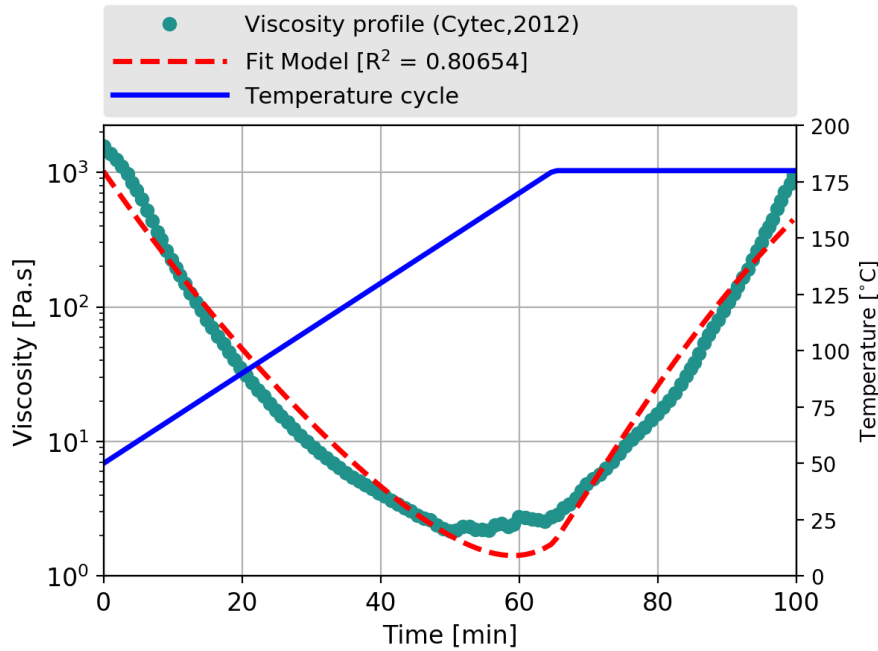


Figure 4.4: Fit of the rheology model to the viscosity profile.

4.2.2 Tool material

The tool is made from the Invar material which is a nickel-iron alloy noted for its low thermal expansion (AZoM, 2001). The tool does not cure, therefore cure properties were not needed for this material. The mechanical properties were obtained from the literature and are presented in Appendix A.

4.2.3 Contact properties

As mentioned in Section 3.2, the contact between the tool and the composite panel was assumed to be frictional which requires defining the friction coefficient to perform simulations. The friction coefficient continually changes with the changing cure conditions and it also depends on the type of release used, i.e. release agent or release film (Zeng and Raghavan, 2010). In this study, it is assumed that a release agent is used instead of a release film. Joven (2013) performed a series of experiments and obtained a friction coefficient of 0.07 when curing a IM7/977-2 composite part on an Invar-tool at 177 °C cure temperature while using a release agent between the part and the tool. Therefore, this friction coefficient was assumed in this study. The contact's thermal conductivity and stiffness were automatically controlled by the solver as they are not known. Furthermore, the Augmented Lagrange formulation theory was used to define the contact because it is less sensitive to the selection of normal contact stiffness and for its ability to control contact penetration.

4.3 Loads and Boundary Conditions

As mentioned in Section 4.1, the full cure simulation procedure is followed, which starts by performing the transient thermal analysis followed by the static structural analysis. During the transient thermal analysis, the composite panel and tool assembly was assumed to be surrounded by air following the cure-temperature cycle conditions shown in Figure 4.5, and with a convection coefficient of 200 W/m²°C on all free surfaces (ANSYS, 2017). The cure-temperature cycle is divided into three load steps and applied as a convection load on all the free surfaces on the top and the bottom of the assembled model. In the first step which is the curing phase, the temperature is ramped up at a rate of 2 °C/min until reaching a cure temperature of 180 °C. Then held at this value for 120 min to allow for complete curing. The second step is the cool-down phase where the temperature is ramped down to room temperature at a rate of 3 °C/min. The room temperature was assumed to be at 20 °C. The third step assumes the composite panel is removed from the tool by removing the contact elements to compute final deformations caused by residual stresses. This last step is beyond the scope of this study, however necessary for the ACCS tool-kit to operate properly (LMAT, 2016).

During the static structural analysis, the tool was assumed to be fixed and the composite panel was pressed against the tool following a cure-pressure cycle, also shown in Figure 4.5. As shown, the pressure is ramped-up simultaneously with the temperature at a rate of 0.5 bar/min to a curing pressure of 10 bar (1 MPa). The pressure ramp-down is also done simultaneously with the temperature cool-down, but at an uncontrolled rate as it is assumed to be vented to the atmosphere. This pressure cycle was applied as a pressure load on the top surface of the composite panel. Furthermore, the composite panel was also constrained to prevent rigid body motion.

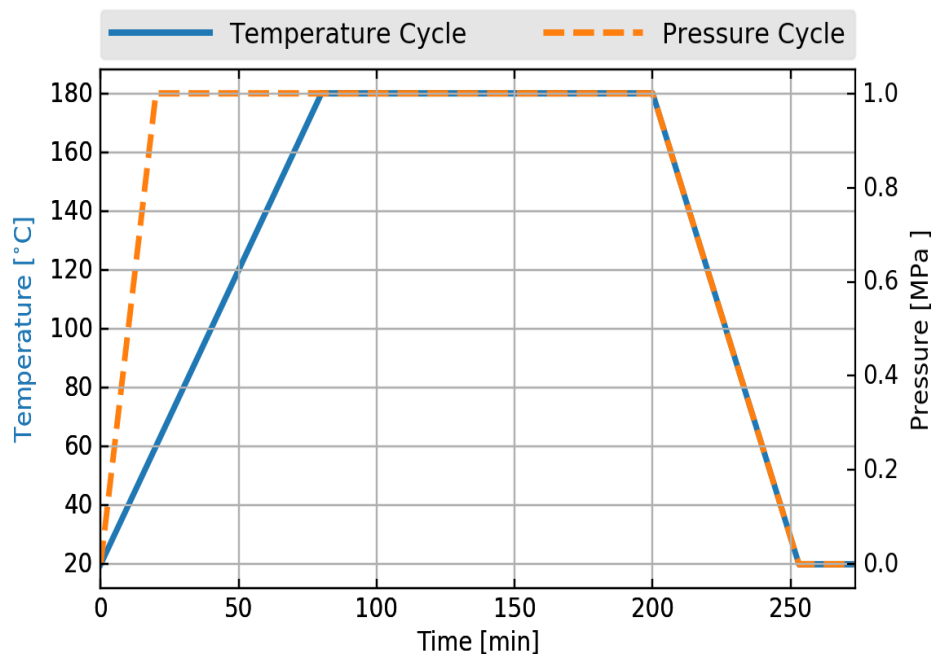


Figure 4.5: Cure cycle for manufacturing composite panel.

4.4 Conclusion

The simulation procedure, the material properties and the loading conditions needed for the FE simulation were presented. The full cure simulation procedure was used which starts by performing the transient thermal analysis followed by a static structural analysis. During the transient thermal analysis, the cure temperature cycle was applied as a convection load on all surfaces on the top and the bottom of the assembled model. The pressure cycle was applied as a pressure load on the top surface of the composite panel. Lastly, when defining the material properties, the Autocatalytic cure kinetic model was chosen since it gave a better fitting of the experimental data obtained from the literature.

Chapter 5

Simulation Results and Validation

The finite element models and cure simulation procedures were presented in Chapters 3 and 4 respectively. In this chapter, the results of the simulations are presented. The discussion starts by analysing the cure results to understand the material evolution of the composite panel during the curing process. These results were validated by comparing against various experimental results obtained from literature. The discussion of the cure-induced stresses/strains development and progression then follows. These stresses/strains development trends will also be validated by various observations from literature. Lastly, strain distributions will be analysed at a single point to predict fibre waviness defects and deduce mechanisms that influence their formation. The predictions will be validated by practical observation after manufacturing.

5.1 Cure Process Results

The evolution of the glass transition temperature, the degree of cure and viscosity were computed during both the transient thermal analysis and the static structural analysis as the cure results. These results are shown in Figure 5.1, which were similar for both thermal and structural analyses. As mentioned in Chapter 2, the composite panel goes through two main transitions during the curing process i.e. gelation and vitrification. Gelation occurs when the degree of cure reaches a predefined value called the gel point (i.e. gelation degree of cure) and vitrification occurs when the glass transition temperature becomes higher than the cured part temperature.

The cure results indicated that gelation occurs at about 95 min cure time when the degree of cure reaches a value of 0.33 as predefined in Chapter 4. This point of cure is not easy to validate using the experimental results from literature because it depends highly on the heat-up rate and the cure temperature which

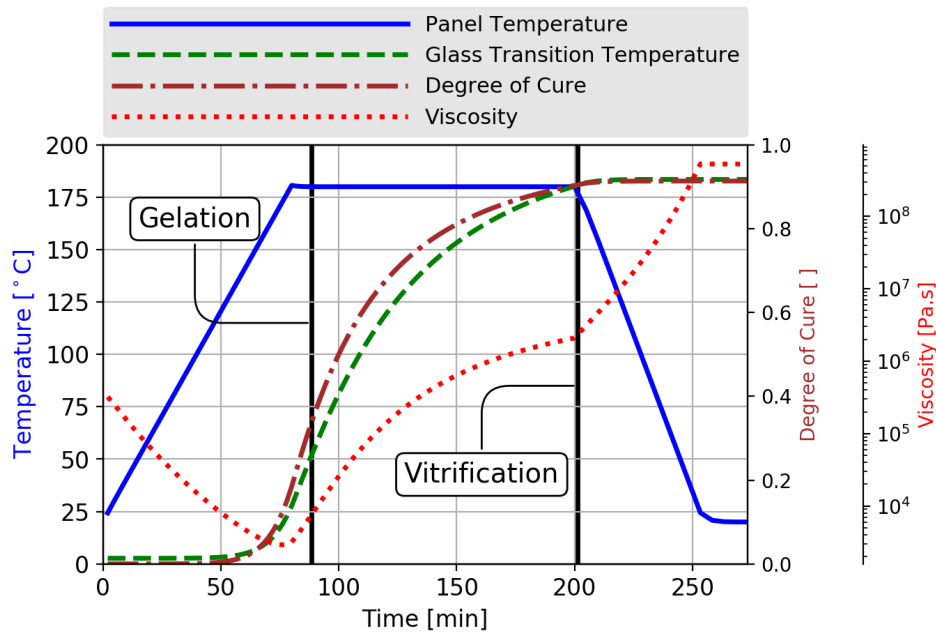


Figure 5.1: Composite panel material evolutions during the curing process.

are often different for manufacturers. Sabzevari (2010) conducted a series of experiments and showed different times of gelation for a number of cure temperatures. For instance, during their study, they obtained a gelation time of about 35 min cure time when using the heat-up rate of 28.9 °C/min and a cure temperature of 180 °C for the same material used in this study (i.e. IM7/977-2 composite).

Vitrification was obtained to occur at about 185 min cure time, which is just before the cool-down. Like gelation, this point depends highly on the cure profile, thus it is difficult to validate from the literature. However, the final degree of cure depends only on the cure temperature and not on the heat-up rate, thus making it easier to validate. The final degree of cure was obtained to be 0.925 and this agrees with the experimental results obtained by Sabzevari (2010) and Alavi-Soltani *et al.* (2012) when curing at 180 °C isothermal cure temperature but using different heat-up rates.

The viscosity results indicate that the composite panel reaches the lowest viscosity before gelation and the highest viscosity after vitrification. This was expected since the resin is believed to be in the liquid state before gelation and in the solid state after vitrification. The high viscosity value at the beginning of the curing process is because the composite panel is built from prepregs, which are partially cured and vitrified for easy handling. As the cure temperature rises, the resin starts melting, reducing the viscosity to a lower value before gelation, then starts increasing as the curing continues. At gelation, the

viscosity is already increasing and has reached the level of an elastic gel state, thus explaining the rubbery state after gelation. Towards vitrification, the viscosity increases even further to an infinite value, thus, explaining the solid state after vitrification. The high viscosity means the resin has lost the ability to flow which will prevent the fibres from buckling. This means fibre waviness can only occur in the viscous liquid state, when the resin has low viscosity and the ability to flow.

It is also important to note that the panel does not cure at the same rate. This is due to varying thermal gradients that the panel experiences. For example, the surface on the bag side experiences higher temperature values compared to the surface on the tool side, thus the bag side cures faster than the tool side. See Figure 5.2 for the degree of cure distribution at gelation time on the top (bag side) and bottom (tool-side) surfaces.

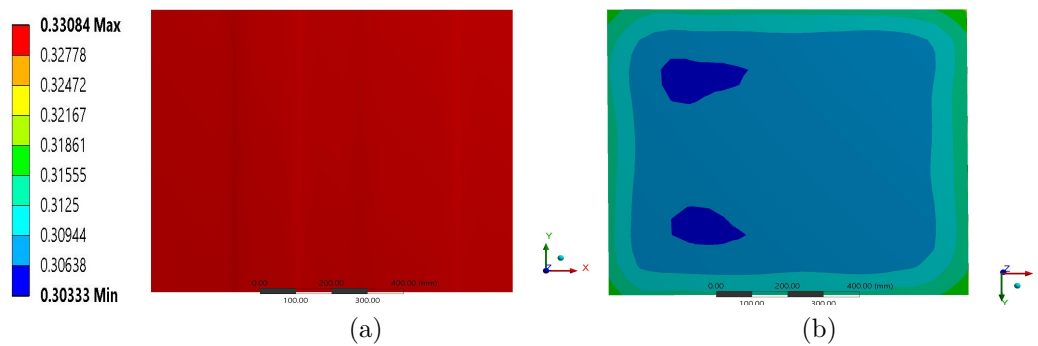


Figure 5.2: Degree of cure distributions at gelation: (a) top surface, (b) bottom surface.

5.2 Development of Cure-induced Stresses

It is mentioned in Chapter 2 that thermosetting composites experience cure-induced stresses and strains during the curing process. The analysis of stresses for composite materials is not recommended due to their complex anisotropic behaviour. However, the equivalent Von-Mises stresses were analysed in this section to understand the overall stress development in the composite panel during the curing process, see Figure 5.3. The plot shows that the composite panel experience stresses right from the start of the curing process, which agrees with the observations made by Mulle *et al.* (2009).

The equivalent stresses reach a constant value in the early stage of the heat-up phase and increase vastly during the cool-down phase. This kind of behaviour was also observed by the numerical studies conducted by White and Kim (1998)

and Li *et al.* (2018) on a carbon fibre-epoxy resin composite material. Various factors such as thermal expansion during the heat-up phase, the interactions of the panel with the tool etc., are believed to be responsible for this early development of cure-induced stresses (Wisnom *et al.*, 2006; Kravchenko *et al.*, 2016; Li *et al.*, 2018). The viscosity plot was used to link these developments of cure-induced stresses to the cure process results. However, no clear relationship was observed.

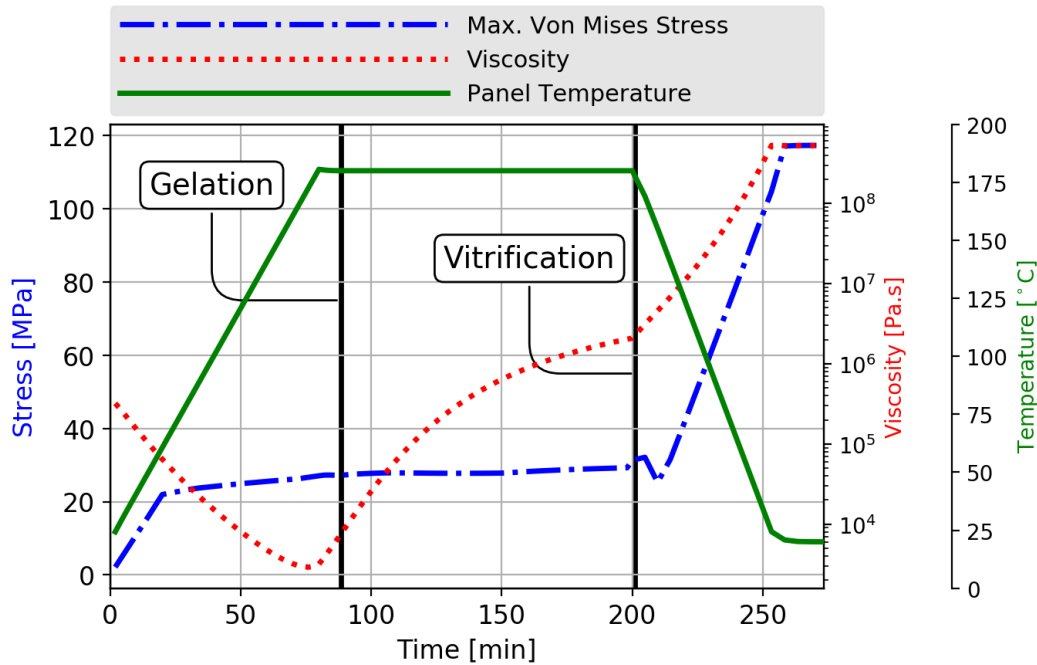


Figure 5.3: Maximum cure-induced Von-Mises stress and average viscosity evolutions during the cure process.

5.3 Development of Cure-induced Strains

The in-plane fibre waviness defect is of concern in this study, therefore only the development of the in-plane cure-induced strains (ε_1 , ε_2 and ε_{12}) were analysed. To better understand how strains are induced at various locations on the panel, the in-plane strains developing at the centre of the drop-off station no. 1 and the thickest section of the panel (Section B) were analysed on plies located on the outer surfaces (bag side and tool side), see Figure 5.4. The same development and progression of strains in the fibre direction (ε_1) were observed on both plies and all locations (Drop-off station and Section B). These strains are very low before gelation and become more and more compressive thereafter. The same observations were made by Niu (1999) by using the FBG sensor.

The transverse strains are in compression and grow larger between gelation and vitrification. This is because the transverse direction is dominated by the resin which experiences the highest chemical shrinkage between gelation and vitrification, i.e. when the curing rate is high. Although the magnitude is lower at the drop-off station on ply 24, the same behaviour is observed at all locations. This variation is believed to be due to the effect of the ply drop-off, since ply 24 is bend into a taper section of the panel at the drop-off station while ply 1 is flat.

Like the transverse strains, the development of shear strains at the drop-off station for ply 24 differs compared to other locations. High shear strains develop at the drop-off station on ply 24, while remaining low for the rest of the panel. This shear strain variation also indicates the effect of ply drop-off on the strain distributions.

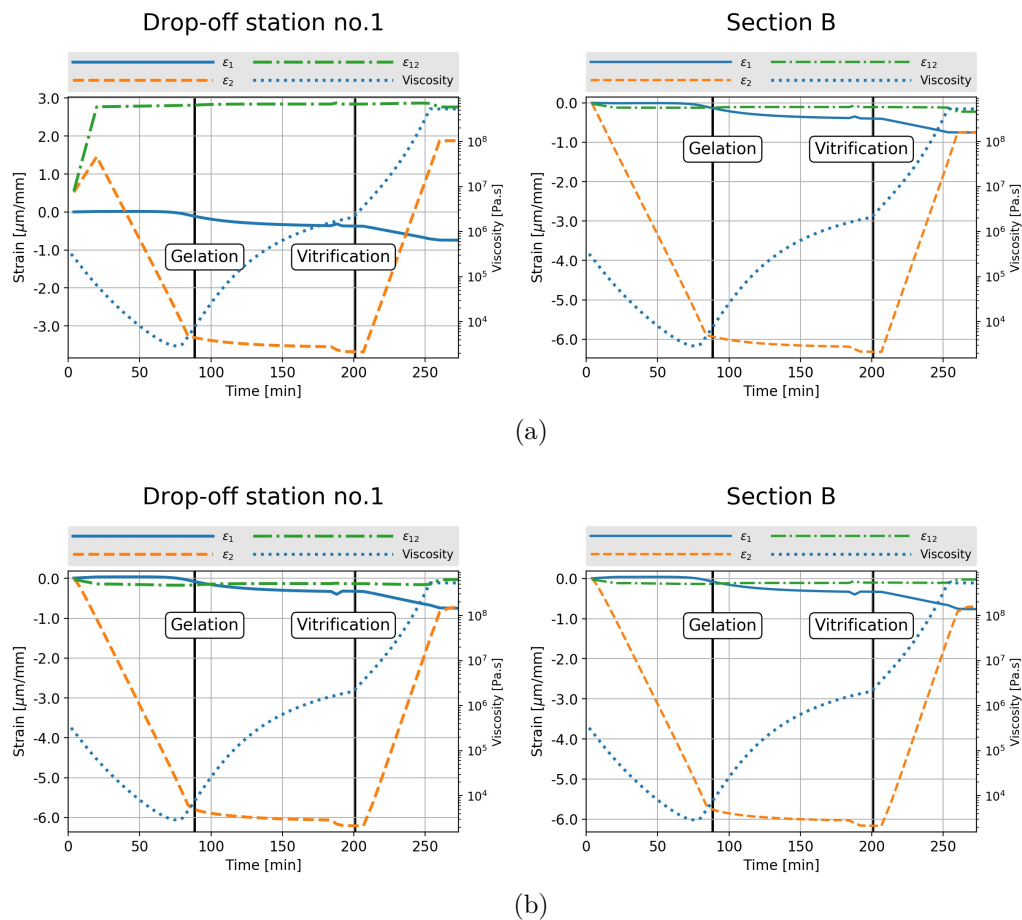


Figure 5.4: Development of in-plane cure-induced strains at drop-off station no. 1 and section B of the panel on, (a) ply 24 (bag-side), (b) ply 1 (tool-side).

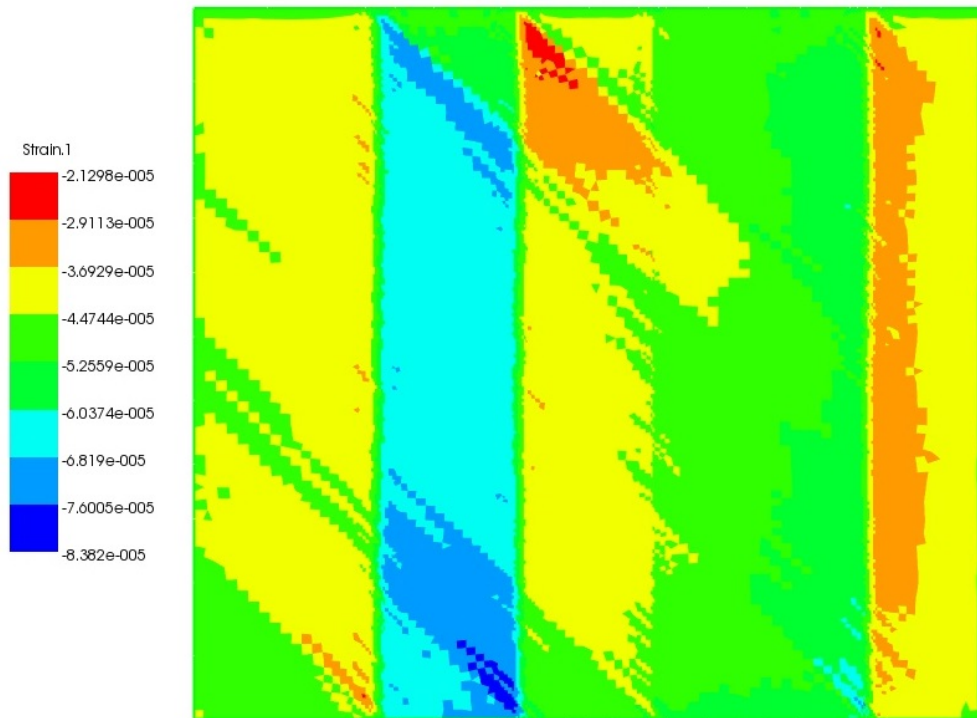
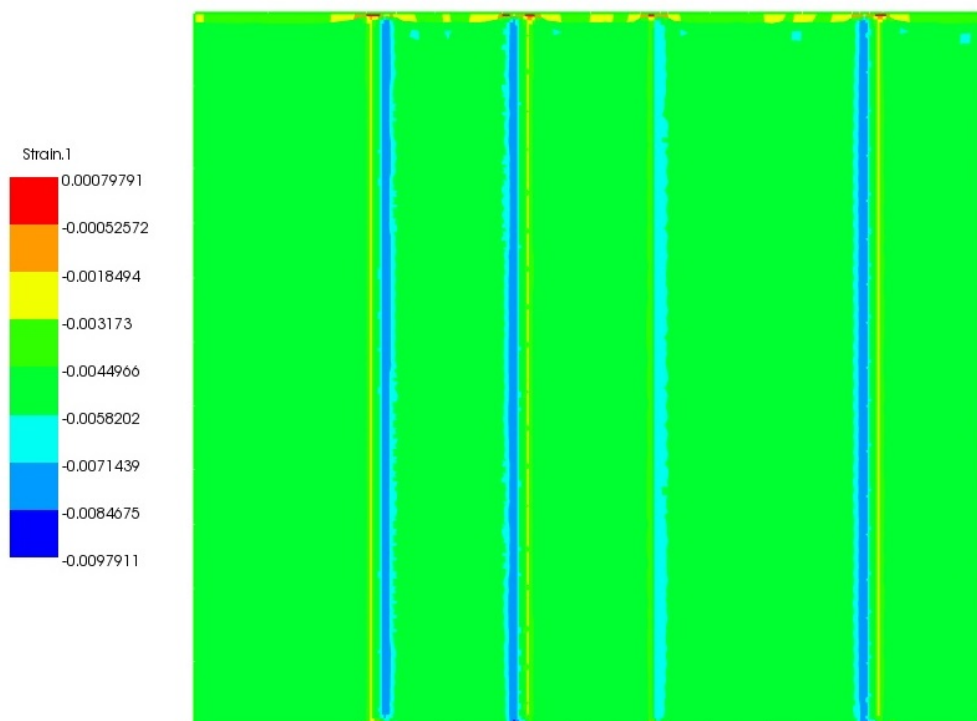
5.4 Cure-strain Distribution

With the stresses and strains developing in the composite panel during the curing process, deformations that result in defects such as fibre waviness are also possible. Fibres are more likely to buckle when the resin has low viscosity and has the ability to flow. Therefore, the in-plane strain distribution in the composite panel were analysed at the point of lowest resin viscosity to observe the possibilities of the buckling of fibres. Furthermore, fibre waviness defects are usually visible on the outer surfaces, therefore, only plies on the outer surfaces, i.e. on the tool side (ply 1) and the bag side (ply 24), were analysed. For the in-plane strain distributions on the rest of the plies, refer to Appendix B.

5.4.1 Bag side (ply 24: -45° fibre direction)

The strains in the fibre direction (ε_1) are in compression. These strains are higher in the thickest section of the panel (Section B) and vary with section thickness. However, this does not give a clear indication if fibres buckle because the loads from the curing process are not pure compressive loads, also these strains are relatively low, i.e. about $83.8 \mu\text{m}/\text{m}$ maximum strain, which might not meet the critical compressive strain (not known) for fibre buckling to occur in a viscous liquid. Therefore, the transverse and the shear strains were also analysed, see Figure 5.9 and 5.10 respectively. Both transverse and shear strains were observed to be concentrated and alternating (high-low-high or vice versa) at the drop-off stations, especially at drop-off stations 1, 2 and 4, and are evenly distributed on the main sections (A through E) of the panel.

The transverse strains are highly compressive with about $9.8 \text{ mm}/\text{m}$ of maximum strain and an alternating difference of about $6 \text{ mm}/\text{m}$. With the resin being in the liquid phase and having the ability to flow, this high alternating transverse strain difference will cause the fibres to buckle due to their low bending stiffness. Shear strains alternate between a positive and a negative value indicating that fibres experience opposing shear angles, thus they will form bends at those drop-off stations.

Figure 5.5: ε_1 strain distribution in ply 24.Figure 5.6: ε_2 strain distribution in ply 24.

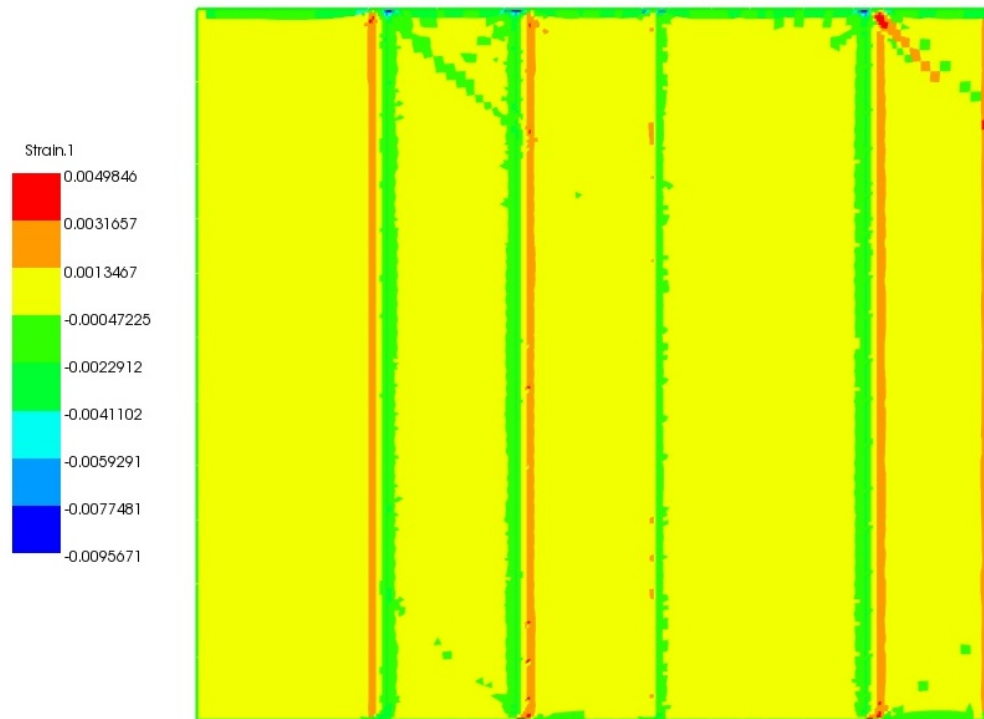
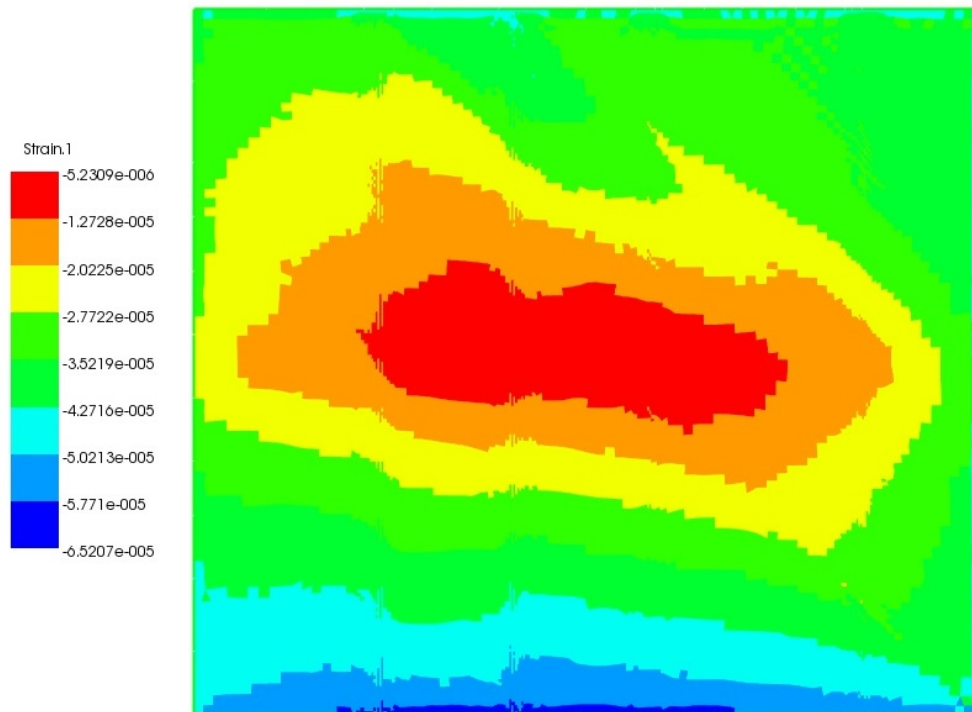
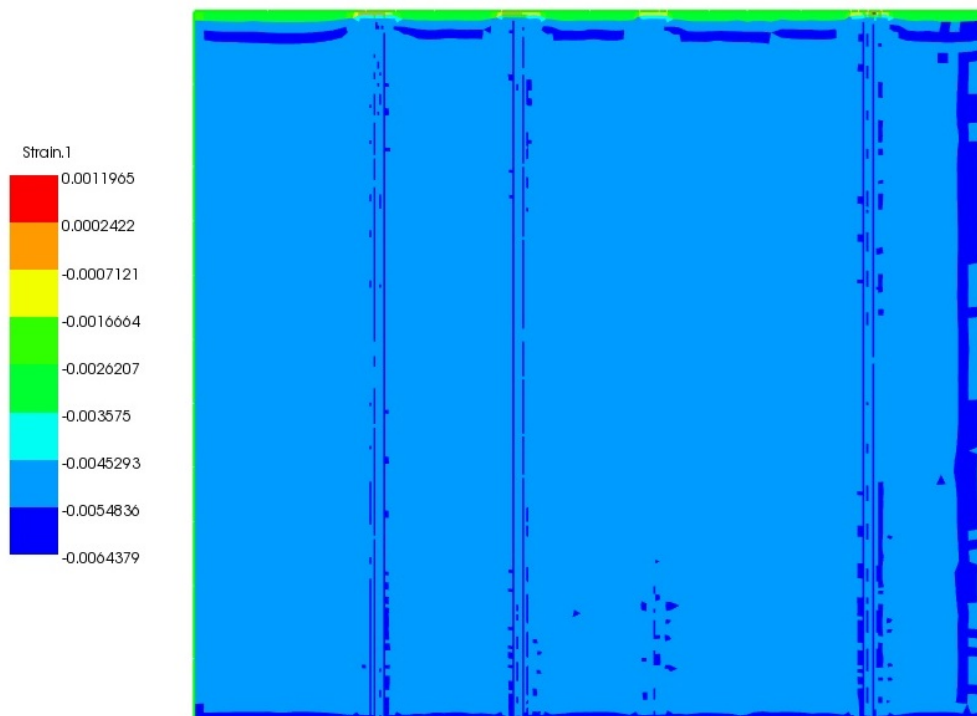


Figure 5.7: ϵ_{12} strain distribution in ply 24.

5.4.2 Tool side (ply 1: -45° fibre direction)

The in-plane strains ϵ_1 , ϵ_2 and ϵ_{12} distributions on ply 1 are shown in Figures 5.8, 5.9 and 5.10 respectively. The strains in the fibre direction (ϵ_1) are very low at the centre of the panel and increase compressively towards the edges. This behaviour is believed to be caused by friction from the tool which restrict cure-induced shrinkage of this ply. The other reason is that fibres have a high compressive stiffness, which also prevents ply shrinkage in the fibre direction.

The transverse (ϵ_2) and the shear (ϵ_{12}) strain distributions are evenly distributed within the ply. Although, minor strain concentrations can be observed at the drop-off stations, the fibres embedded in this ply will experience uniform deformations with little to no chance of buckling.

Figure 5.8: ε_1 strain distribution in ply 1.Figure 5.9: ε_2 strain distribution in ply 1.

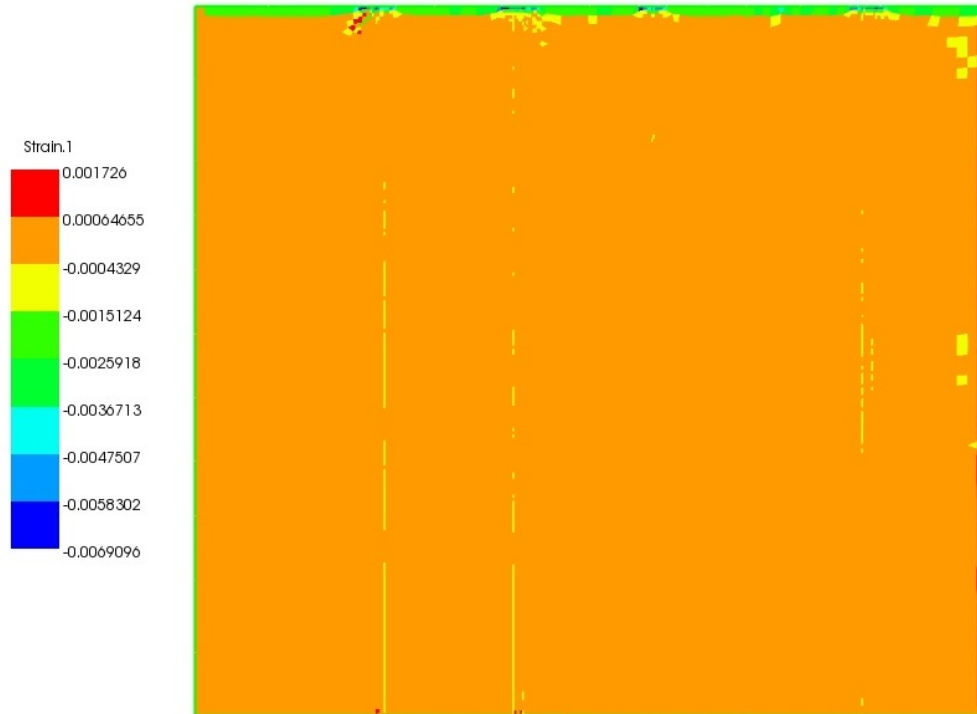


Figure 5.10: ε_{12} strain distribution in ply 1.

5.5 Fibre Waviness Predictions

Based in the strain distribution discussed in Section 5.4, the transverse and the shear strains proved to be good indicators of fibre waviness defects. Ply 24 showed signs of fibre waviness defects at drop-off stations 1, 2 and 4, while no sign was observe in ply 1. To study this even further, the in-plane strains were analysed along the length of the panel on the lines located at the panel-centre and 50 mm from both edges as shown in Figure 5.11. Again, the two plies on the outer surfaces are analysed, i.e. ply 1 and ply 24. Although the fibres on these plies are oriented at an angle of -45° , this will help understand how fibres experience strains within the plies.

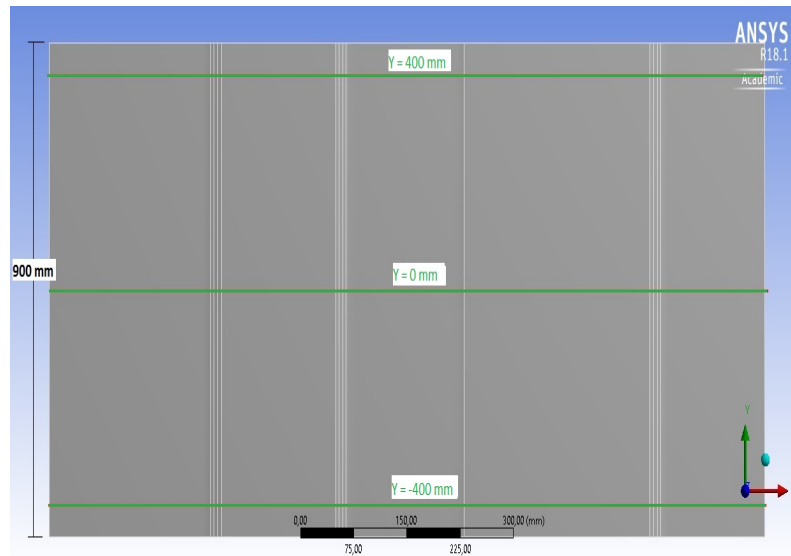


Figure 5.11: Locations along the panel analysed for fibre waviness defects.

On the tool side (ply 1), the variations in fibre direction strains (ϵ_1) were not evenly distributed along the width of the panel but they were following similar trends along the length of the panel at all locations, see Figure 5.12. The entire panel was in compression with maximum strains experienced at the thickest section (Section B). Since fibres have low bending stiffness, the alternation of transverse strains (between high and low values) and the change in shear strain directions (between positive and negative values) at the drop-off stations 1, 2 and 4 will result in the buckling of fibres, thus forming fibre waviness defects at these locations. Furthermore, the fibre waviness defects will occur over the entire width of the panel as there are no variations in the transverse and shear strains along the width.

On the tool side (ply 1), the variations of the strains in the fibre direction were almost even on all locations with the lowest strains occurring at the centre of the panel where they are sometimes in tension, see Figure 5.13. Putting the fibres in tension will increase their bending stiffness which will make it harder for them to buckle. Also, the transverse and shear strains are evenly distributed along both the width and the length of the panel indicating even deformations of fibres without buckling.

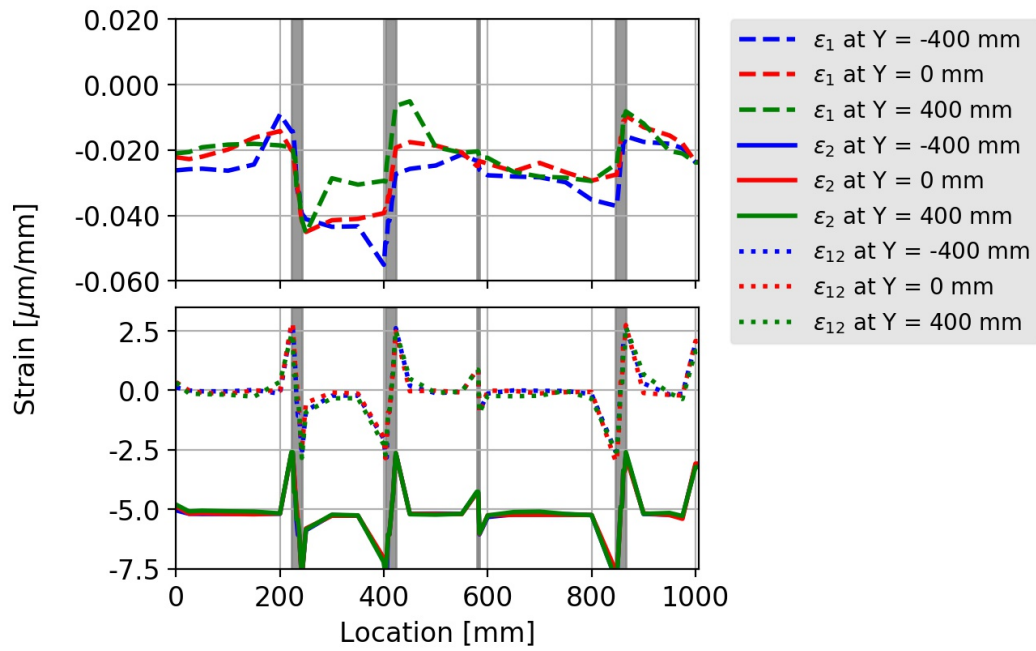


Figure 5.12: Strain variations in ply 24 along the length of the panel at various locations.

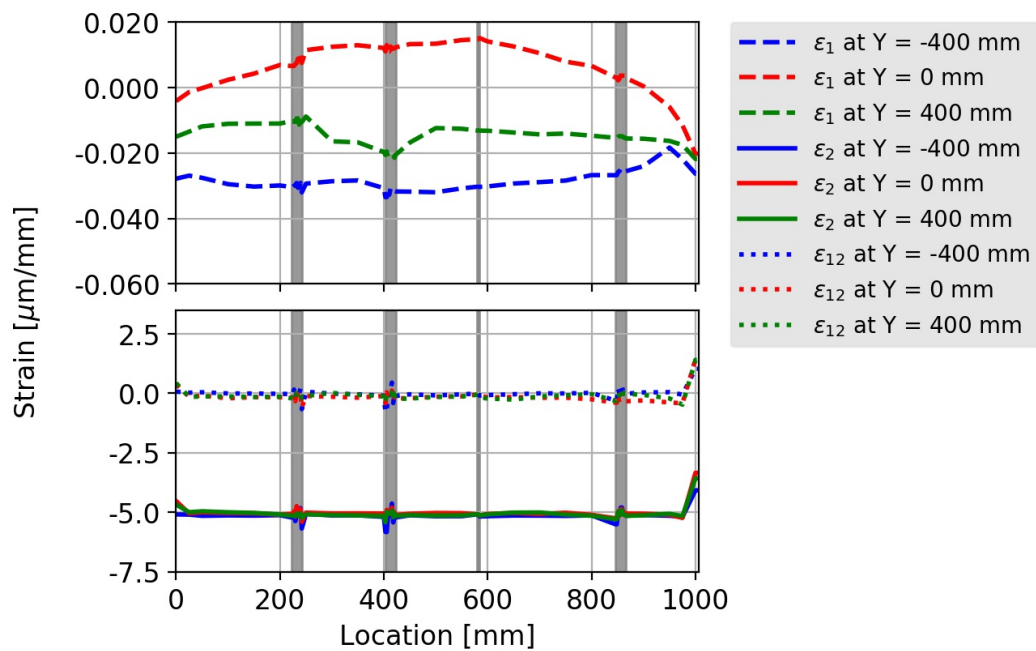


Figure 5.13: Strain variations in ply 1 along the length of the panel at various locations.

5.6 Experimental Validation

As mentioned in Chapter 3, the composite panel was designed by an aerospace partner company as the spar-component of an aeroplane's tail wing. This company has been manufacturing the panel for some time, following the same curing conditions discussed in Chapter 4. During the manufacturing, fibre waviness defects were observed on the top surface of the panel and at the drop-off stations 1 and 2 as shown in Figure 5.14.

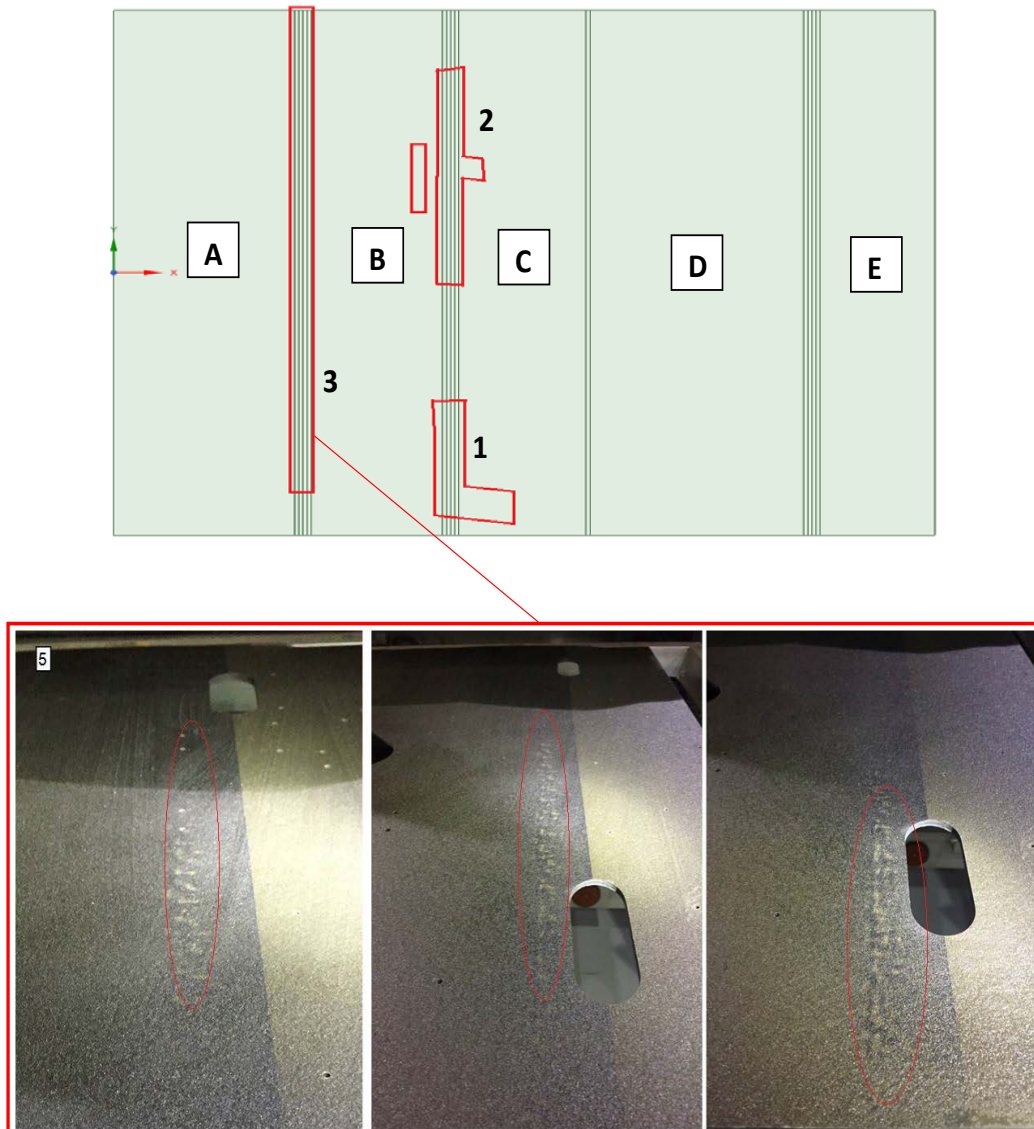


Figure 5.14: Locations of fibre waviness defects observed practically after manufacturing the composite panel.

The practical observations showed agreement with the predictions from the simulations, however, the numerical simulations also predicted fibre waviness at drop-off station 4. This difference in practical observations and numerical prediction is because, during the manufacturing of the panel, other features were added to the panel which were not considered in this study. Some of these extra features are stiffeners which were added at drop-off stations 3 and 4, and parallel to the drop-off. These stiffeners tend to work as stress intensifiers on the panel, which restrict the contraction of plies during curing and enforcing those plies to be in tension. When fibres are in tension, their bending stiffness increase and they will not buckle.

According to Qu (2010), the size of fibre buckling deformations is controlled by both compressive loading and transverse viscous forces. Therefore, since section B experiences higher compressive strains than both sections D and E, fibre buckling will be more intense at the drop-off stations 1 and 2, thus more practically visible. The practical fibre waviness defects at locations 1 and 2 of the drop-off station number 2 are shown in Figures 5.15 and 5.16 respectively.

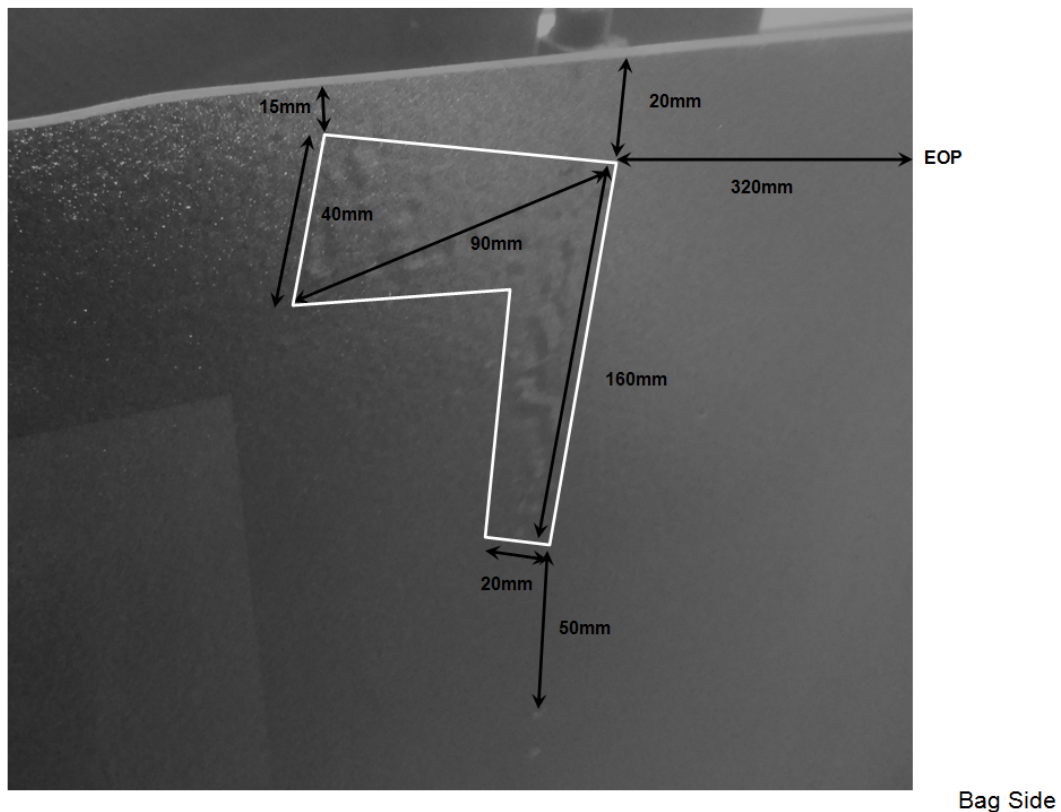


Figure 5.15: Fibre waviness defects at location 1 of drop-off station 2.



Figure 5.16: Fibre waviness defects at location 2 of drop-off station 2.

5.7 Conclusion

The results of the cure simulations were presented and discussed. The results showed that the composite panel goes through material evolutions during the curing process, which were validated by various observations from literature. During this process of material evolutions, stresses and strains develop in the composite panel, also validated using observations from literature. These stresses and strains cause fibre waviness defects due to buckling of fibres when the resin is in the liquid phase with low viscosity. Fibre waviness defects were predicted to occur at drop-off stations 1, 2 and 4 on the bag side (ply 24) of the panel. These fibre waviness defects occur when fibres are in compression and also experiencing alternating transverse (between high and low) strains and changing shear strain directions (alternate between positive and negative values) causing fibres to buckle. The predictions agreed with practical observations only at drop-off stations 1 and 2. This was because extra features (not considered in the study), were added at drop-off stations 3 and 4 of the panel during manufacturing, that prevented fibres from buckling. Following a similar analysis on the internal plies, only plies 23 and 24 showed signs of fibre waviness defects.

Chapter 6

Parametric Study

The mechanism behind the fibre waviness defect formation was identified in Chapter 5 stating: when fibres are in compression, they have a reduced bending stiffness, therefore the alternation of transverse strains (i.e. between high and low values) and in-plane shear strains (i.e. between negative and positive values) causes them to buckle, forming fibre waviness defects. This chapter investigates the effect of various parameters on the formation of fibre waviness defects using the identified mechanism. Three groups of parameters were investigated, i.e. ply drop-off, the cure cycle and material properties effects. The analyses were done by studying the strains induced when resin viscosity is the lowest (remember, this is when fibres are easy to buckle), and these strains are analysed along the length of the panel at a line passing through the centre, for both plies on the outer surfaces, i.e. ply 1 on the tool side and ply 24 on the bag side. This is because it was shown in Chapter 5 that both transverse and shear strains do not vary along the width of the panel and they are also shown to be good indicators of fibre waviness defects.

6.1 Ply Drop-off Effects

Fibre waviness occurred at the drop-off stations. The number of plies dropped at a single drop-off station has already been shown to have an effect on the formation of fibre waviness defects. To recap, the numerical predictions showed that fibre waviness defects occur at drop-off stations 1, 2 and 4 which all had four plies dropped and not at drop-off station 3 where only one ply has been dropped. Dropping many plies at a single station is necessary to achieve a high degree of tapering within a small span (Mukherjee and Varughese, 2001). Therefore, the ply drop-off effects focused only on two parameters. The first parameter is the drop-off sequence which defines the order in which the plies are dropped at a station with more than one ply dropped. The second parameter is the stagger length, which defines the distance between two successive ply drop-offs at a single station.

6.1.1 Drop-off sequence

Two drop-off sequences as shown in Figure 6.1 were studied. The first sequence is the original (design) drop-off sequence applied to the panel where bottom plies are dropped first when moving from the thick to the thin section of the drop-off station. The second sequence is the reverse of the original drop-off sequence where top plies are dropped first instead.

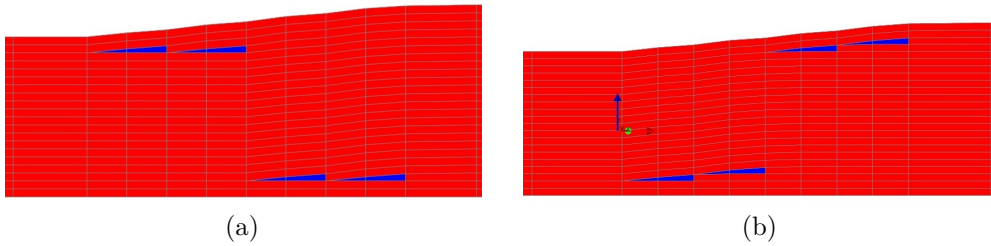


Figure 6.1: Drop-off sequence, (a) original order, (b) reversed order.

The change in the drop-off sequence had no significant effect on the fibre direction strains (ε_1) in both plies, see Figure 6.2, and in both transverse (ε_2) and shear (ε_{12}) strains in ply 24, see Figures 6.3 and 6.4 respectively. The only effect was in ply 1 (tool side), where both transverse (ε_2) and shear (ε_{12}) strain concentrations at the drop-off stations got reduced slightly by reversing the drop-off sequence. Even though, the change in drop-off sequence has no effect on the formation of fibre waviness defects since it occurs on the bag side (ply 24) where all strains are not affected.

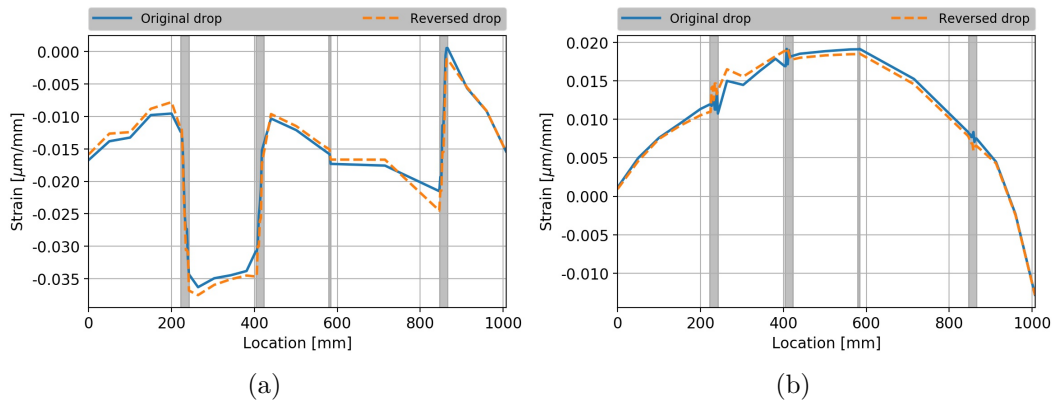


Figure 6.2: Effect of drop-off sequence on ε_1 , (a) ply 24 (bag side), (b) ply 1 (tool side).

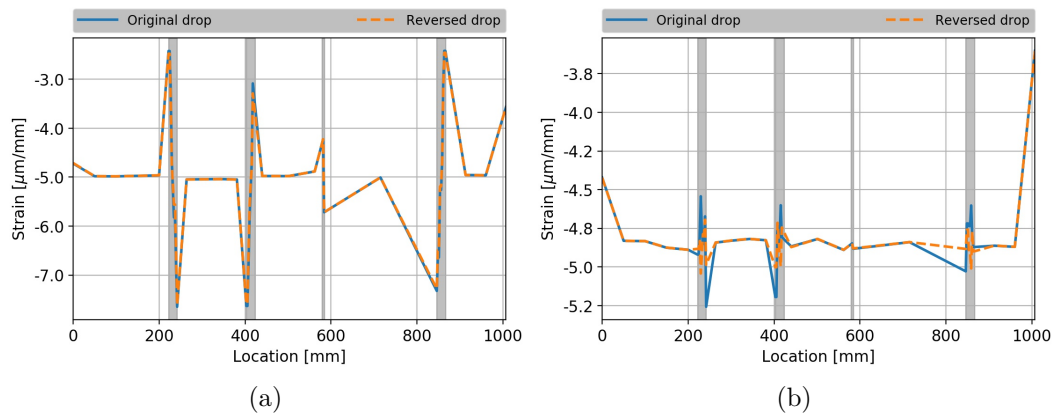


Figure 6.3: Effect of drop-off sequence on ε_2 , (a) ply 24 (bag side), (b) ply 1 (tool side).

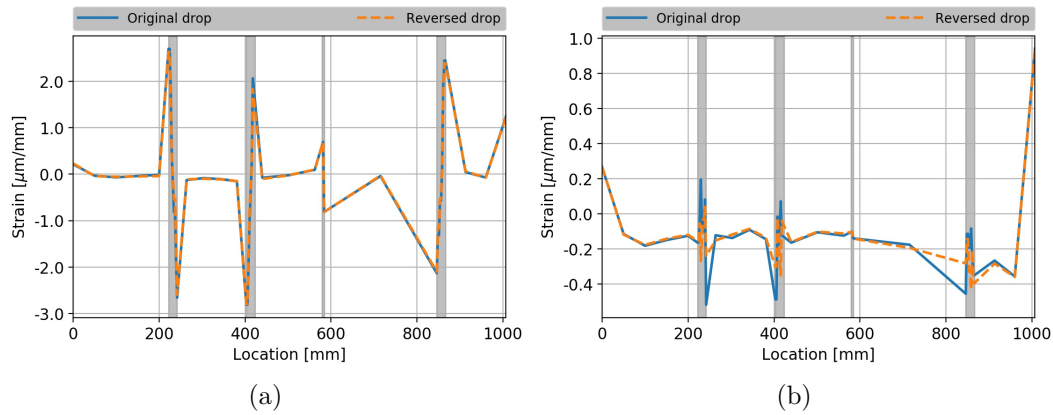


Figure 6.4: Effect of drop-off sequence on ε_{12} , (a) ply 24 (bag side), (b) ply 1 (tool side).

6.1.2 Stagger length

Stagger length was chosen as one of the parameters because it is believed to have an effect on the stress concentrations induced by ply drop-offs (Mukherjee and Varughese, 2001). In this study, the stagger length was increased at intervals of 5 mm from the design stagger length of 5 mm.

Like changing the drop-off sequence, changing the stagger length had no significant effect on the fibre direction strains (ε_1) in both plies. However, both transverse (ε_2) and shear (ε_{12}) strains were affected by the change in stagger length, see Figures 6.6 and 6.7 respectively. Increasing the stagger length reduced the alternating peaks of both transverse and shear strains at the drop-off

stations in both plies. This indicates and agrees with the effect stagger length have on strain concentrations as stated by Mukherjee and Varughese (2001).

The reduction in alternation peaks of transverse and shear strains indicates that fibres will experience almost even deformations in the transverse direction, thus reducing their buckling intensity and so on the fibre waviness defects. Although, the use of longer stagger lengths is not always recommended in practice as they might create an irregular taper surface (Mukherjee and Varughese, 2001).

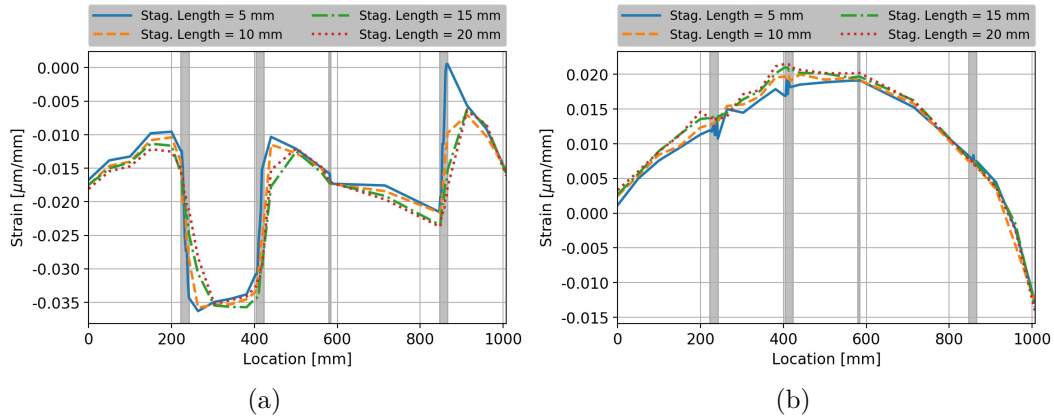


Figure 6.5: Effect of drop-off stagger length on ϵ_1 , (a) ply 24 (bag side), (b) ply 1 (tool side).

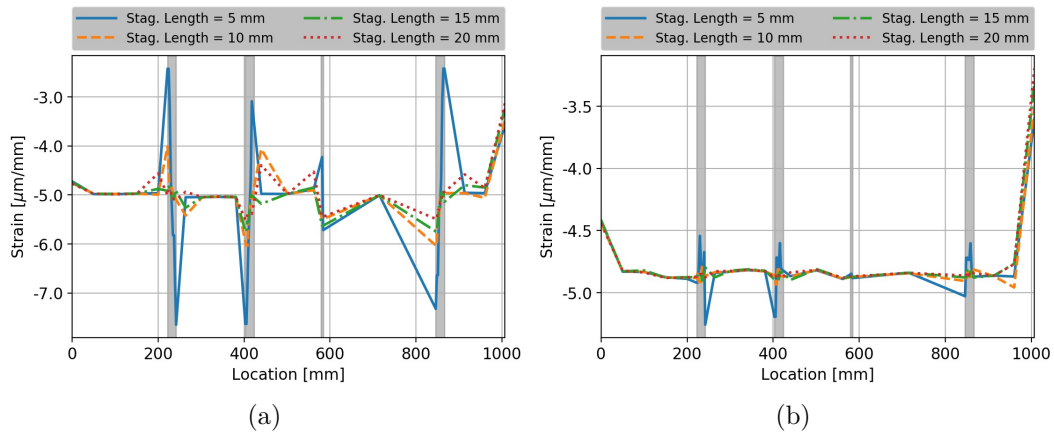


Figure 6.6: Effect of drop-off stagger length on ϵ_2 , (a) ply 24 (bag side), (b) ply 1 (tool side).

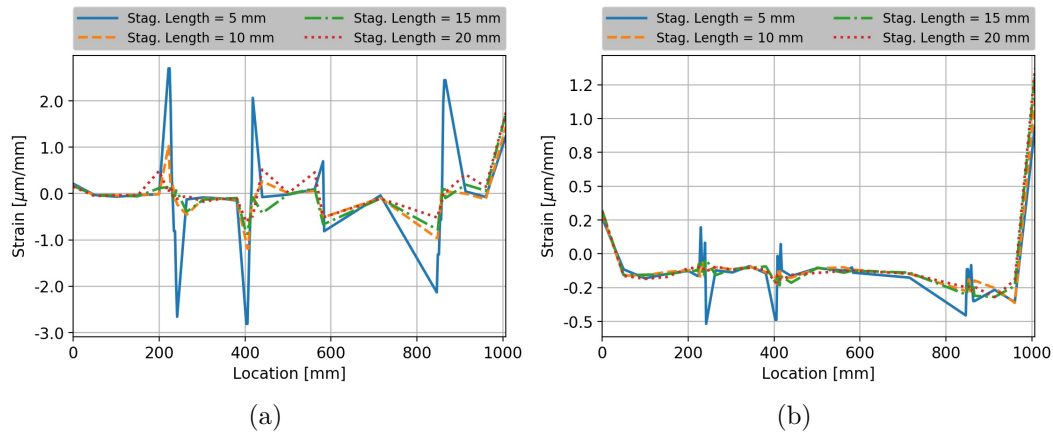


Figure 6.7: Effect of drop-off stagger length on ε_{12} , (a) ply 24 (bag side), (b) ply 1 (tool side).

6.2 Cure Cycle Effects

As mentioned in Section 5.1, the cure cycle has an effect on the material evolutions of the composite panel, thus, on the stresses and strains. The cure cycle is governed by many parameters. For example, Kugler and Moon (2002) identified cure cycle parameters such as the cooling-rate, cure pressure and the cure temperature as the most significant in the formation of fibre waviness in a thermoplastic composite. The difference between thermoplastic composite and the thermosetting composite is that thermosetting composite undergoes chemical reactions during the curing process while thermoplastic composites consolidate through softening.

In this section, only three cure process parameters, i.e the cure-pressure, pressure ramp-up rate and the heat-up rate were investigated for their influence on the formation of fibre waviness defects. These parameters were first analysed on the effects they have on the development of cure-induced in-plane strains, followed by the effects on strain distributions within the panel. The effect on strain development was analysed at points located at the centre of drop-off station 1 for both outer surface plies.

6.2.1 Cure-pressure

It is believed that, under the action of pressure, shear strains are generated at the tool-part interface (Mulle *et al.*, 2009; Joven, 2013). This is the reason the cure-pressure was chosen as one of the cure cycle parameters. In this study, the pressure was reduced at intervals of 2 bar from the design cure pressure of 10 bar.

The change in cure pressure had no significant effect on the development of fibre direction strains (ε_1) in both plies, see Figure 6.8. Reducing the cure pressure increased (compressively) the transverse strains that develop on the bag side (ply 24) of the panel but no effect on the tool side (ply 1), see Figure 6.9. The development of shear strains was affected by the change in cure pressure in both plies, see Figure 6.10. Reducing the cure pressure reduced the shear strains that develop at the drop-off station.

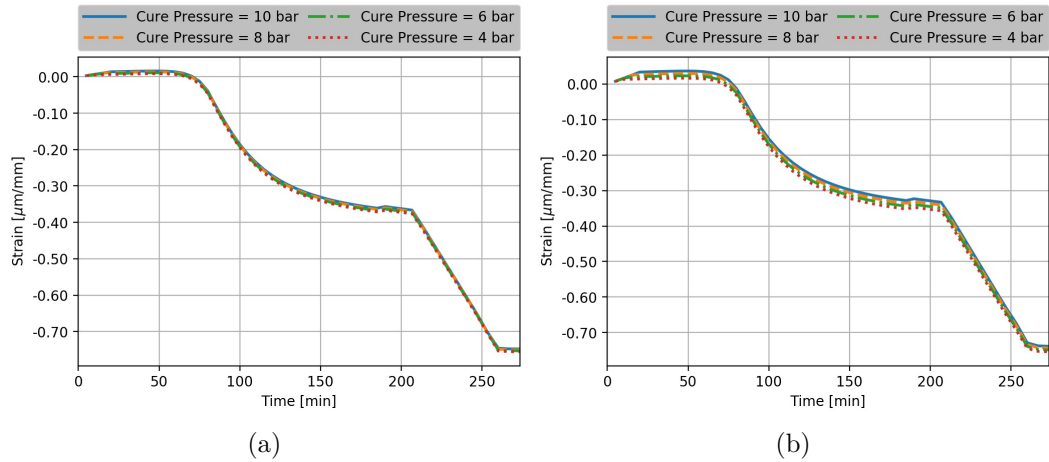


Figure 6.8: Effect of cure pressure on the development of ε_1 , (a) ply 24 (bag side), (b) ply 1 (tool side).

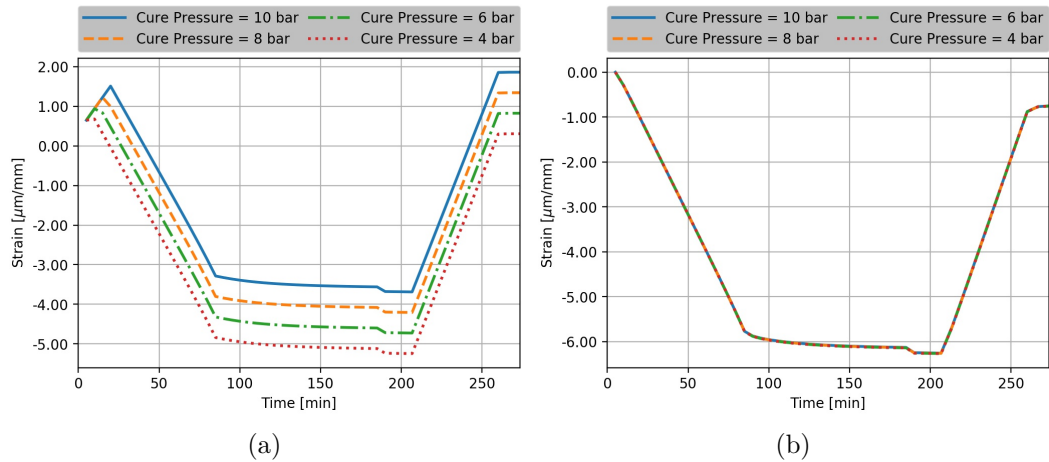


Figure 6.9: Effect of cure pressure on the development of ε_2 , (a) ply 24 (bag side), (b) ply 1 (tool side).

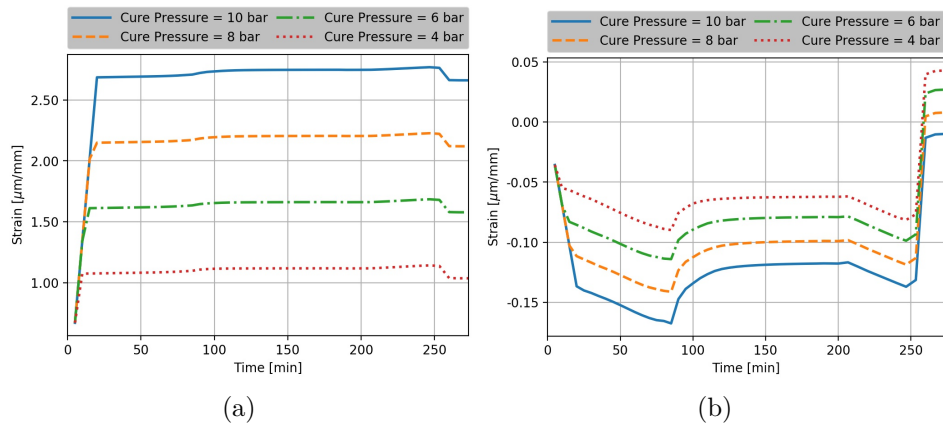


Figure 6.10: Effect of cure pressure on the development of ϵ_{12} , (a) ply 24 (bag side), (b) ply 1 (tool side).

The change in cure-pressure had an effect on the distributions of all the in-plane strains ϵ_1 , ϵ_2 and ϵ_{12} within the panel. The fibre direction strains (ϵ_1) were affected differently in both plies, see Figure 6.11. On the bag side (ply 24), reducing the cure pressure resulted in the alternation of fibre direction strains among the panel sections. The strains on the thickest section (Section B) of the panel reduces while it increases on the other sections. Therefore, it can be said that a reduction in cure pressure reduces the fibre direction strain gradients at the drop-off stations. On the tool side (ply 1), reducing the cure pressure reduces the fibre direction strains over the entire length of the panel. Although it must be noted that, the reduction of fibre direction strains is when in tension, meaning they are increasing compressively. This indicates that the fibres on the tool side can become vulnerable to buckling at low cure pressures.

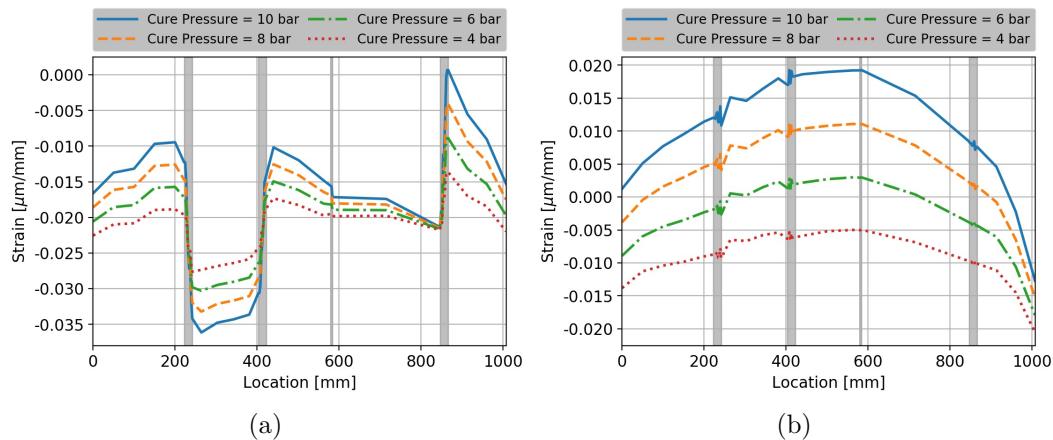


Figure 6.11: Effect of cure pressure on ϵ_1 , (a) ply 24 (bag side), (b) ply 1 (tool side).

Both transverse and shear strains, see Figures 6.12 and 6.13 respectively, were affected in the same way by the change in cure pressure in both plies. Their alternation peak values reduced with the reduction in cure pressure. This indicates that, at low pressures, the transverse and the shear strain distributions are low and evenly distributed within the panel reducing the possibility of the buckling of fibres. However, care must be taken that the cure pressure is not reduced to the point where fibre direction strains on the tool side (ply 1) increase compressively beyond the critical fibre buckling compressive strain. Furthermore, the cure-pressure helps reduce the void content in the panel during the curing process, which has a huge effect on mechanical properties, i.e. Koushyar (2011) has stated that many studies have confirmed that reducing the cure pressure will increase the porosity, thus, reducing mechanical properties.

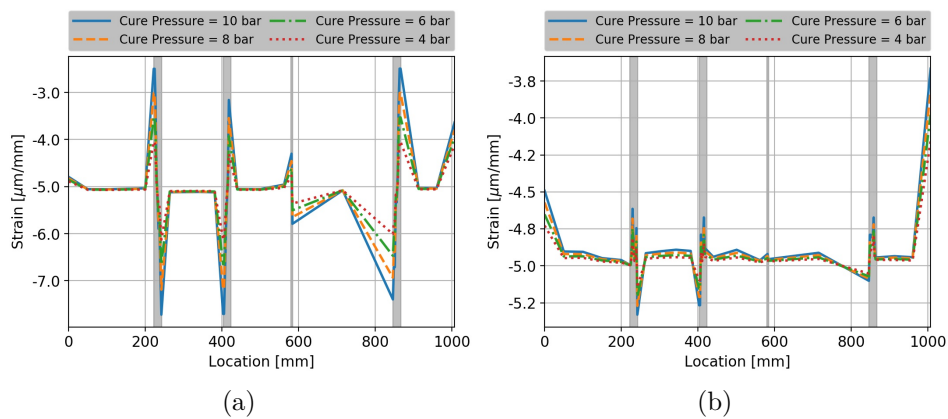


Figure 6.12: Effect of cure pressure on ε_2 , (a) ply 24 (bag side), (b) ply 1 (tool side).

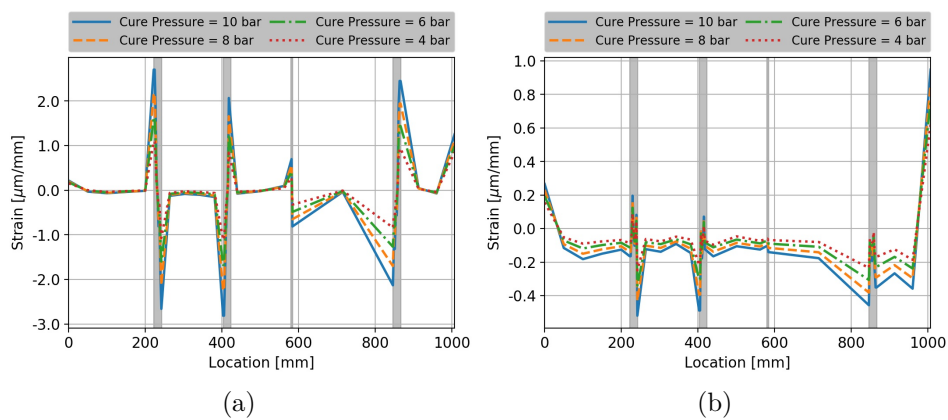


Figure 6.13: Effect of cure pressure on ε_{12} , (a) ply 24 (bag side), (b) ply 1 (tool side).

6.2.2 Pressure ramp-up rate

Like the cure pressure, the pressure ramp-up rate was chosen as one of the investigated parameters because of the shear strains that are generated at the tool-part interface due to the action of pressure during the curing process. In this study, the pressure ramp-up rate was reduced at ratios of 1:2 from the design pressure ramp-up rate of 0.1 bar/min. The change in pressure ramp-up rate had no significant effect on the development of fibre direction strains (ε_1) in both plies, see Figure 6.14, also on the development of transverse strains (ε_2) in ply 1 only, see Figure 6.15. However, the rate at which transverse strains in ply 24 develop increases with the reduction in pressure ramp-up rate, so is the rate at which shear strains (ε_{12}) develop in both plies as shown in Figure 6.16. For example, at a high-pressure ramp-up rate, these strains raised quickly and slowly for a low-pressure ramp-up rate.

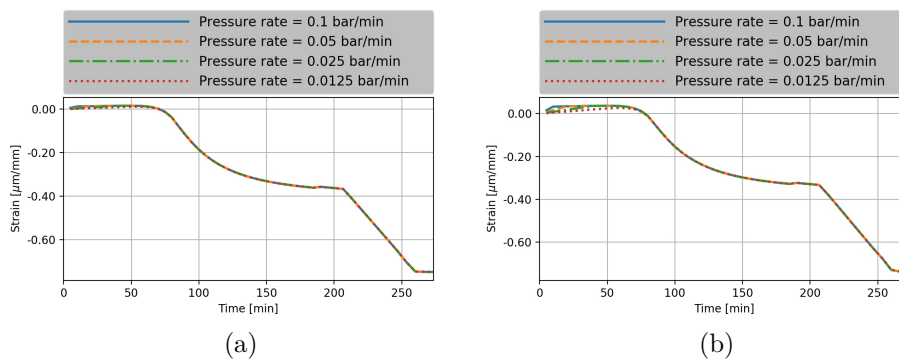


Figure 6.14: Effect of pressure ramp-up rate on the development of ε_1 , (a) ply 24 (bag side), (b) ply 1 (tool side).

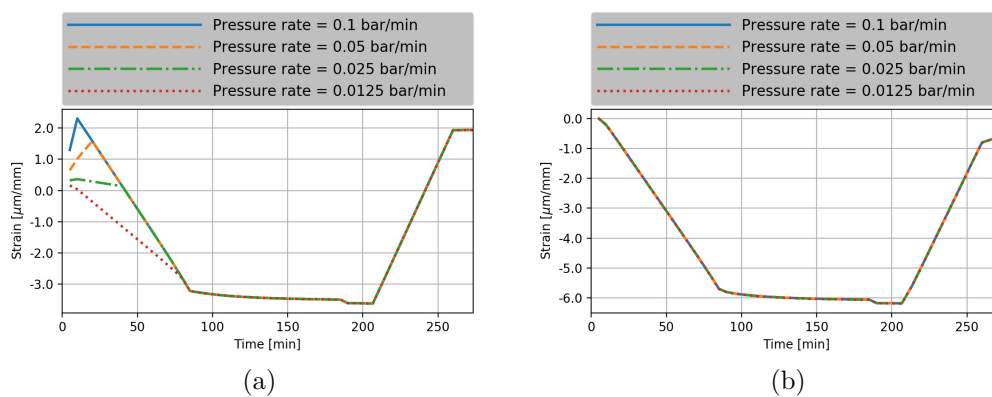


Figure 6.15: Effect of pressure ramp-up rate on the development of ε_2 , (a) ply 24 (bag side), (b) ply 1 (tool side).

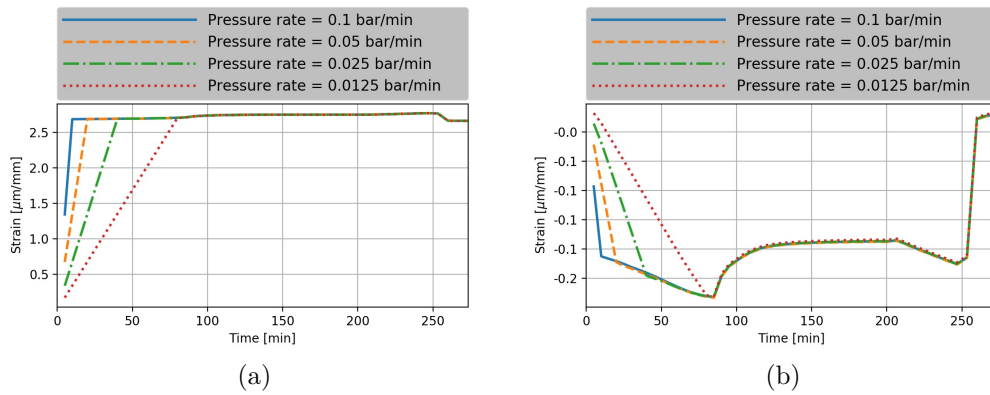


Figure 6.16: Effect of pressure ramp-up rate on the development of ϵ_{12} , (a) ply 24 (bag side), (b) ply 1 (tool side).

The change in pressure ramp-up rate had no effect on all the in-plane strains ϵ_1 , ϵ_2 and ϵ_{12} distributions within the panel, see Figures 6.17, 6.18 and 6.19 respectively. However, only minor reduction in fibre direction strains were observed in ply 1 for the lowest value of pressure ramp-up rate. This behaviour is because, at low-pressure ramp-up rates, strains develop at a slow rate. However, this effect was not clearly observed during the analysis of effects on the development of strains. Regardless, changing the pressure ramp-up rate does not affect the formation of fibre waviness defects.

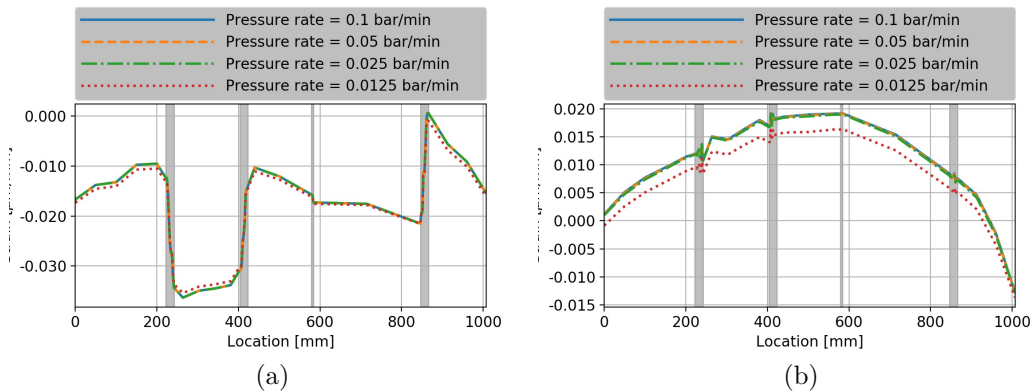


Figure 6.17: Effect of pressure ramp-up rate on ϵ_1 , (a) ply 24 (bag side), (b) ply 1 (tool side).

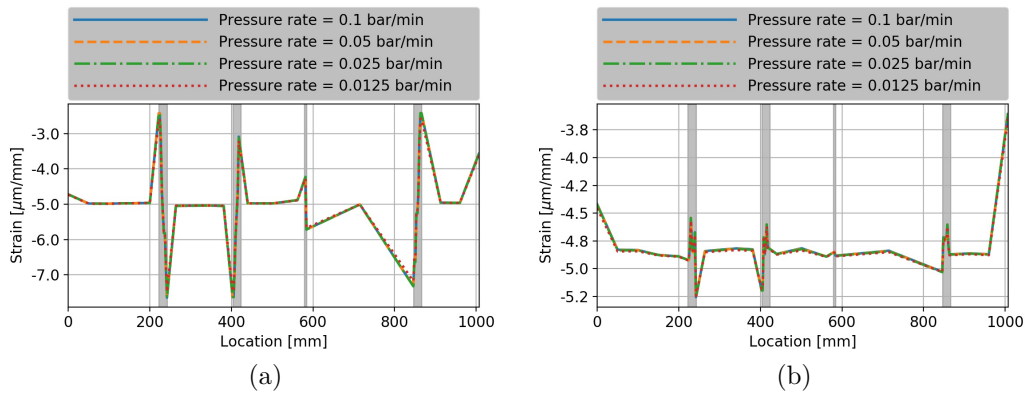


Figure 6.18: Effect of pressure ramp-up rate on ε_2 , (a) ply 24 (bag side), (b) ply 1 (tool side).

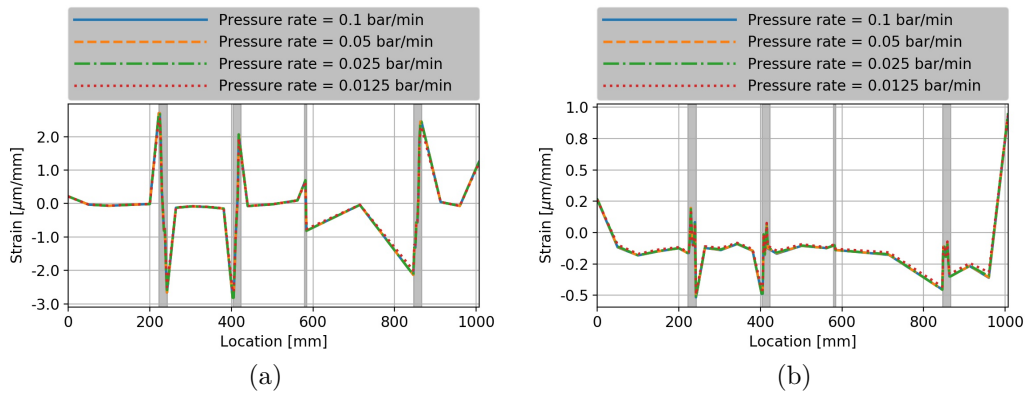


Figure 6.19: Effect of pressure ramp-up rate on ε_{12} , (a) ply 24 (bag side), (b) ply 1 (tool side).

6.2.3 Heat-up rate

Temperature is the main driver of chemical reactions during the curing process. Since fibre waviness occurs at a point of low viscosity which is before gelation, the rate at which temperature is raised (heat-up rate) to the cure temperature was chosen as one of the cure cycle parameters. The heat-up rate was increased at intervals of $0.5\text{ }^{\circ}\text{C}/\text{min}$ from the design heat-up rate of $2\text{ }^{\circ}\text{C}/\text{min}$. Clearly, the heat-up rate has an effect on the material evolutions, see Figure 6.20. Increasing the heat-up rate reduces (linearly) the time it takes the resin viscosity to reach a minimum value and the times of both gelation and vitrification.

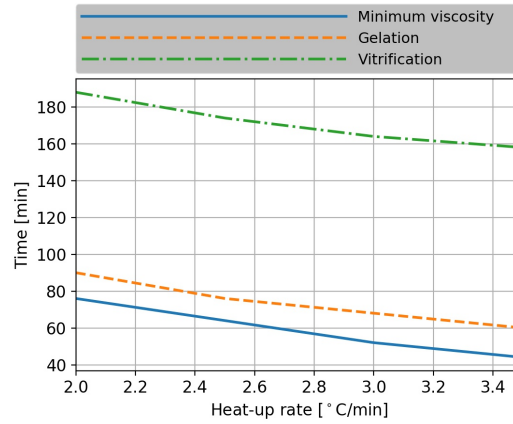


Figure 6.20: Effect of heat-up rate on the material transition times.

The change in heat-up rate had no effect on the early development of fibre direction strains in both plies, rather had an effect on their progression between the point of minimum viscosity and vitrification, see Figure 6.21. As the curing process begins in the heat-up phase, the resin melts and expand. This resin behaviour, together with the thermal expansion of fibres, results in tensile strains dominating in the early stages of the curing process. Once the resin viscosity reaches a minimum value and starts increasing, the cure reaction rate becomes higher, thus resulting in the increase of chemical shrinkages. This chemical shrinkage becomes dominant as the curing continues, thus resulting in compressive strains after the point of minimum viscosity. Therefore, since the time of the point of minimum viscosity decreases with the increasing heat-up rate, causing the chemical shrinkages to occur early, thus causing early development of compressive strains.

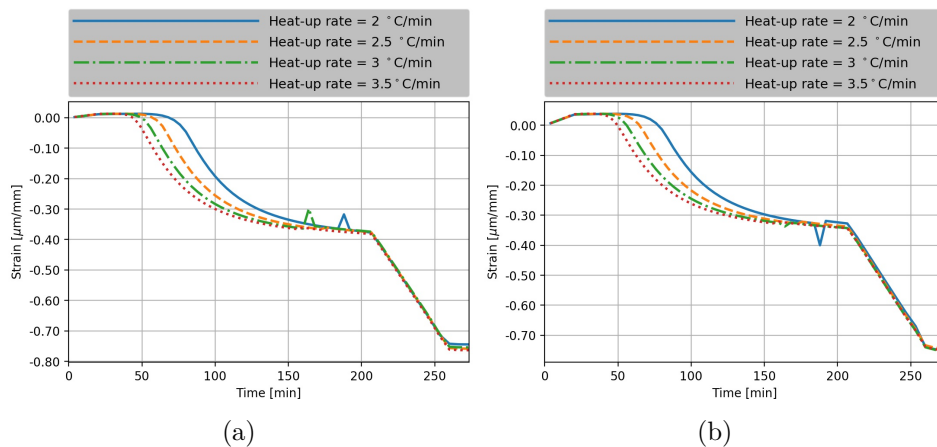


Figure 6.21: Effect of heat-up rate on the development of ϵ_1 , (a) ply 24 (bag side), (b) ply 1 (tool side).

Like the fibre direction strains, increasing the heat-up rate results in the early development of compressive strains in the transverse direction in both plies, see Figure 6.22. This behaviour is because the ply properties in the transverse direction are dominated by the resin. As the resin melts and its viscosity decreases, cure-reactions also increase though at a slow rate until the point of minimum viscosity. As this happens, the chemical shrinkage strains develop which are dominant in the transverse direction. Once the cure temperature has been reached and all thermal expansion strains (which are in tension during the heat-up phase) have been eliminated, these chemical shrinkage strains reach a peak value.

Therefore, changing the heat-up rate also changes the times at which chemical shrinkage strains reach a peak value. The development of the shear strains (ε_{12}) on ply 24 (bag side) was not affected by the heat up rate, however, on ply 1 (tool side) the effect was observed on the peak values, although the effect relationship was not clear, see Figure 6.23.

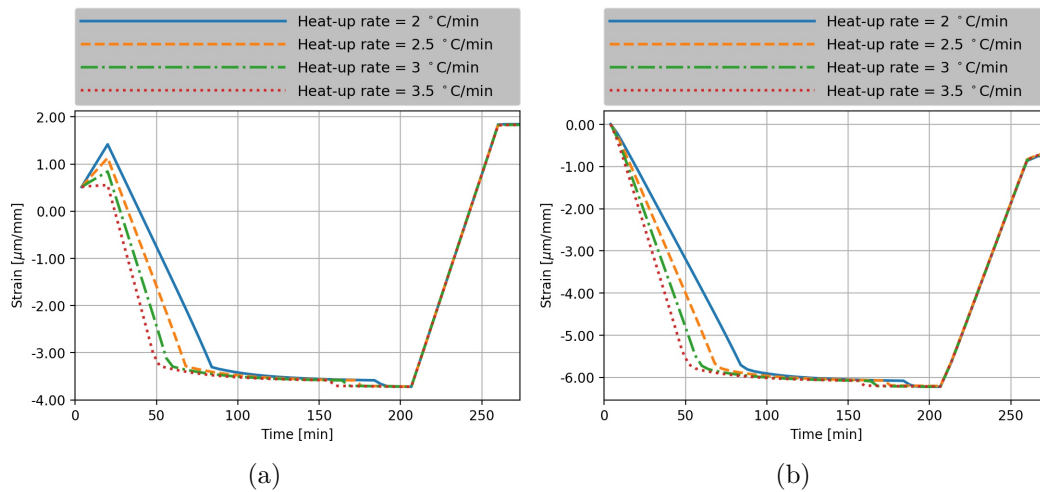


Figure 6.22: Effect of heat-up rate on the development of ε_2 , (a) ply 24 (bag side), (b) ply 1 (tool side).

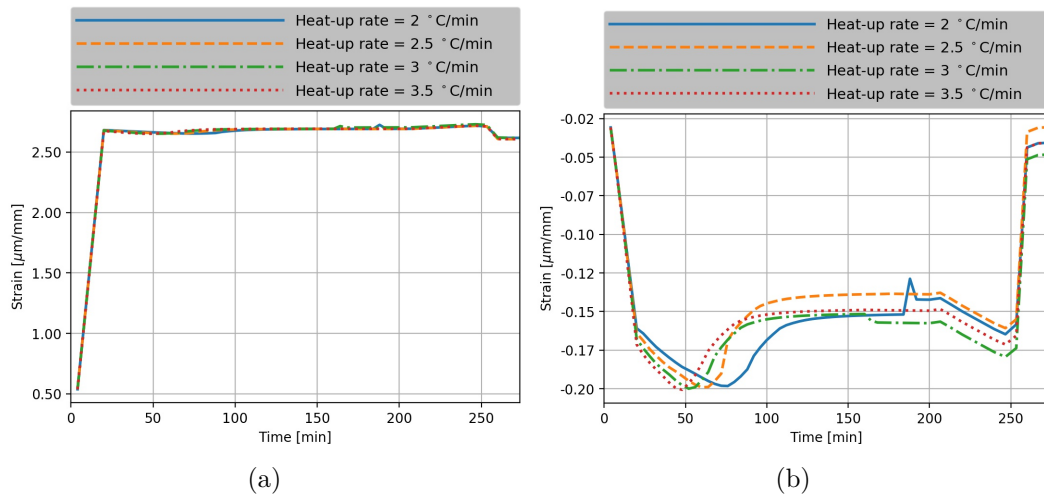


Figure 6.23: Effect of heat-up rate on the development of ϵ_{12} , (a) ply 24 (bag side), (b) ply 1 (tool side).

The change in heat up rate had an effect on the values of both fibre direction (ϵ_1) and transverse (ϵ_2) strains in both plies as shown in Figures 6.24 and 6.25 respectively, however, did not affect how they are distributed within the panel. The values (intensity) of these strains were varied without a clear relationship to the heat-up rate changes. Even so, the alternating differences of the transverse strains were affected. The shear strains in both plies were also not affected by the changes in the heat-up rate, see Figure 6.26. Therefore, the change in heat-up rate does not have an effect on fibre waviness formation.

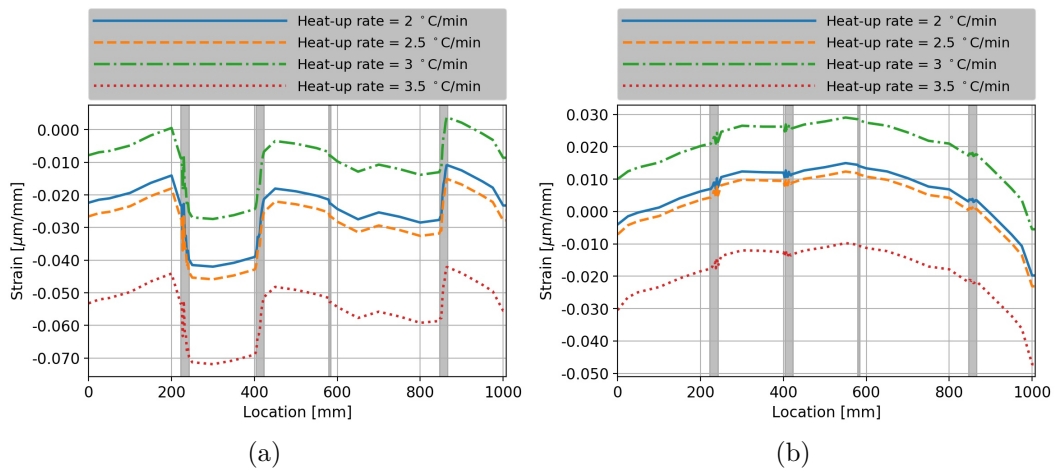


Figure 6.24: Effect of heat-up rate on ϵ_1 , (a) ply 24 (bag side), (b) ply 1 (tool side).

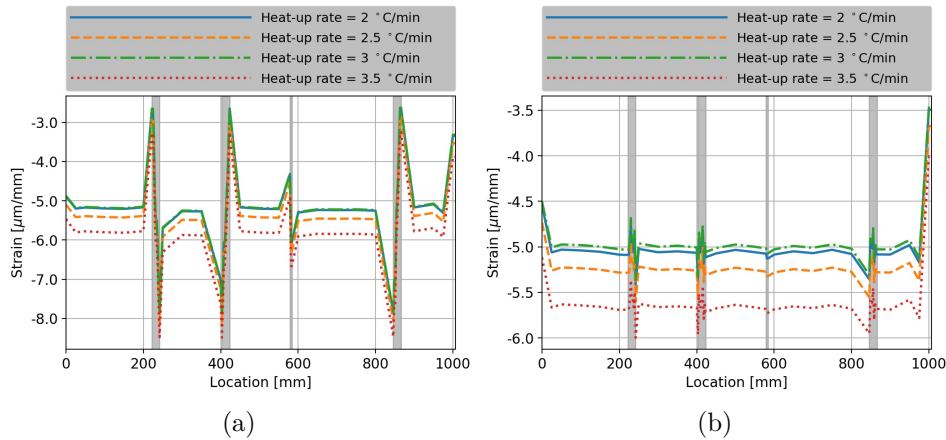


Figure 6.25: Effect of heat-up rate on ϵ_2 , (a) ply 24 (bag side), (b) ply 1 (tool side).

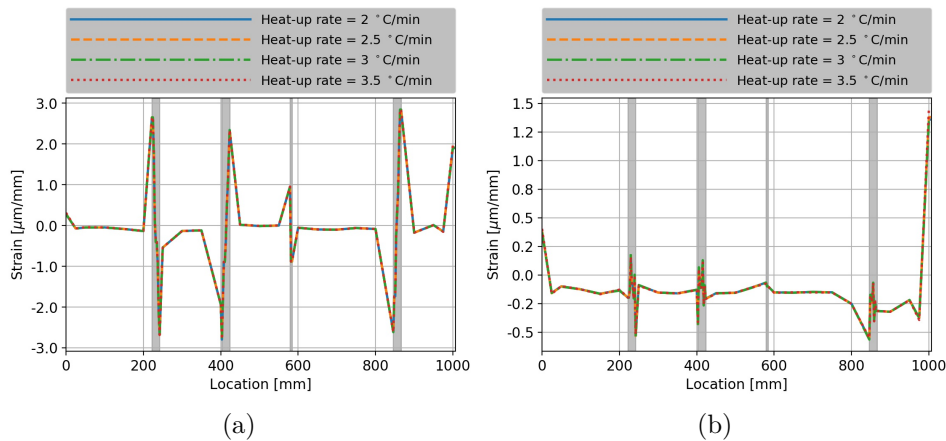


Figure 6.26: Effect of heat-up rate on ϵ_{12} , (a) ply 24 (bag side), (b) ply 1 (tool side).

6.3 Tool Material

The last parameter investigated was the tool material. Two materials were chosen in this study, i.e. invar and aluminium. Invar is the material used in the design and it is noted for its low thermal expansions, while aluminium is the most common material used in tools for composite manufacturing. The friction coefficient between the IM7/977-2 composite and aluminium tool is unknown, therefore the same friction coefficient of 0.07 for invar and the IM7/977-2 composite is used.

Changing the tool material from the invar to aluminium had no effect on the development of fibre direction and transverse strains in both plies, see Figures 6.27 and 6.28 respectively. However, the aluminium tool slightly increased the peak values of the shear strains in both plies, see Figure 6.29. This strains analysis was performed at a point located at the centre of the thickest section (Section B) and width-centre of the panel.

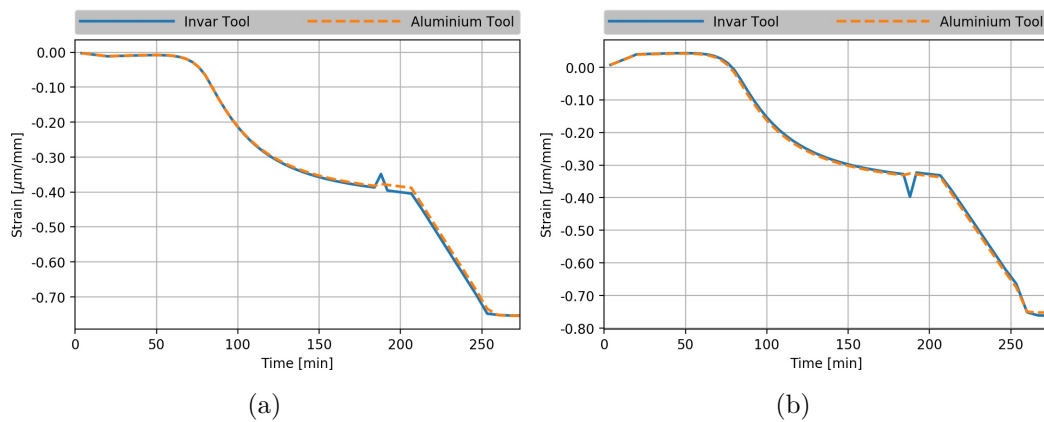


Figure 6.27: Effect of tool material on the development of ϵ_1 , (a) ply 24 (bag side), (b) ply 1 (tool side).

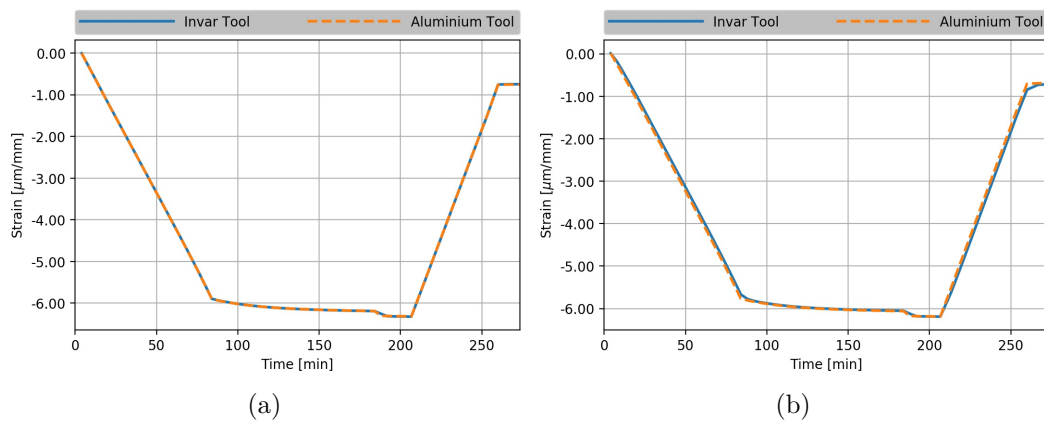


Figure 6.28: Effect of tool material on the development of ϵ_2 , (a) ply 24 (bag side), (b) ply 1 (tool side).

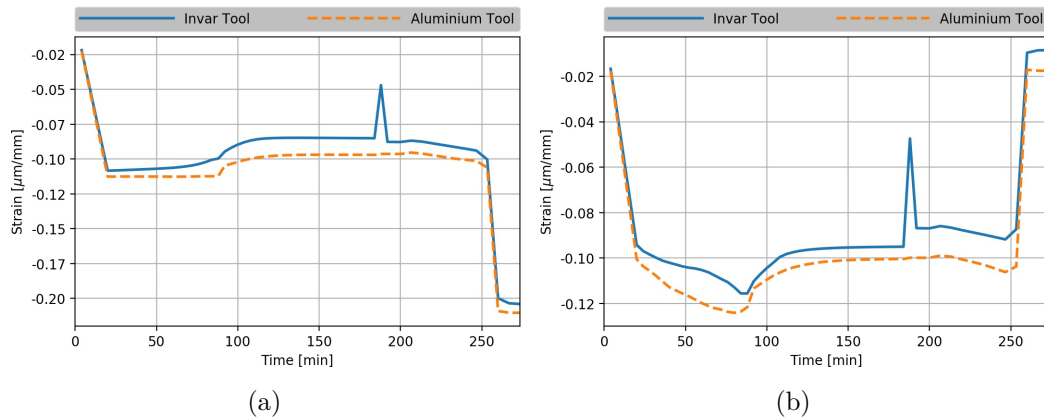


Figure 6.29: Effect of tool material on the development of ε_{12} , (a) ply 24 (bag side), (b) ply 1 (tool side).

Changing the tool material had no effect on all the in-plane strain distributions in ply 24 (bag side), rather had effects on the strains in ply 1 (tool side). Figures 6.30, 6.31 and 6.32 respectively shows the ε_1 , ε_2 and ε_{12} strain distributions along the length of the panel at its width-centre in both plies. Using the aluminium tool reduced the fibre direction strains (ε_1) from tension into compression. This behaviour is because the invar material has low thermal expansion than the aluminium, therefore, it restricts the contraction of plies on the tool side resulting in more tensile strains. Also, the aluminium tool increases the transverse strains on the tool side. However, no effect is observed on the shear strain in both plies, therefore changing the tool material does not affect fibre waviness formation.

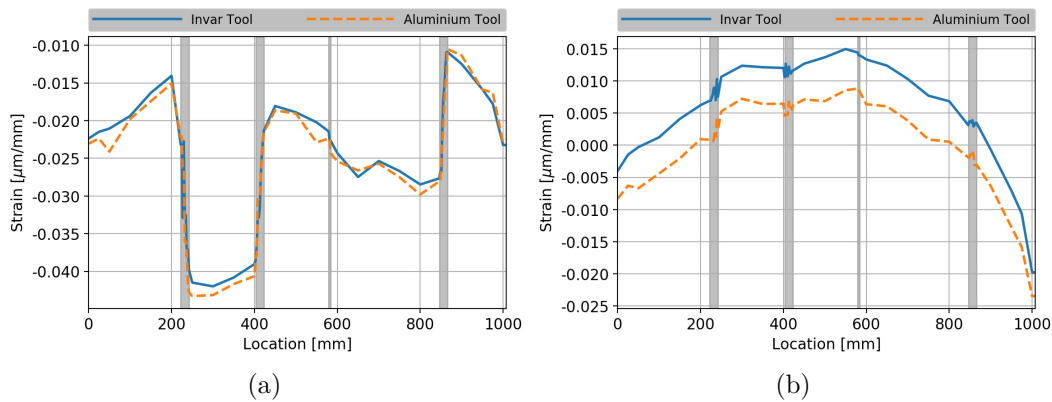


Figure 6.30: Effect of tool material on ε_1 , (a) ply 24 (bag side), (b) ply 1 (tool side).

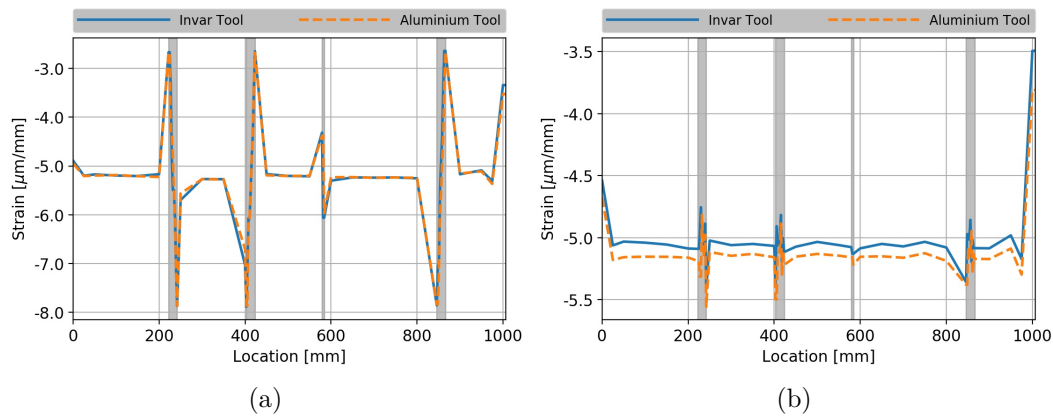


Figure 6.31: Effect of tool material on ε_2 , (a) ply 24 (bag side), (b) ply 1 (tool side).

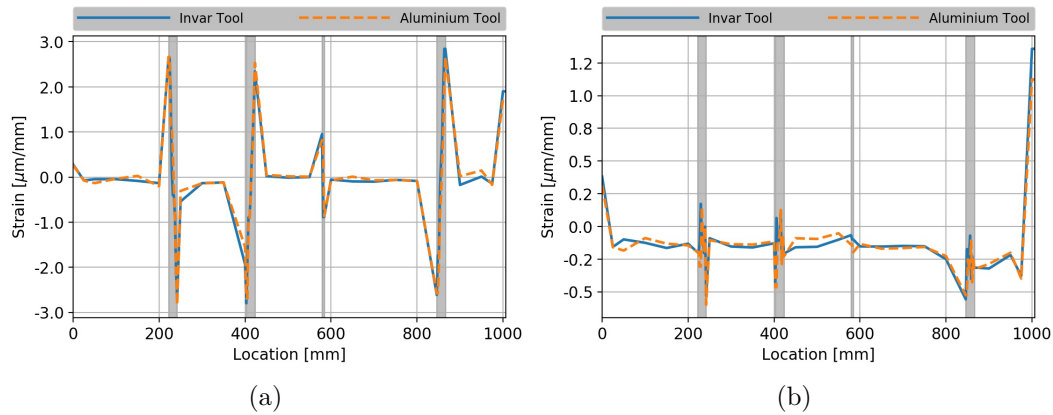


Figure 6.32: Effect of tool material on ε_{12} , (a) ply 24 (bag side), (b) ply 1 (tool side).

6.4 Conclusion

The study on the influence of various manufacturing parameters on the formation of fibre waviness defects was presented. The first parameters investigated were the drop-off sequence and the stagger length. The drop-off sequence showed no effect on the formation of fibre waviness, however, reversing the drop-off sequences slightly reduced the strain concentration at drop-off stations on the tool side. On the other hand, the stagger length had a huge effect on formation of fibre waviness defects. Increasing the stagger length reduced the alternation peaks occurring at the drop-off stations on both transverse and shear strain distributions in both plies, thus, reducing fibre waviness defects

intensity. On the cure cycle parameters, only the change of cure-pressure had an effect on fibre waviness formation. Both the pressure ramp-up rate and the heat-up rate had effect on the development of strain, however, did not affect the distributions within the panel. The change of the tool material only had effect on the development of shear strains, and also the strain distributions on the tool side. Even so, the tool had no effect on fibre waviness formation. Therefore, to avoid fibre waviness defects, one has to increase the stagger length and reduce the pressure as much as practically possible.

Chapter 7

Conclusion and Recommendations

7.1 Conclusion

The aim for this study was to predict the formation of fibre waviness defects in a thermosetting composite panel that comprises ply drop-offs. This study was done by performing cure process simulations using a newly developed Ansys Composite Cure Simulation (ACCS) analytical tool-kit and validating the predictions with practical observations after manufacturing. The cure process simulations had to calculate the material evolutions (i.e. the degree of cure, glass transition temperature, viscosity, etc.) and stress/strain distributions in the composite panel, using material properties from literature. The stress/strain distributions was then used to predict the locations of possible fibre waviness defects and to identify mechanisms for fibre waviness formation. The manufacturing of the composite panel followed the autoclave curing process with the same curing conditions as the simulations. Lastly, numerical experimentation was conducted to study the effect of various parameters (i.e. geometric, cure cycle or tool material) on the formation of fibre waviness. Manufacturing recommendations were then made based on these numerical experiments.

The composite panel was modelled in Ansys Composite PrePost (ACP). The ply drop-offs in the composite panel created triangular gaps called resin pockets in the model. The plies were modelled using the solid-shell elements which specified the ply material (i.e. IM7/977-2 unidirectional tape), ply thickness and fibre orientations. The resin pockets were modelled using solid elements with an isotropic material (i.e. 977-2 epoxy resin).

The tool was also modelled using solid elements with an isotropic material (Invar). The contact between the tool and the composite panel was modelled as a frictional contact with a release agent applied on the tool surface.

The cure process simulation of the composite panel was divided into two steps, i.e. transient thermal analysis followed by the static structural analysis. In the transient thermal analysis, the composite panel and the tool were assumed to be surrounded by air following a cure temperature cycle (i.e. convection heat transfer loading on all outer surfaces). Then, the ACCS tool-kit was used to compute the temporal temperature distributions and material evolutions. In the static structural analysis, a cure pressure cycle was applied to the composite panel. Then, the temporal temperature distributions generated in the transient thermal analysis was applied to compute the stress/strains distributions in the composite panel, also using the ACCS tool-kit. This process was identified as the ACCS's full cure simulation procedure and the best way to completely capture temporal material evolutions.

The material evolution results showed the two main material transitions occurring in the composite panel during the curing process. The first was when the resin transforms from the liquid state into the rubbery state, i.e. gelation. This transition occurred when the degree of cure reached a predefined value called the gel point at about 85 min of the curing time. The second transition was when the resin transforms from the rubbery state into a glassy solid, i.e. vitrification. This transition occurred when the glass transition temperature exceeded the panel temperature at about 185 min of the curing time. The viscosity of the composite panel was the lowest just before gelation which is when fibre waviness was assumed to occur due to the low bending stiffness of fibres and the ability of the resin to flow.

Stresses and strains in the composite panel developed right from the start of the curing process. The in-plane strains were the highest in the transverse direction (ε_2) and in compression for all plies. The fibre direction strains (ε_1) were very low due to the high compressive stiffness of the fibres and they gradually increased compressively as the cure progressed to completion. The in-plane shear strains (ε_{12}) were also low, however, they progress differently at the drop-off stations on the bag side. This was believed to be due to the stress concentrations induced by ply drop-off and the tapering on the bag side plies. These inconsistencies and the early development of cure-induced strains led to the belief that they might cause the fibres to buckle when the resin has low viscosity and is able to flow. Therefore, the in-plane strains were analysed further at the point of minimum viscosity to predict fibre waviness defects.

The analysis of strain distributions in the composite panel when the resin viscosity was at the minimum showed that the transverse strains alternate (i.e. high-low-high values or vice versa), and also the in-plane shear strains (i.e. between negative and positive values) at the drop-off stations 1, 2 and 4; in a ply located on the bag side of the composite panel. The fibre direction strains

on this ply were in compression which indicated that these uneven transverse strain distributions will cause fibres to buckle due to their low bending stiffness. The ply on the tool side experienced even transverse and shear distributions while fibre direction strains were low at the centre of the panel and in compression towards the edges. Thus, indicating that the fibres does not buckle on this ply.

The predictions agreed with practical observations after manufacturing the panel, however, in practise fibre waviness did not occur at drop-off station 4 as predicted. This was because other features such as stiffeners were added parallel and at drop-off stations 3 and 4 of the panel during the manufacturing, which were not considered during the predictions. These stiffeners work as stress intensifiers, which restrict the plies from contracting during the curing process resulting in tensile strains, thus, preventing fibres to buckle by alternating transverse and shear strains, due to their increased bending stiffness.

Therefore, fibre waviness defects were predicted successfully and mechanism behind their formation was formulated saying: when fibres are in compression, they have a reduced bending stiffness, therefore the alternation of transverse strains (i.e. high-low-high values or vice versa) and in-plane shear strains (i.e. between negative and positive values) causes them to buckle forming fibre waviness defects. Following this mechanism, the effect of various parameters was investigated on the formation of fibre waviness defects.

The first group of parameters investigated was the ply drop-off effect which included the drop-off sequence and the stagger length. The drop-off sequence did not have any effect on fibre waviness formation while increasing the stagger length reduced the alternation peaks of the transverse and shear strains bringing them closer to even distributions on the fibres, thus, reducing fibre waviness defects intensity. However, longer stagger lengths are not always recommended in practice as they will create irregular taper surfaces.

The second group of parameters investigated was the cure cycle effects which included the cure-pressure, the pressure ramp-up rate and the heat-up rate. Both the pressure ramp-up and heat-up rates did not have any effect on the formation of fibre waviness defects, however they had an effect on the development of strains in the panel. The cure pressure had effect on the fibre waviness. Reducing the pressure reduced the intensity of fibre waviness defects formation, but may results in high void content in the panel.

The last group of parameters investigated was the tool material where the effects of invar tool were compared to the effects of aluminium tool. Changing the tool material had no effect on the fibre waviness defects. Only the fibre direction and transverse strains on the tool side were affected but not for the

formation of fibre waviness defects.

To summarise, the parametric study found that to minimize fibre waviness in composites comprising ply drop-off's, one should increase the stagger length as much as practically possible. In addition, it is beneficial to reduce cure-pressure as much as practically possible.

7.2 Recommendations

Upon the review of the predictions and the parametric study, some improvements could be identified as well as the opportunities for future research. This section discusses these points.

The ACCS tool-kit predicts the formation of fibre waviness defects very well. However, the material properties of the composite need to be determined in full, i.e. both cure and mechanical properties, due to properties from the literature being diverse. The friction between the tool and the panel also needs to be determined since it changes with cure conditions and this study assumed it to be constant throughout the curing process.

Fibre waviness defects in this study were not quantified. Therefore, a multi-scale simulation needs to be performed to isolate the stresses and strains experienced by the fibres. This will also help identify the critical fibre buckling strains since the stress concentrations induced by the ply drop-off's are unavoidable.

The other consideration is that the parametric study was only performed numerically. Therefore, experimental studies needs to be conducted to validate the results.

List of References

1. Ahmed, A., Tavakol, B., Das, R., Joven, R., Roozbehjavan, P. and Minaie, B. (2012). Study of thermal expansion in carbon fiber-reinforced polymer composites. In: *SAMPE International Symposium Proceedings*.
2. Alavi-Soltani, S., Sabzevari, S., Koushyar, H. and Minaie, B. (2012). Thermal, rheological, and mechanical properties of a polymer composite cured at different isothermal cure temperatures. *Journal of Composite Materials*, vol. 46, no. 5, pp. 575–587. ISSN 00219983.
3. ANSYS (2017). LMAT Composite Cure Simulation Toolbox - White Paper. Available at: <http://www.ansys.com/Resource-Library/white-paper/lmat-composite-cure-simulation-toolbox>
4. AZoM (2001). Invar - Nickel Iron Alloy. Available at: <https://www.azom.com/article.aspx?ArticleID=515>
5. Cytec (2012). Cycom 977-2 Epoxy Resin System - Technical Data Sheet. Tech. Rep., Cytec - Engineered Materials.
6. Dhurvey, P. and Mittal, N.D. (2012). Finite Element Analysis of Internally Ply Drop-off Composite Laminates. *International Journal of Engineering Research*, vol. 1, no. 1, pp. 12–16.
7. Ding, A., Li, S., Wang, J., Ni, A. and Zu, L. (2017). A new path-dependent constitutive model predicting cure-induced distortions in composite structures. *Composites Part A: Applied Science and Manufacturing*, vol. 95, pp. 183–196. ISSN 1359835X.
8. Guo, Z.S., Zhang, B. and Du, S.Y. (2007). Theoretical and experimental studies on residual stresses of advanced polymer composites. *Advances in Composite Materials and Structures, Pts 1 and 2*, vol. 334-335, pp. 37–40. ISSN 0277786X.
9. Hallett, S.R., Belnoue, J.P.-H., Nixon-Pearson, O.J., Mesogitis, T., Kratz, J., Ivanov, D.S., Partridge, I.K. and Potter, K.D. (2016). Understanding and Prediction of Fibre Waviness Defect Generation. *American Society for Composites Thirty-First Technical Conference*.
10. He, K., Hoa, S.V. and Ganesan, R. (2000). The study of tapered laminated composite structures: A review. *Composites Science and Technology*, vol. 20, no. 2000, pp. 2643–2657. ISSN 02663538.

11. Johnston, A. (1997). *An integrated model of the development of process-induced deformation in autoclave processing of composite structures*. Ph.D. thesis, University of British Columbia.
12. Joven, R. (2013). *Characterization and modeling of shear stress during manufacturing and thermal properties of structural composite materials*. Phd, Wichita State University.
13. Joven, R., Das, R., Ahmed, A., Roozbehjavan, P. and Minaie, B. (2012). Thermal properties of carbon fiber epoxy composites with different fabric weaves. In: *SAMPE International Symposium Proceedings*, p. 14.
14. Karami, G. and Garnich, M. (2005). Micromechanical study of thermoelastic behavior of composites with periodic fiber waviness. *Composites Part B: Engineering*, vol. 36, no. 3, pp. 241–248. ISSN 13598368.
15. Koushyar, H. (2011). EFFECTS OF VARIATION IN AUTOCLAVE PRESSURE, CURE TEMPERATURE, AND VACUUM-APPLICATION TIME ON THE POROSITY AND MECHANICAL PROPERTIES OF A CARBON/EPOXY COMPOSITE. Tech. Rep..
16. Kravchenko, O.G., Kravchenko, S.G. and Pipes, R.B. (2016). Chemical and thermal shrinkage in thermosetting prepreg. *Composites Part A: Applied Science and Manufacturing*, vol. 80, pp. 72–81. ISSN 1359835X.
17. Kugler, D. and Moon, T.J. (2002). Identification of the Most Significant Processing Parameters on the Developments of Fiber Waviness in Thin Laminates. *Journal of Composite Materials*, vol. 36, no. 12, pp. 1451–1479.
18. Li, D., Li, X., Dai, J. and Xi, S. (2018). A Comparison of Curing Process-Induced Residual Stresses and Cure Shrinkage in Micro-Scale Composite Structures with Different Constitutive Laws. *Application Composite Materials*, vol. 25, pp. 67–84.
19. Li, W. and Lee, L.J. (1998). Shrinkage control of low-profile unsaturated polyester resins cured at low temperature. *Polymer*, vol. 39, no. 23, pp. 5677–5687. ISSN 00323861.
20. Liang, G. and Chandrashekhara, K. (2006). Cure kinetics and rheology characterization of soy-based epoxy resin system. *Journal of Applied Polymer Science*, vol. 102, no. 4, pp. 3168–3180. ISSN 00218995.
Available at: <https://doi.org/10.1002/app.24369>
21. Lightfoot, J.S., Wisnom, M.R. and Potter, K. (2013). A new mechanism for the formation of ply wrinkles due to shear between plies. *Composites Part A: Applied Science and Manufacturing*, vol. 49, pp. 139–147.
22. LMAT (2016). ANSYS Composite Cure Simulation: User Guide, theory reference and tutorials.

23. Mukherjee, A. and Varughese, B. (2001). Design guidelines for ply drop-off in laminated composite structures. *Composites Part B: Engineering*, vol. 32, no. 2, pp. 153–164. ISSN 13598368.
24. Mulle, M., Collombet, F., Olivier, P. and Grunevald, Y.H. (2009). Assessment of cure residual strains through the thickness of carbon-epoxy laminates using FBGs, Part I: Elementary specimen. *Composites Part A: Applied Science and Manufacturing*, vol. 40, no. 1, pp. 94–104. ISSN 1359835X.
25. Niu, X. (1999). *PROCESS INDUCED RESIDUAL STRESSES AND DIMENSIONAL DISTORTIONS IN ADVANCED LAMINATED COMPOSITES*. Phd, UNIVERSITY OF FLORIDA.
26. Pain, D. and Drinkwater, B.W. (2013). Detection of fibre waviness using ultrasonic array scattering data. *Journal of Nondestructive Evaluation*, vol. 32, no. 3, pp. 215–227. ISSN 01959298.
27. Parlevliet, P.P., Bersee, H.E.N. and Beukers, A. (2007). Residual stresses in thermoplastic composites-A study of the literature. Part III: Effects of thermal residual stresses. *Composites Part A: Applied Science and Manufacturing*, vol. 38, no. 6, pp. 1581–1596. ISSN 1359835X.
28. Pian, T.H. and Tong, P. (1969). Basis of finite element methods for solid continua. *International Journal for Numerical Methods in Engineering*, vol. 2, pp. 1333–1336. ISSN 10970207.
29. Piggott, M. (1995 jan). The effect of fibre waviness on the mechanical properties of unidirectional fibre composites: A review. *Composites Science and Technology*, vol. 53, no. 2, pp. 201–205. ISSN 02663538.
30. Potter, K.D. (2009 oct). Understanding The Origins of Defects And Variability in Composites Manufacture. *17 th International Conference on Composite Materials*, pp. 27–31. ISSN 1359835X.
31. Qu, B.B. (2010). Modelling Generation of Fibre Waviness. In: *14th European Conference on Composite Materials*, pp. 1–10.
32. Ruiz, E. and Trochu, F. (2005). Thermomechanical properties during cure of glass-polyester RTM composites: Elastic and viscoelastic modeling. *Journal of Composite Materials*, vol. 39, no. 10, pp. 881–916. ISSN 00219983.
33. Sabzevari, S.M. (2010). *Cure Kinetics and Process Modeling of a Carbon-Fiber Thermoplastic-Toughened Epoxy Resin Prepreg*. Ph.D. thesis, Sharif University of Technology.
34. Schulz, W.A., Myers, D.G., Singer, T.N., Ifju, P.G. and Haftka, R.T. (2005). Determination of residual stress and thermal history for IM7/977-2 composite laminates. *Composites Science and Technology*, vol. 65, no. 13, pp. 2014–2024. ISSN 02663538.

35. Shanku, R., Vaughan, J.G. and Roux, J.A. (1997). Rheological characteristics and cure kinetics of EPON 862/W epoxy used in pultrusion. *Advances in Polymer Technology*, vol. 16, no. 4, pp. 297–311. ISSN 07306679.
36. Sun, L. (2002). *Thermal Rheological Analysis of Cure Process of Epoxy Prepeg*. Phd, Louisiana State University and Agricultural and Mechanical College. [arXiv: 1011.1669v3](https://arxiv.org/abs/1011.1669v3).
37. Tabiei, A. and Chen, Q. (1999). Micromechanics Based Composite Material Model for Impact and Crashworthiness Explicit Finite Element Simulation. In: *PROCEEDINGS-AMERICAN SOCIETY FOR COMPOSITES*, pp. 317–334.
38. Tavakol, B., Roozbehjavan, P., Ahmed, A., Das, R., Joven, R., Koushyar, H., Rodriguez, A. and Minaie, B. (2013). Prediction of residual stresses and distortion in carbon fiber-epoxy composite parts due to curing process using finite element analysis. *Journal of Applied Polymer Science*, vol. 128, no. 2, pp. 941–950. ISSN 00218995.
39. Vidyashankar, B. and Krishna Murty, A. (2001). Analysis of laminates with ply drops (Layered Elements). *Composites Science and Technology*, vol. 61, no. 5, pp. 749–758. ISSN 02663538.
Available at: www.elsevier.com/locate/compscitechhttp://linkinghub.elsevier.com/retrieve/pii/S0266353801000100
40. Vizzini, A. (1995). Influence of Realistic Ply-Drop Geometries on Interlaminar Stresses in Tapered Laminates. *Composite Materials: Fatigue and Fracture: Fifth Volume*, vol. 5, pp. 467–485. ISSN 10403094.
41. White, S.R. and Kim, Y.K. (1998). Process-Induced Residual Stress Analysis of As4/3501-6 Composite Material. *Mechanics of Advanced Materials and Structures*, vol. 5, no. 2, pp. 153–186. ISSN 1537-6494.
42. Wisnom, M.R., Gigliotti, M., Ersoy, N., Campbell, M. and Potter, K.D. (2006). Mechanisms generating residual stresses and distortion during manufacture of polymer-matrix composite structures. *Composites Part A: Applied Science and Manufacturing*, vol. 37, no. 4, pp. 522–529. ISSN 1359835X.
43. Zeng, X. and Raghavan, J. (2010). Role of tool-part interaction in process-induced warpage of autoclave-manufactured composite structures. In: *Composites Part A: Applied Science and Manufacturing*, vol. 41, pp. 1174–1183. ISBN 1359-835X. ISSN 1359835X.
44. Zhang, J.T., Zhang, M., Li, S.X., Pavier, M.J. and Smith, D.J. (2016). Residual stresses created during curing of a polymer matrix composite using a viscoelastic model. *Composites Science and Technology*, vol. 130, pp. 20–27. ISSN 02663538.
45. Zobeiry, N., Forghani, A., Li, C., Gordnian, K., Thorpe, R., Vaziri, R., Fernlund, G. and Poursartip, A. (2016). Multiscale characterization and representation of composite materials during processing. In: *Philosophical Transactions of the Royal Society A: Mathematical, Physical and Engineering Sciences*, vol. 374. ISSN 1364503X.

Appendices

Appendix A

Material Properties

A.1 IM7/977-2

Table A.1: Mechanical properties of IM7/977-2 composite (Cytec, 2012; Ahmed *et al.*, 2012; Joven *et al.*, 2012; Tavakol *et al.*, 2013).

Property	Symbol	Value	Units
Destiny	ρ	1.31	g/cm^3
Elastic Modulus:	$E1$	165	GPa
	$E2$	9	GPa
	$E3$	9	GPa
Poison's Ratio:	ν_{12}	0.29	
	ν_{23}	0.46	
	ν_{13}	0.29	
Shear Modulus:	G_{12}	4.74	GPa
	G_{23}	5.96	GPa
	G_{13}	4.74	GPa
Thermal Expansion:	α_1	-0.76	$10^{-6}/^\circ\text{C}$
	α_2	36.15	$10^{-6}/^\circ\text{C}$
	α_3	36.15	$10^{-6}/^\circ\text{C}$
Thermal Conductivity:	$K1$	8	W/m.K
	$K2$	0.85	W/m.K
	$K3$	0.85	W/m.K
Specific Heat	c	1.13	J/g.K

A.2 CYCOM 977-2 epoxy resin

Table A.2: Mechanical properties of pure CYCOM 977-2 epoxy resin (Tabiei and Chen, 1999; Cytec, 2012; Joven *et al.*, 2012).

Property	Value	Units
Destiny	1.31	g/cm^3
Elastic Modulus	3.52	GPa
Poison's Ratio	0.4	
Coefficient of Thermal Expansion	55.84	$10^{-6}/^{\circ}\text{C}$
Thermal Conductivity	0.48	W/m.K
Specific Heat	0.0013	J/g.K

A.3 Invar

Table A.3: Mechanical properties of Invar (AZoM, 2001).

Property	Value	Units
Destiny	8.15	Mg/m^3
Elastic Modulus	141	GPa
Poison's Ratio	0.29	
Coefficient of thermal Expansion	1.25	$10^{-6}/\text{K}$
Thermal Conductivity	13.5	W/m.K
Specific Heat	515	J/Kg.K

Appendix B

Ply Strain Distributions

B.1 Ply 2

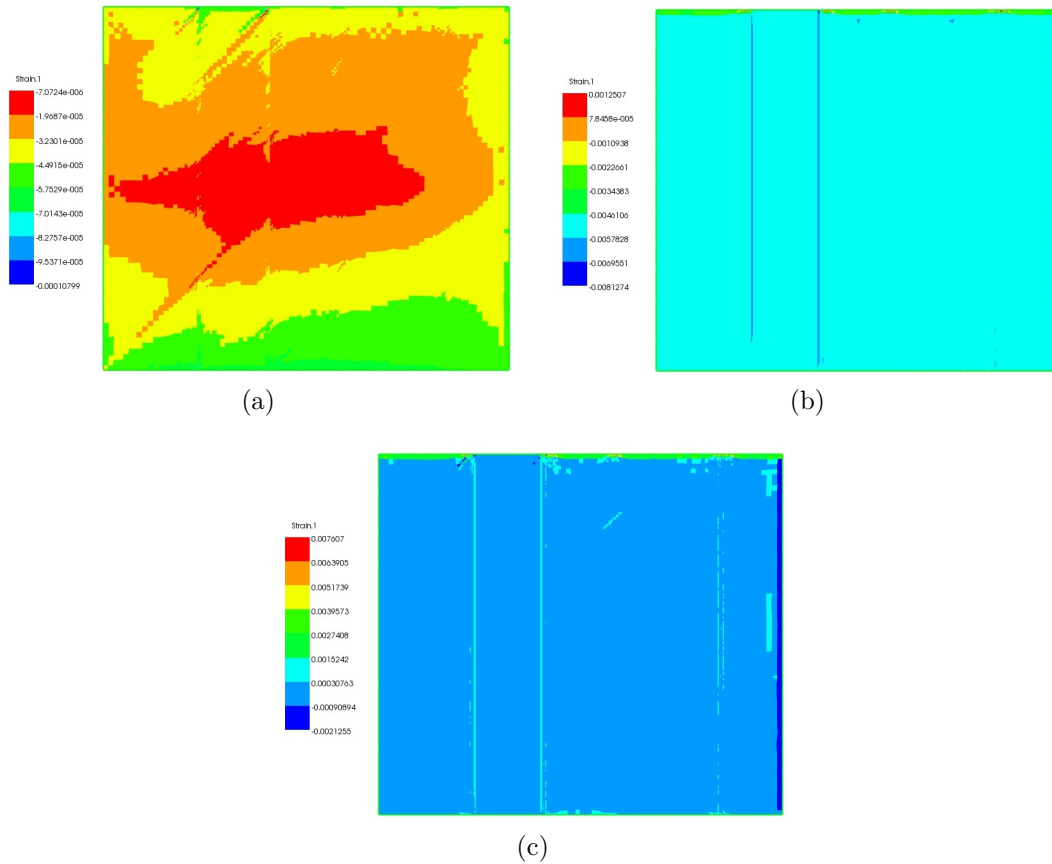


Figure B.1: Strain distributions in ply 2, (a) ϵ_1 , (b) ϵ_2 , (c) ϵ_{12} .

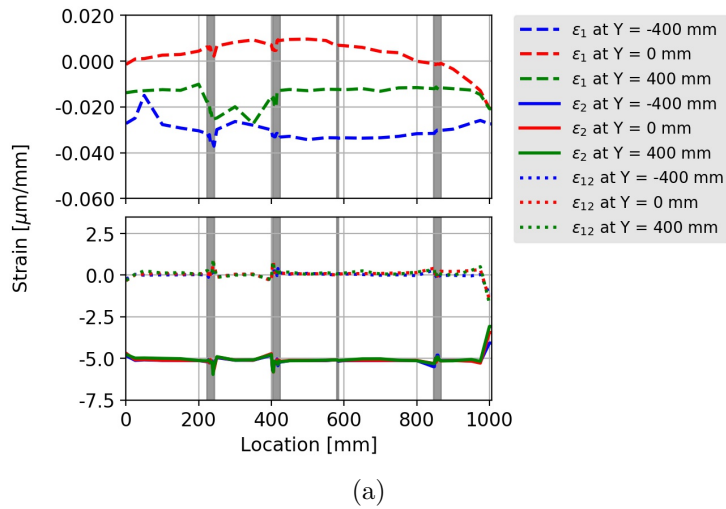
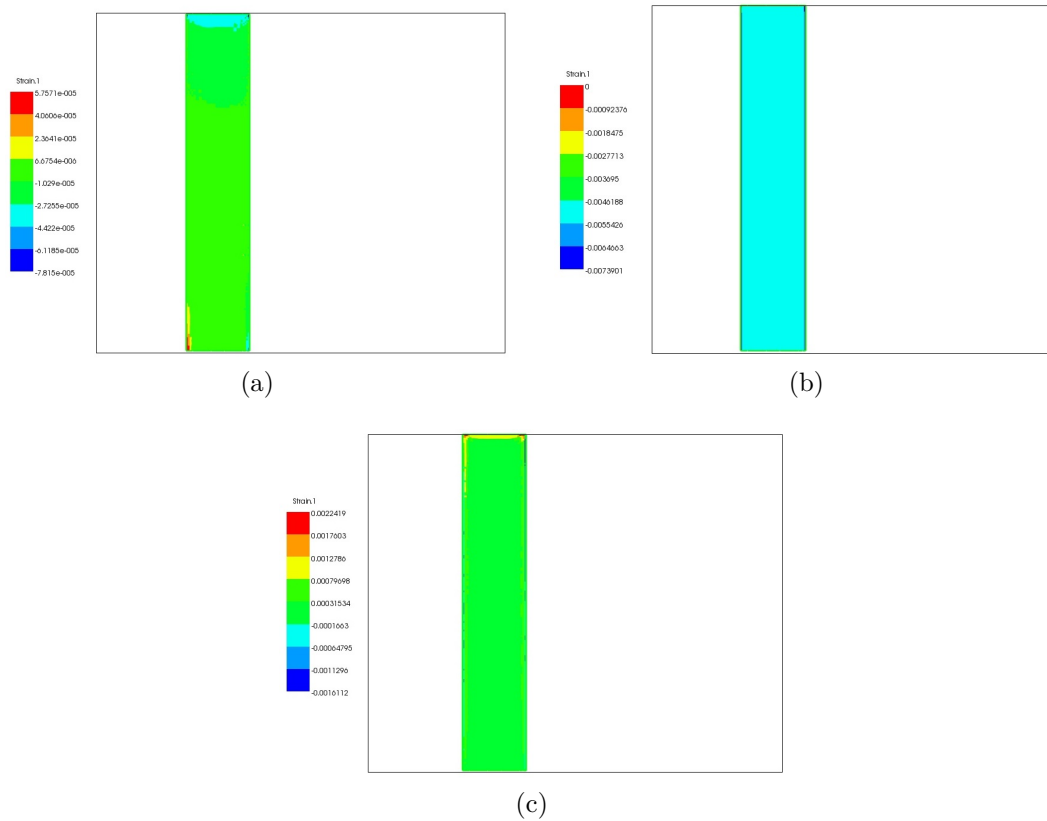


Figure B.2: Strains in ply 2 along ply length at various locations.

B.2 Ply 3 (Dropped)

Figure B.3: Strain distributions in ply 3, (a) ϵ_1 , (b) ϵ_2 , (c) ϵ_{12} .

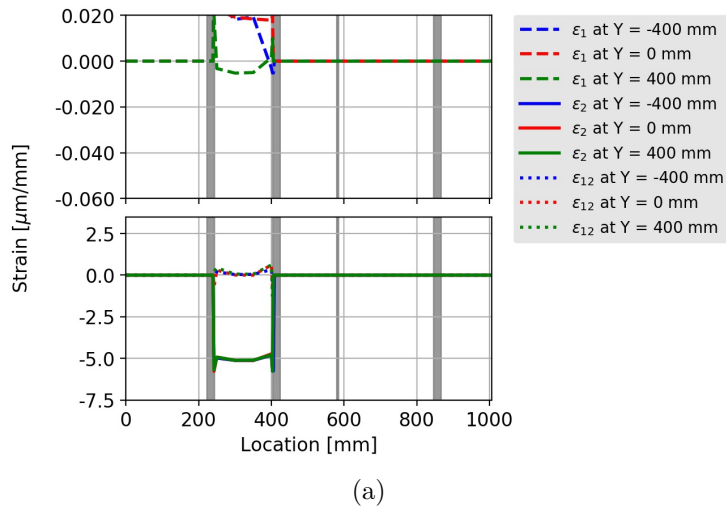
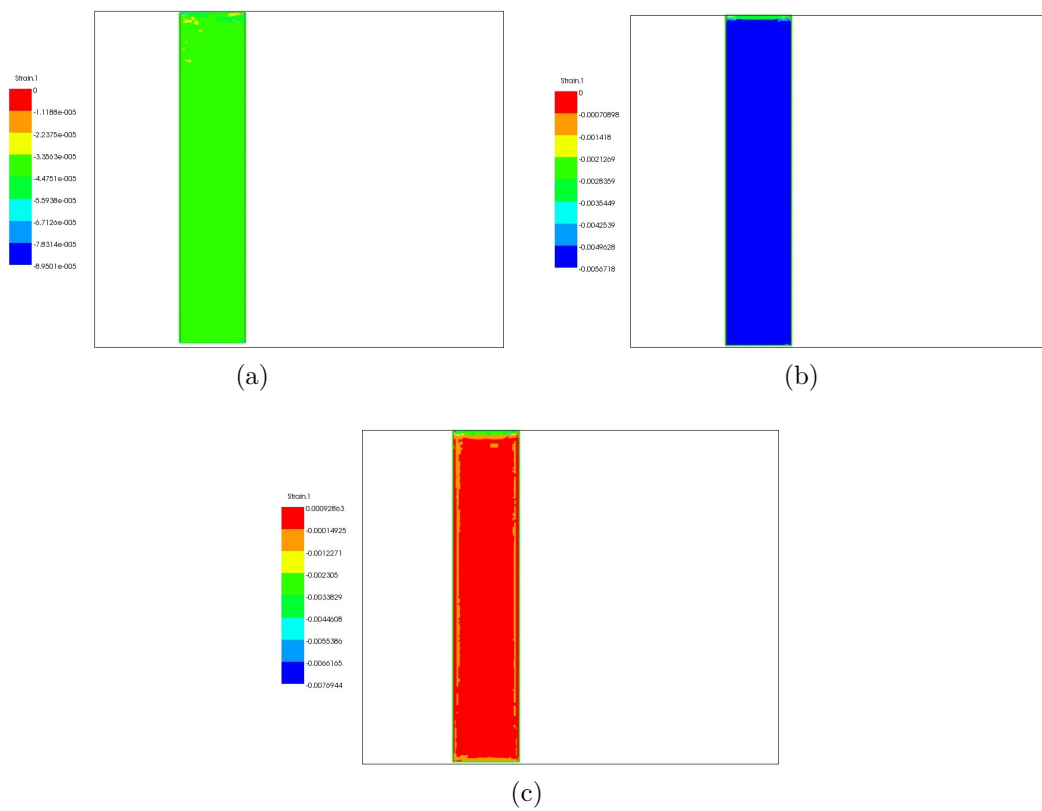


Figure B.4: Strains in ply 3 along ply length at various locations.

B.3 Ply 4 (Dropped)

Figure B.5: Strain distributions in ply 4, (a) ϵ_1 , (b) ϵ_2 , (c) ϵ_{12} .

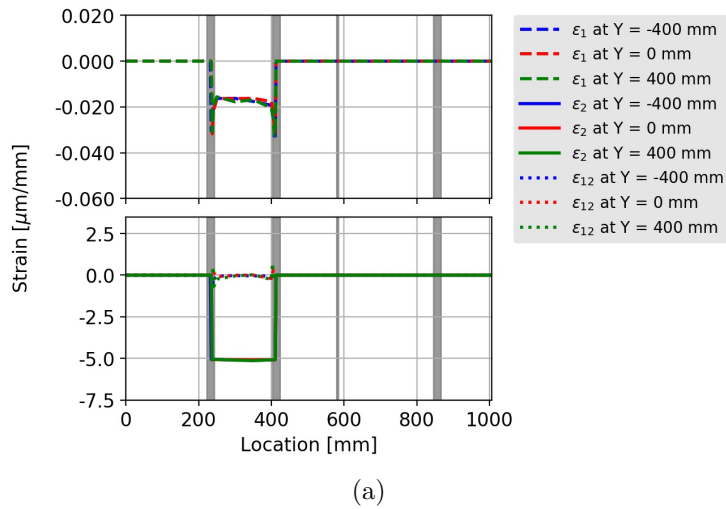
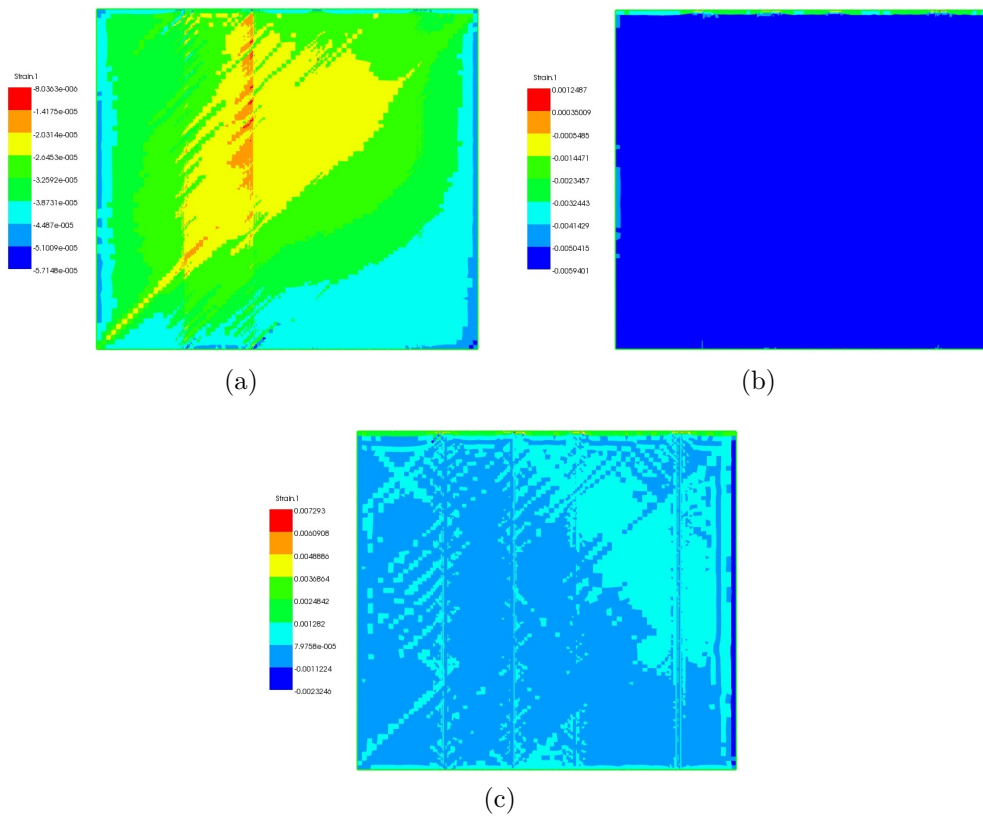


Figure B.6: Strains in ply 4 along ply length at various locations.

B.4 Ply 5

Figure B.7: Strain distributions in ply 5, (a) ε_1 , (b) ε_2 , (c) ε_{12} .

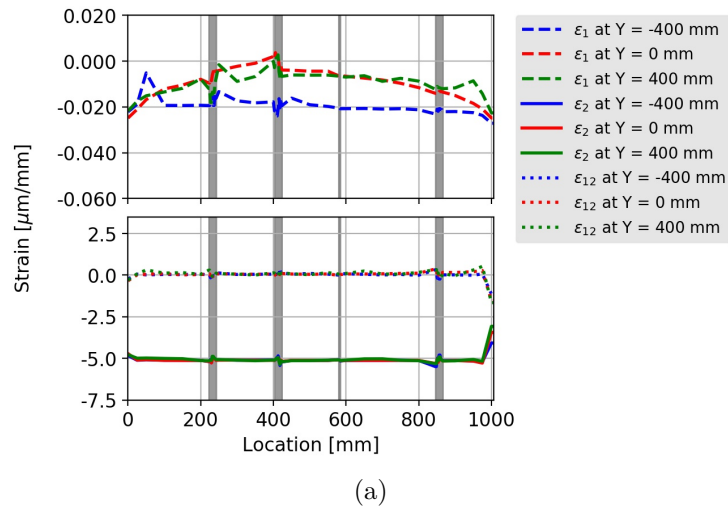
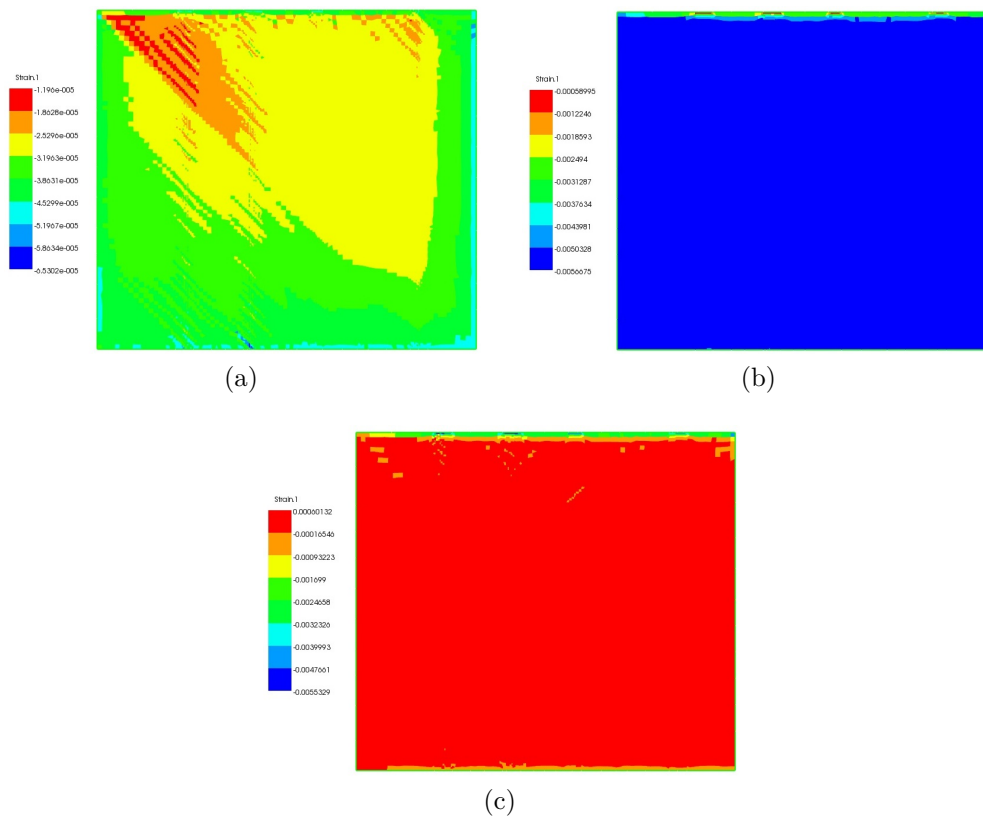


Figure B.8: Strain in ply 5 along ply length at various locations.

B.5 Ply 6

Figure B.9: Strain distributions in ply 6, (a) ϵ_1 , (b) ϵ_2 , (c) ϵ_{12} .

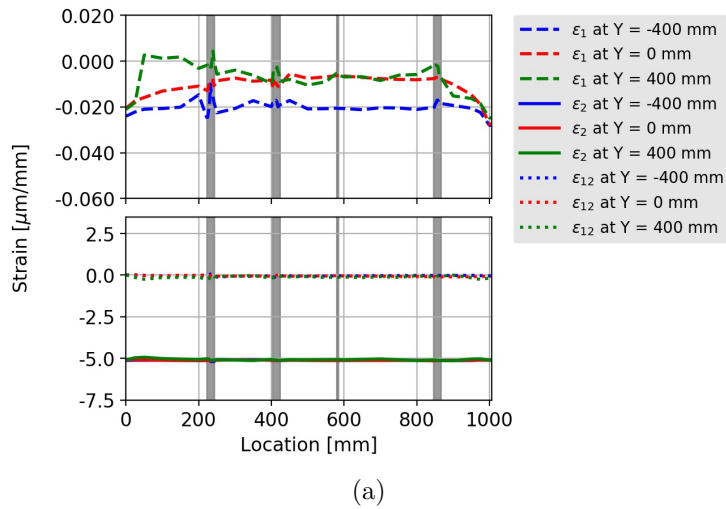
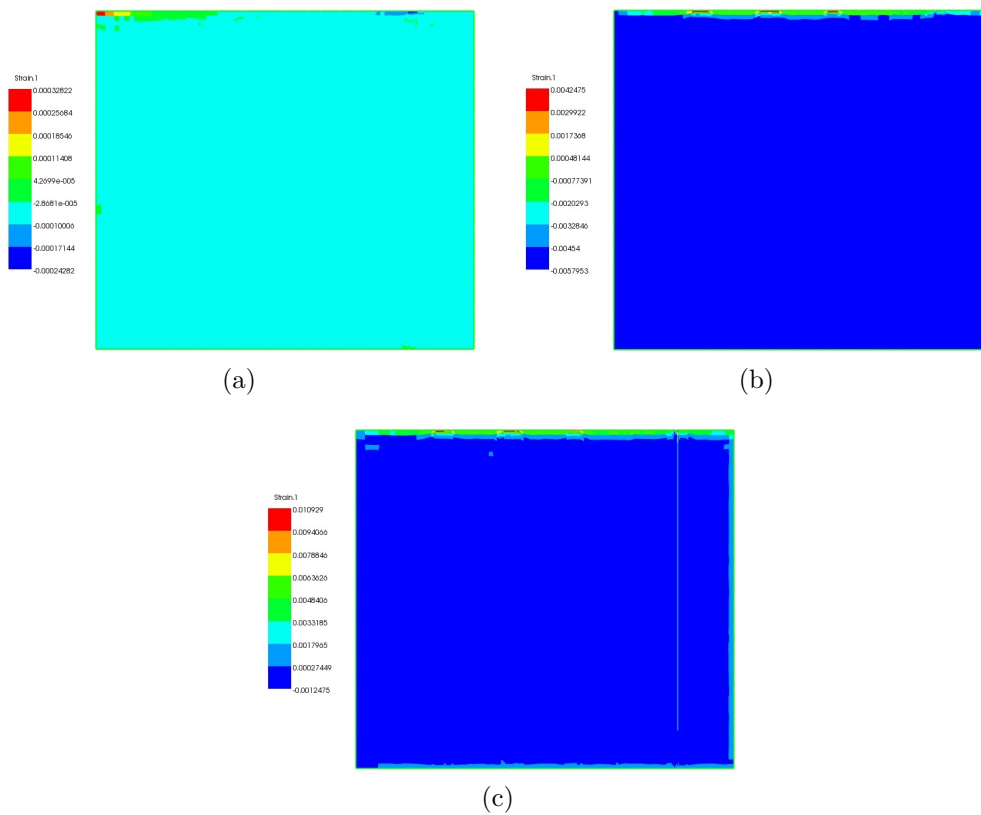


Figure B.10: Strains in ply 6 along ply length at various locations.

B.6 Ply 7

Figure B.11: Strain distributions in ply 7, (a) ϵ_1 , (b) ϵ_2 , (c) ϵ_{12} .

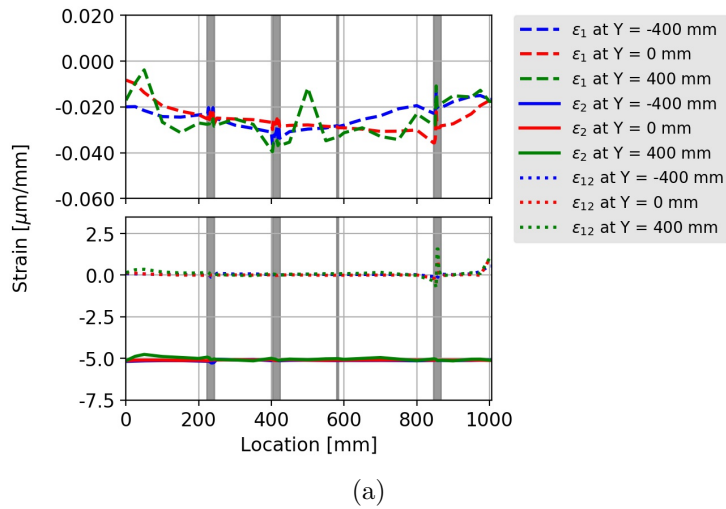
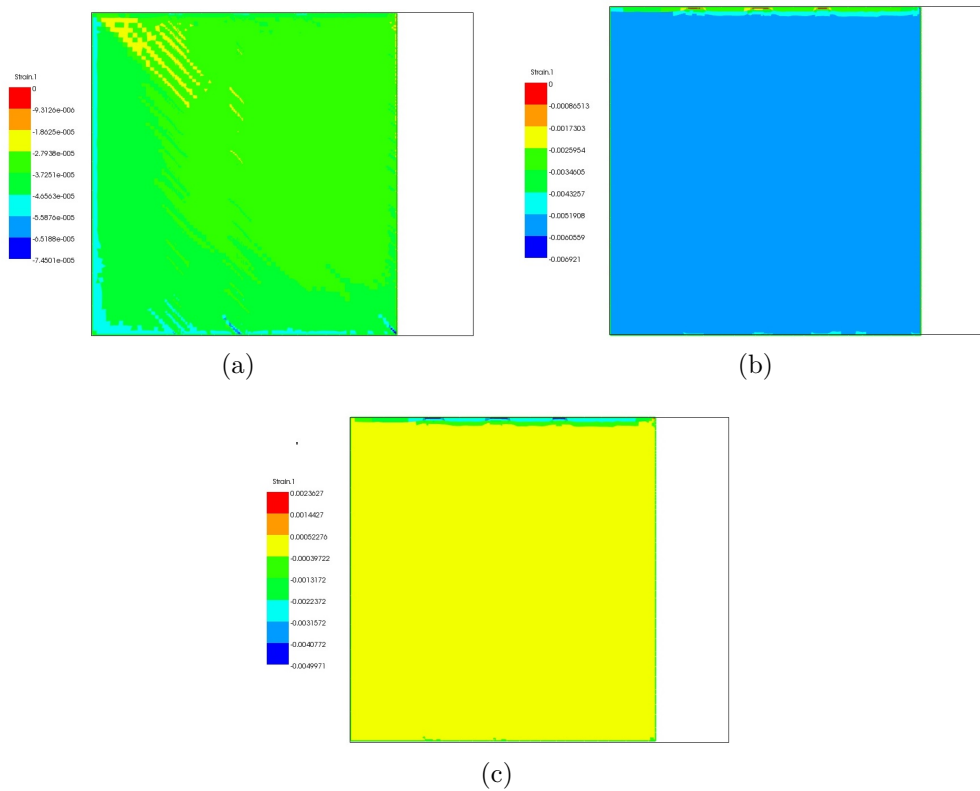


Figure B.12: Strains in ply 7 along ply length at various locations.

B.7 Ply 8 (Dropped)

Figure B.13: Strain distributions in ply 8, (a) ϵ_1 , (b) ϵ_2 , (c) ϵ_{12} .

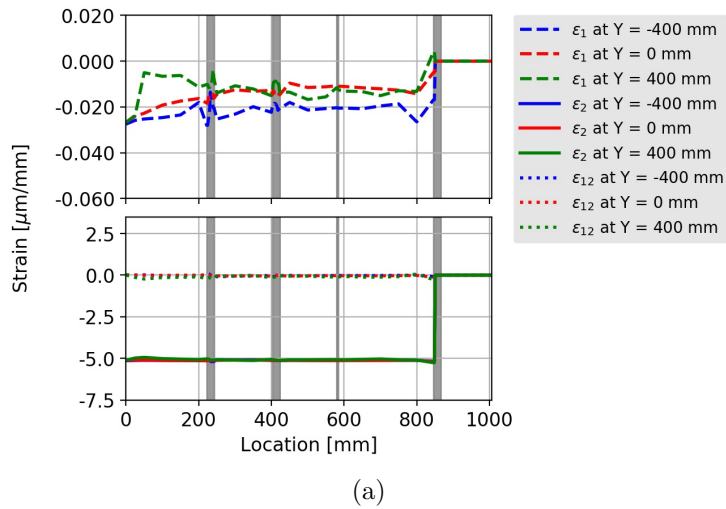
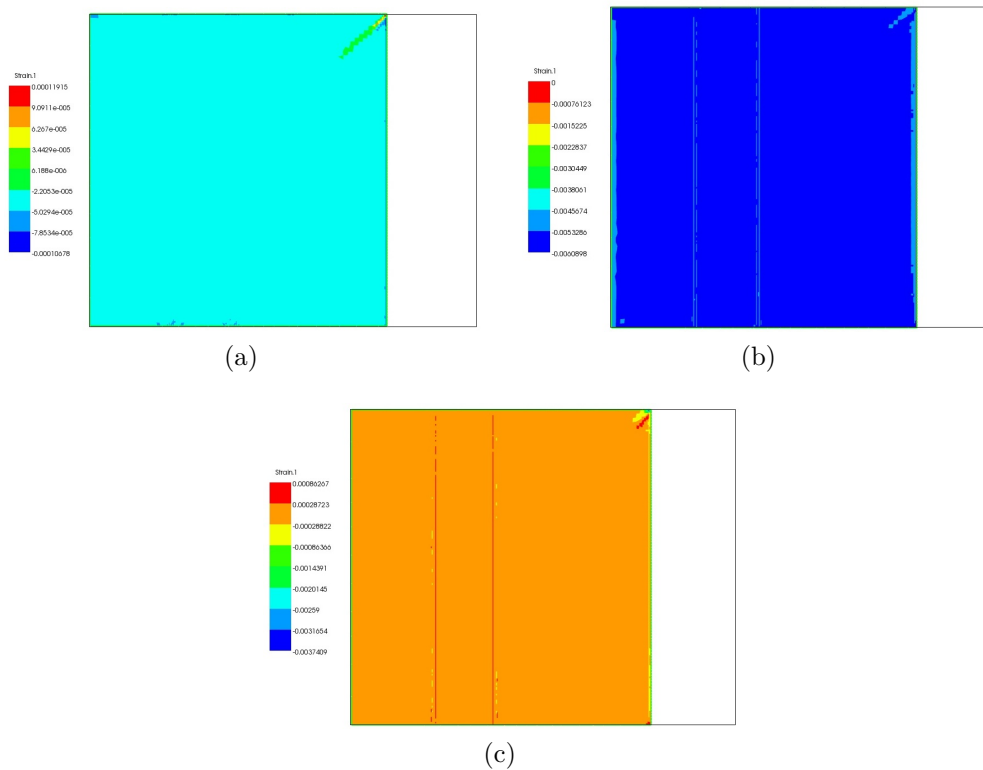


Figure B.14: Strains in ply 8 along ply length at various locations.

B.8 Ply 9 (Dropped)

Figure B.15: Strain distributions in ply 9, (a) ϵ_1 , (b) ϵ_2 , (c) ϵ_{12} .

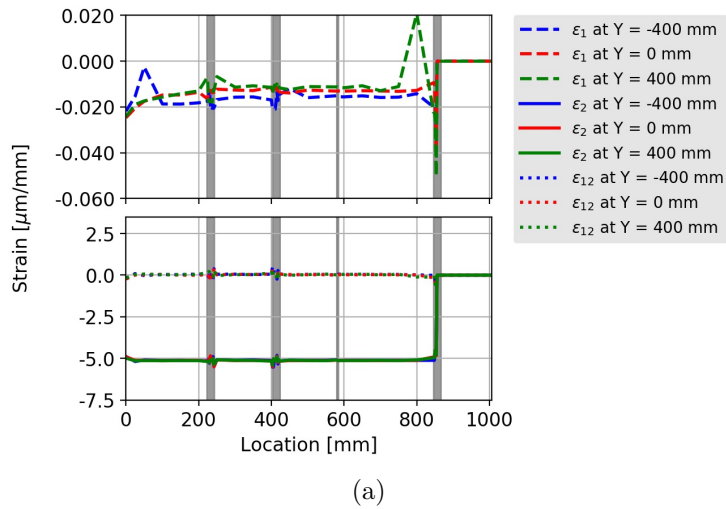
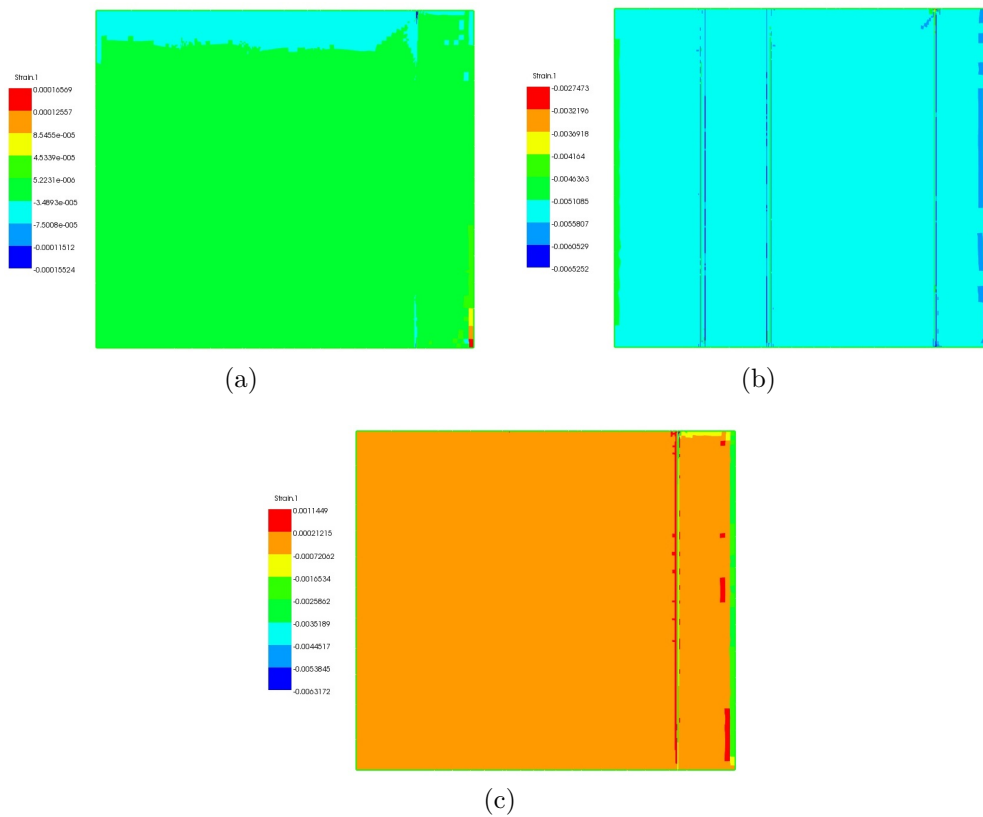


Figure B.16: Strains in ply 9 along ply length at various locations.

B.9 Ply 10

Figure B.17: Strain distributions in ply 10, (a) ε_1 , (b) ε_2 , (c) ε_{12} .

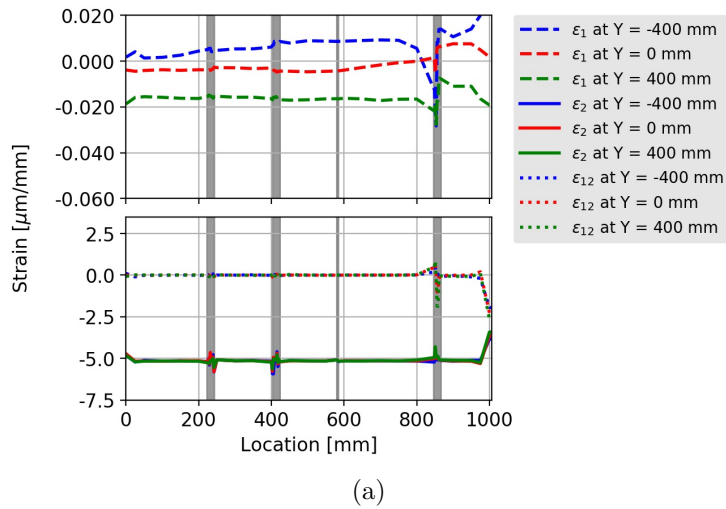
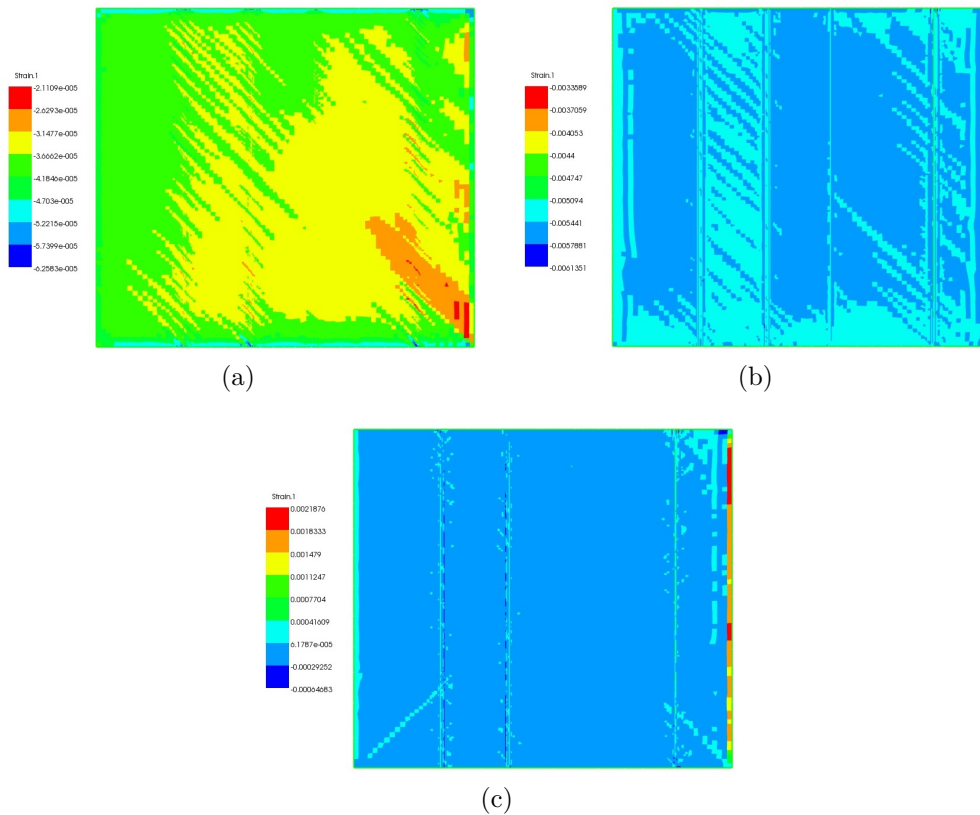


Figure B.18: Strains in ply 10 along ply length at various locations.

B.10 Ply 11

Figure B.19: Strain distributions in ply 11, (a) ε_1 , (b) ε_2 , (c) ε_{12} .

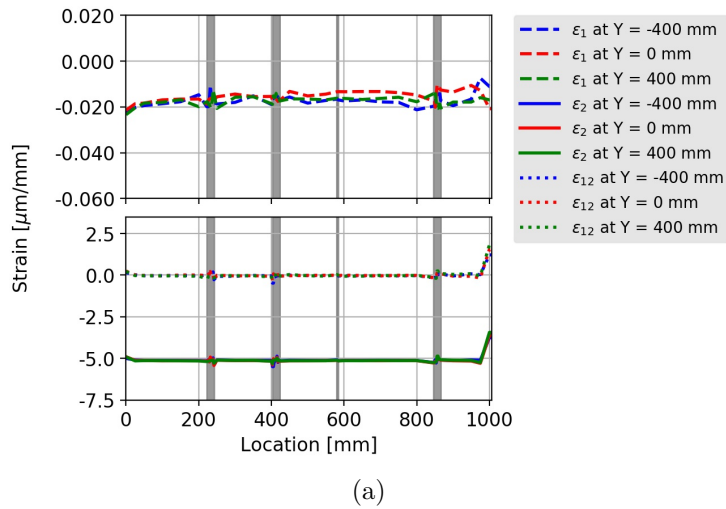
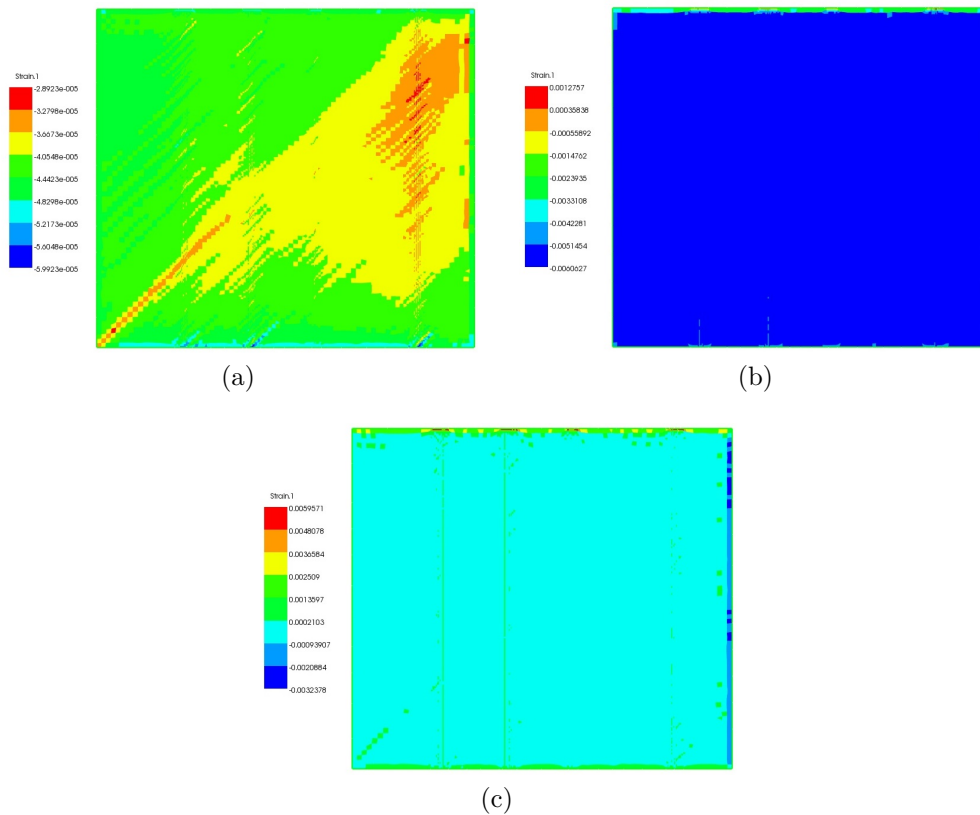


Figure B.20: Strains in ply 11 along ply length at various locations.

B.11 Ply 12

Figure B.21: Strain distributions in ply 12, (a) ε_1 , (b) ε_2 , (c) ε_{12} .

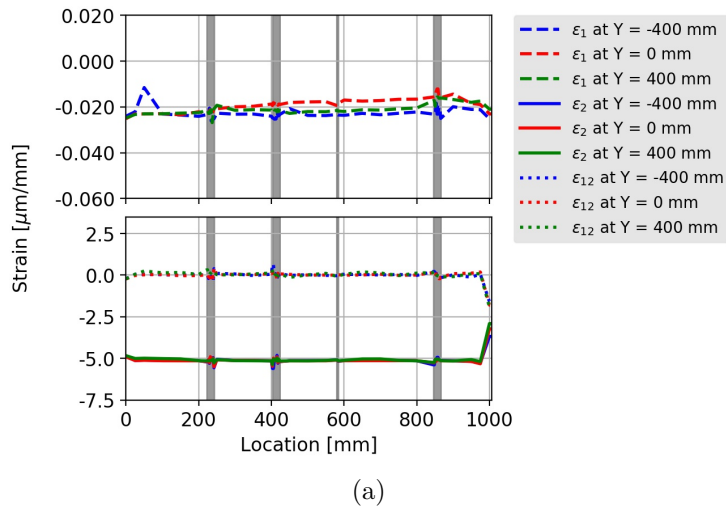
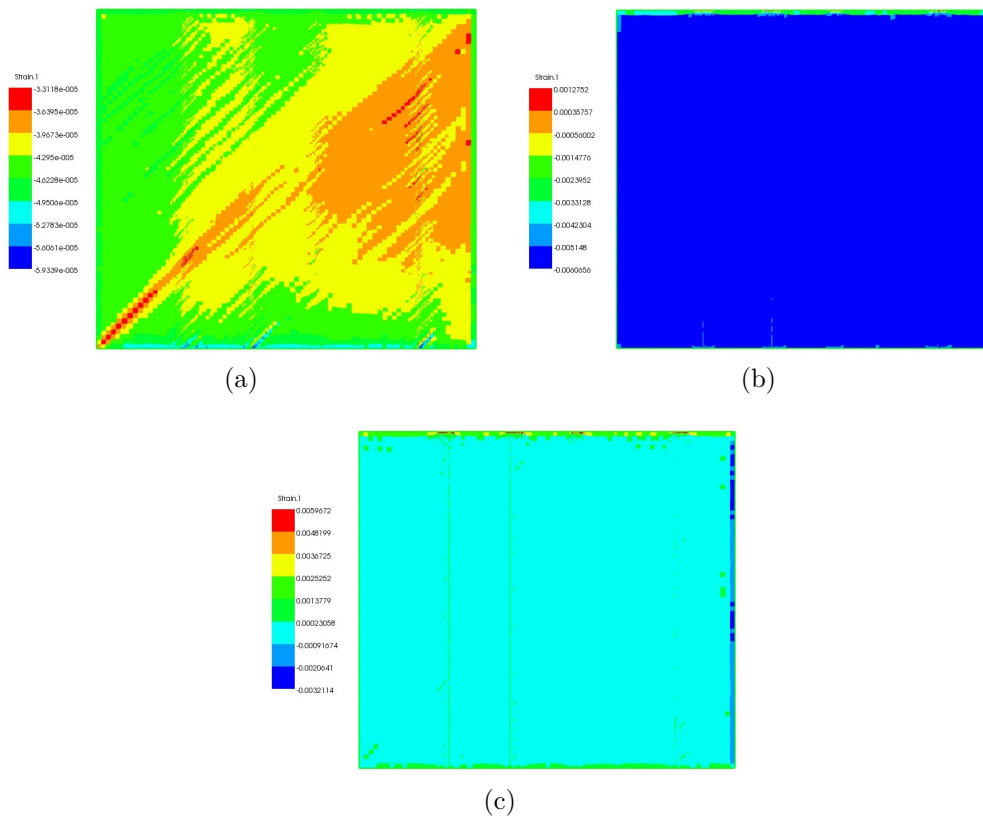


Figure B.22: Strains in ply 12 along ply length at various locations.

B.12 Ply 13

Figure B.23: Strain distributions in ply 13, (a) ϵ_1 , (b) ϵ_2 , (c) ϵ_{12} .

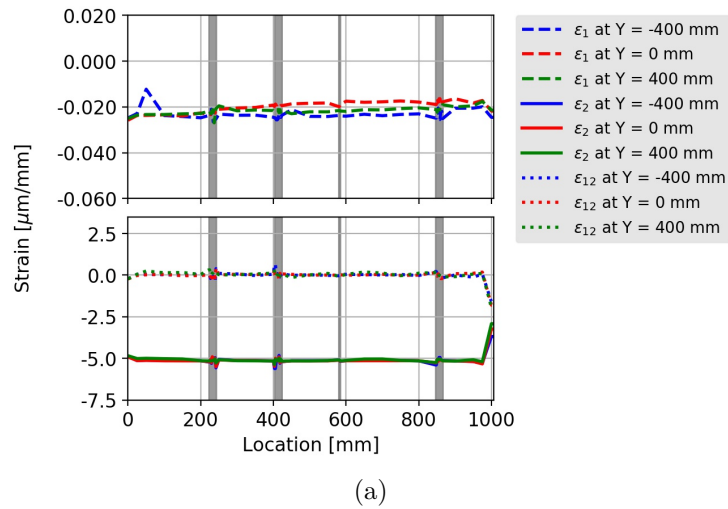
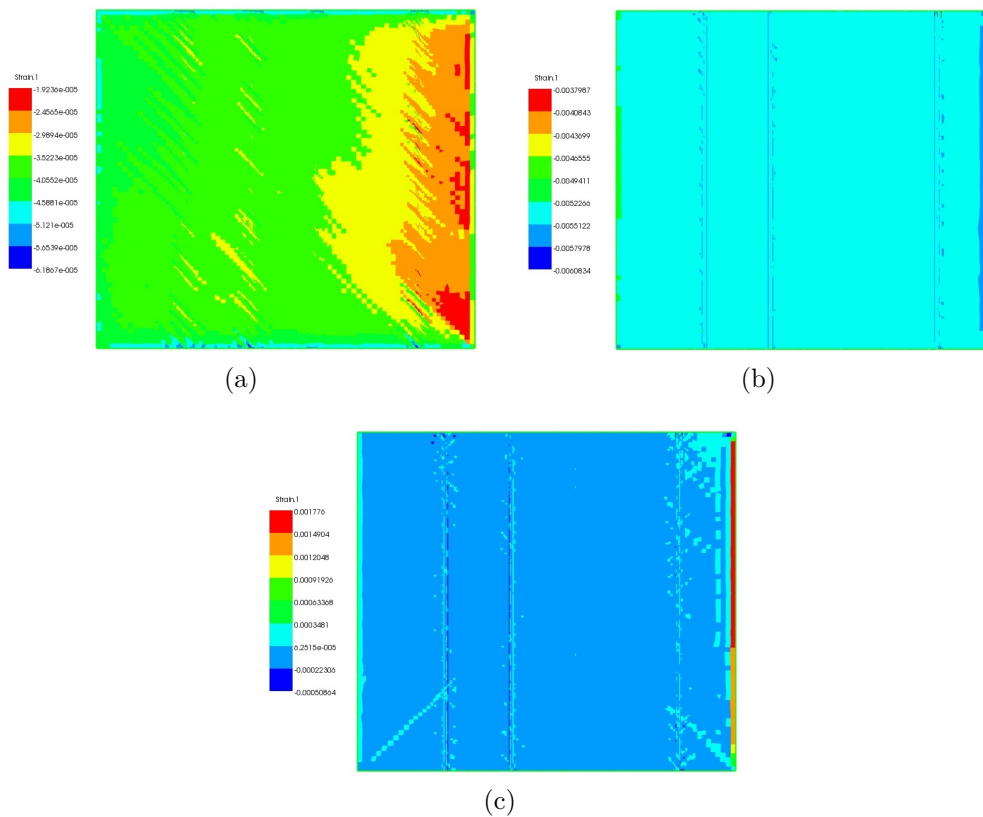


Figure B.24: Strains in ply 13 along ply length at various locations.

B.13 Ply 14

Figure B.25: Strain distributions in ply 14, (a) ϵ_1 , (b) ϵ_2 , (c) ϵ_{12} .

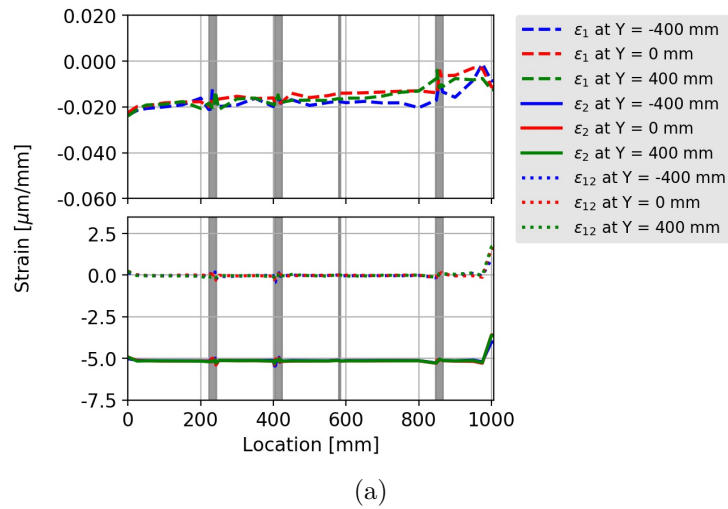
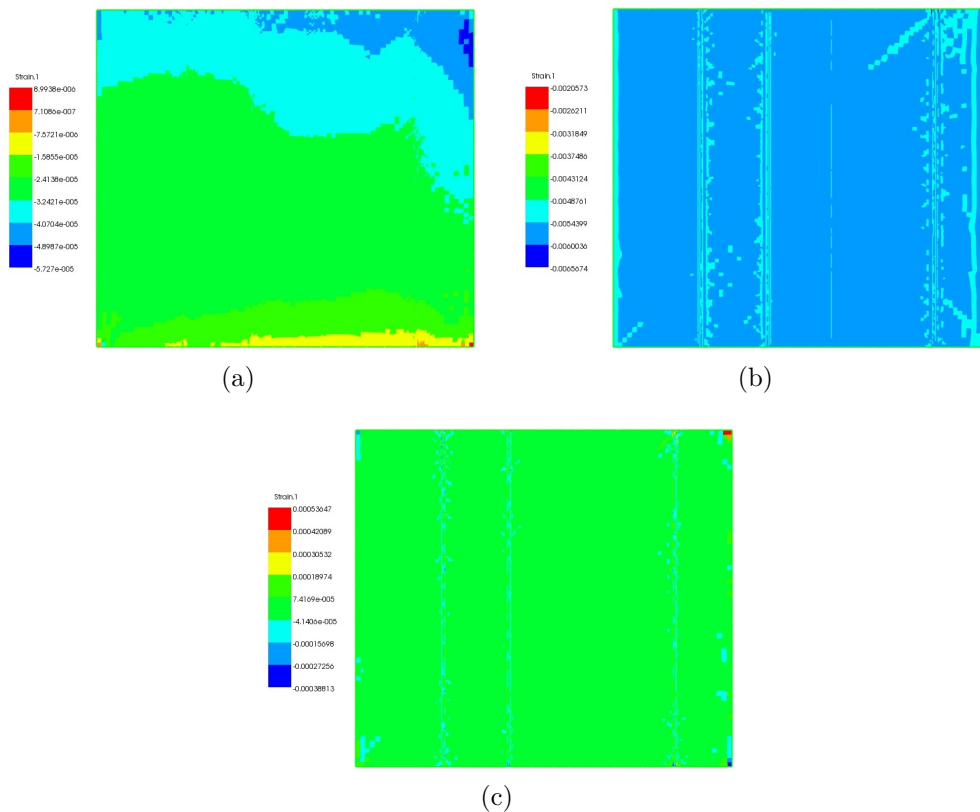


Figure B.26: Strains in ply 14 along ply length at various locations.

B.14 Ply 15

Figure B.27: Strain distributions in ply 15, (a) ϵ_1 , (b) ϵ_2 , (c) ϵ_{12} .

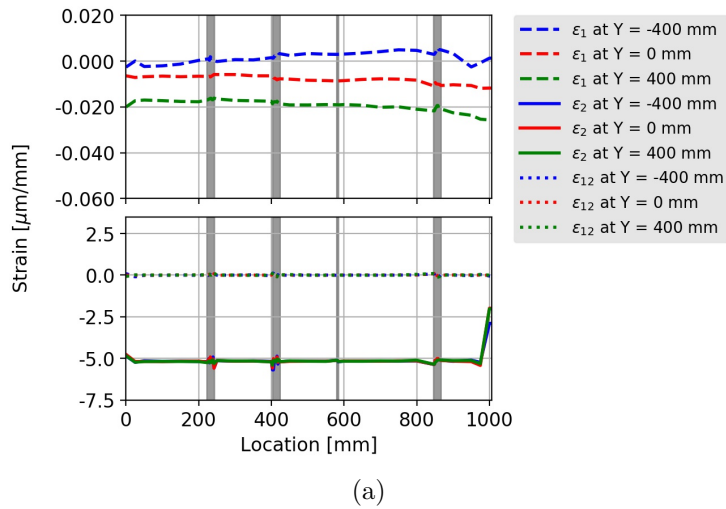
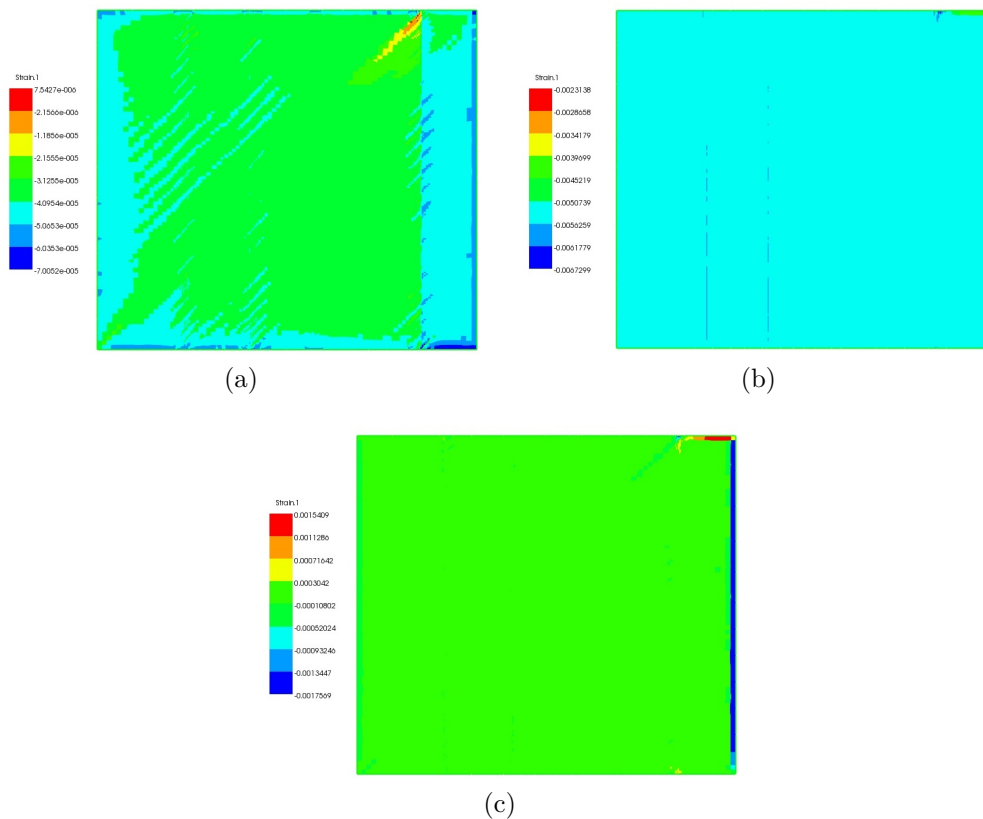


Figure B.28: Strains in ply 15 along ply length at various locations.

B.15 Ply 16

Figure B.29: Strain distributions in ply 16, (a) ε_1 , (b) ε_2 , (c) ε_{12} .

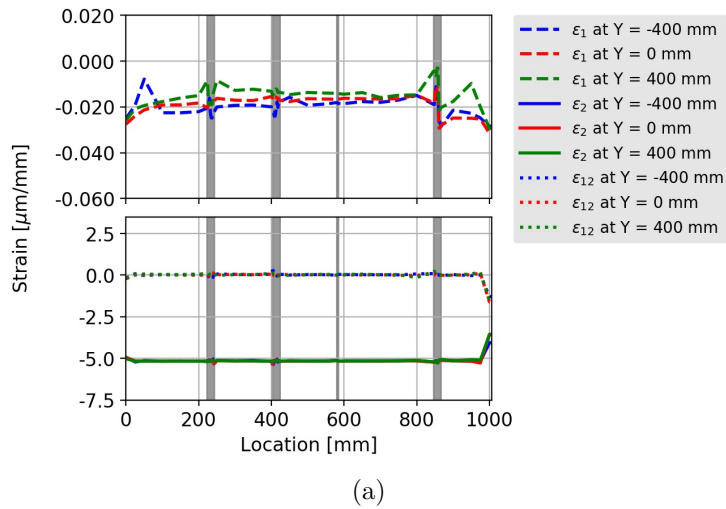
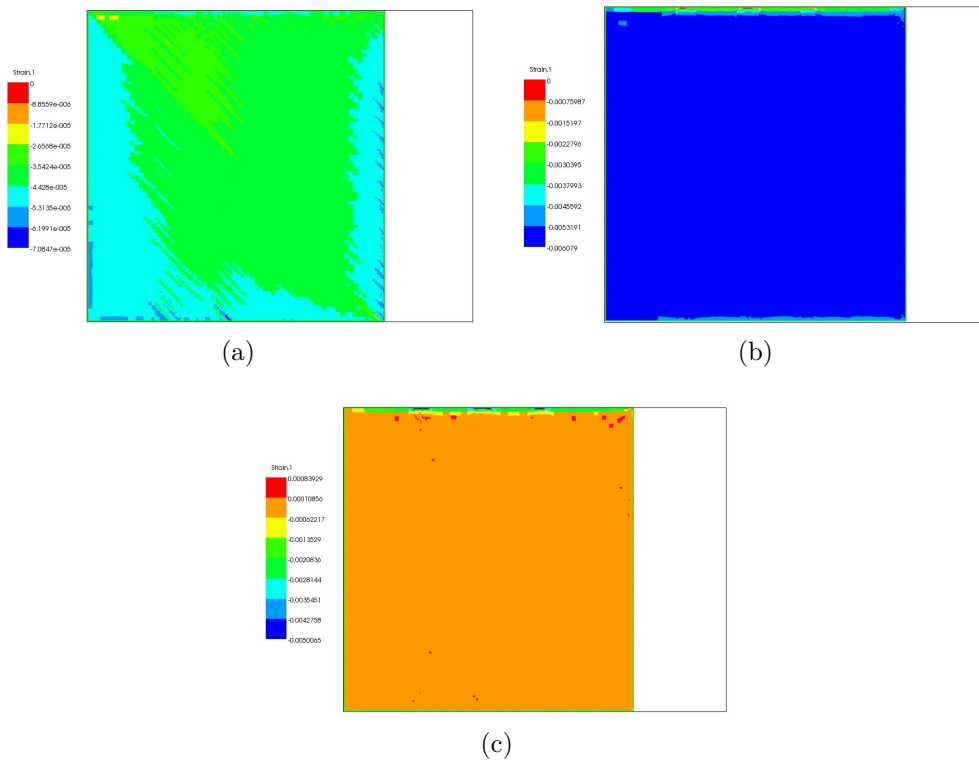


Figure B.30: Strains in ply 16 along ply length at various locations.

B.16 Ply 17 (Dropped)

Figure B.31: Strain distributions in ply 17, (a) ϵ_1 , (b) ϵ_2 , (c) ϵ_{12} .

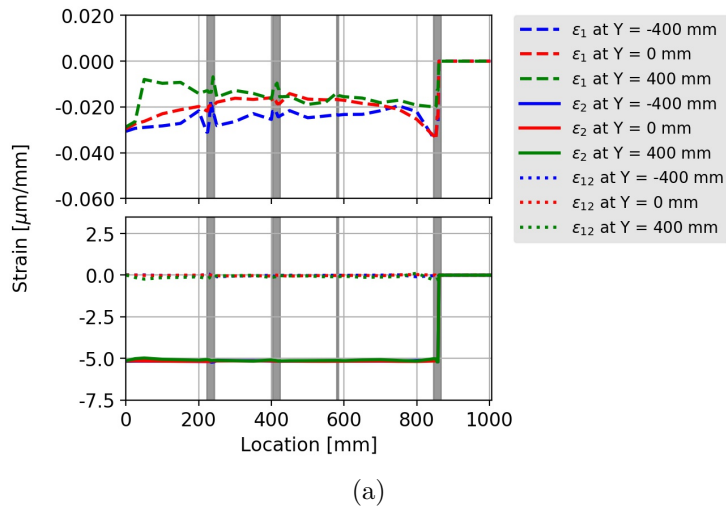
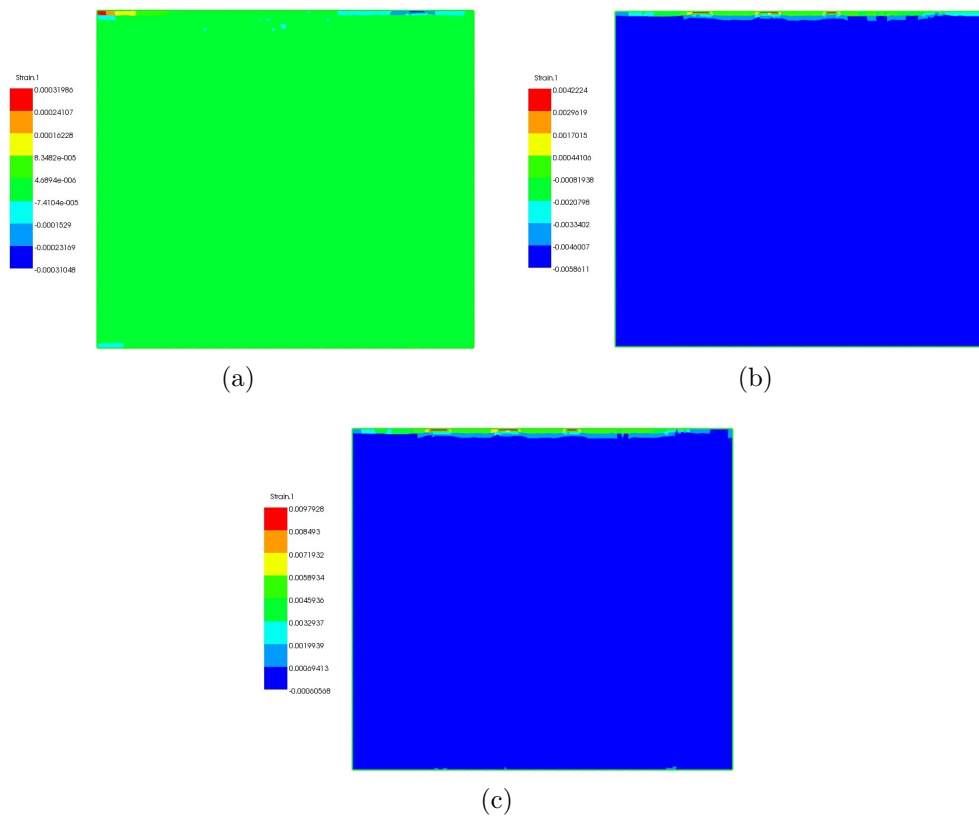


Figure B.32: Strains in ply 17 along ply length at various locations.

B.17 Ply 18

Figure B.33: Strain distributions in ply 18, (a) ϵ_1 , (b) ϵ_2 , (c) ϵ_{12} .

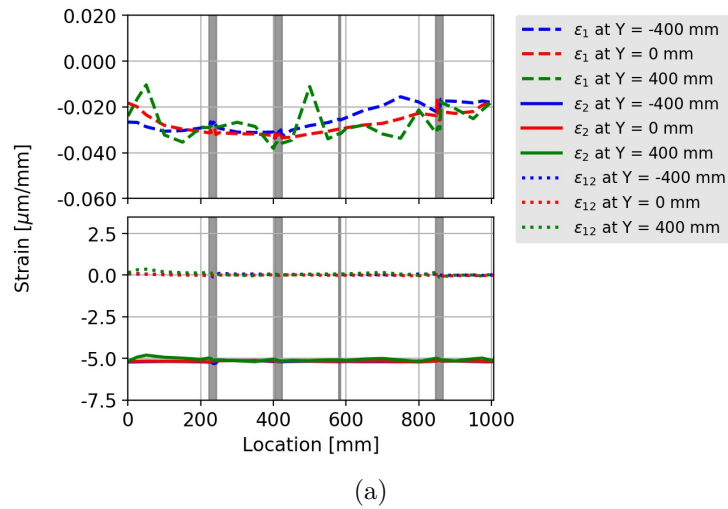
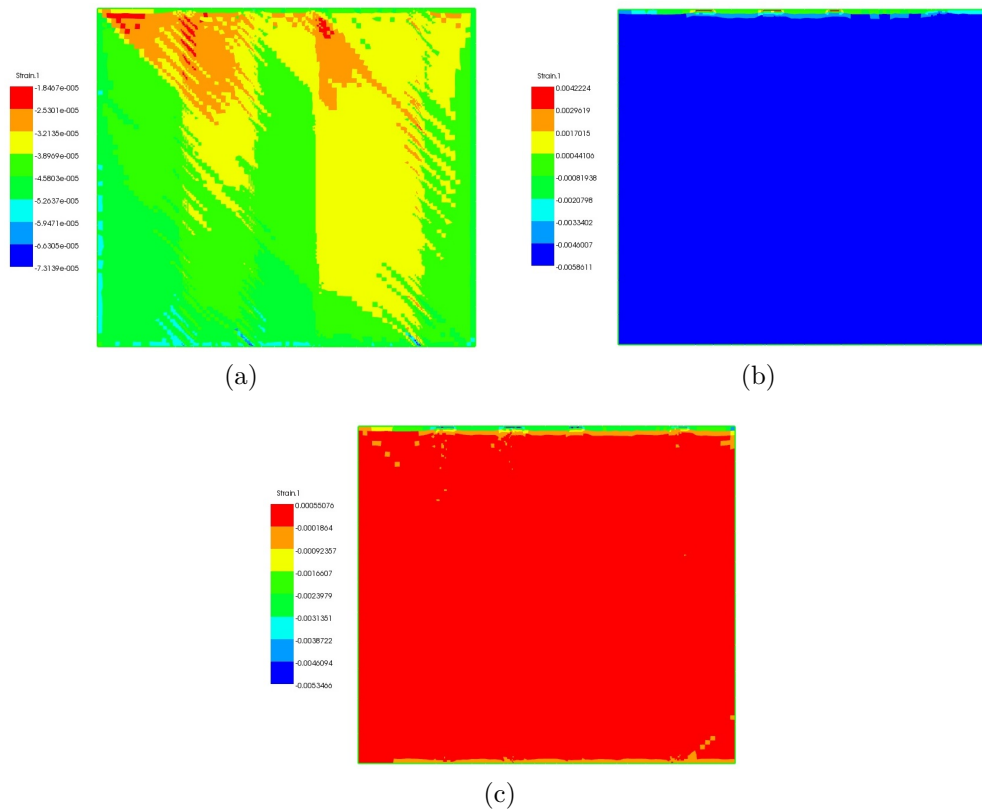


Figure B.34: Strains in ply 18 along ply length at various locations.

B.18 Ply 19

Figure B.35: Strain distributions in ply 19, (a) ϵ_1 , (b) ϵ_2 , (c) ϵ_{12} .

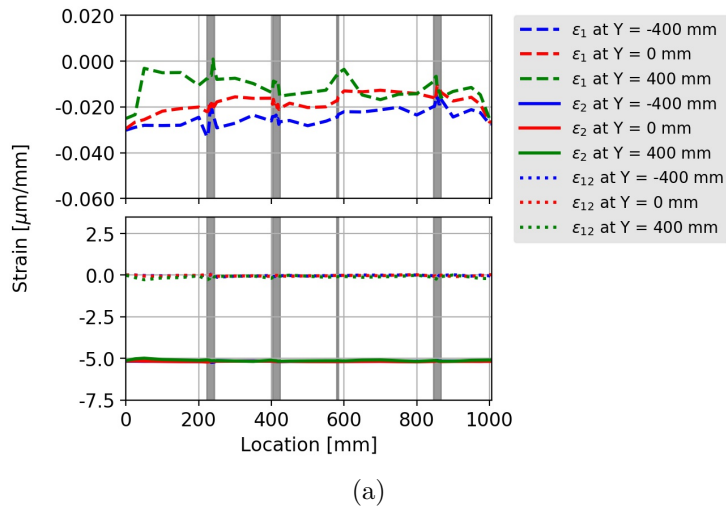
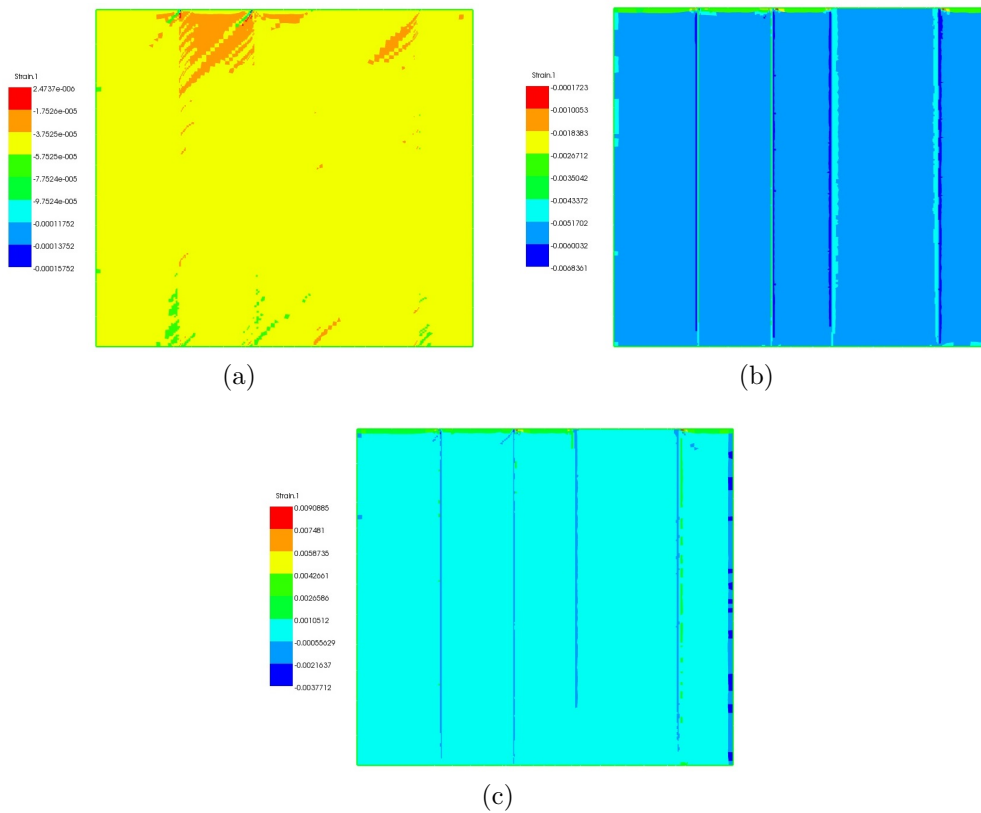


Figure B.36: Strains in ply 19 along ply length at various locations.

B.19 Ply 20

Figure B.37: Strain distributions in ply 20, (a) ϵ_1 , (b) ϵ_2 , (c) ϵ_{12} .

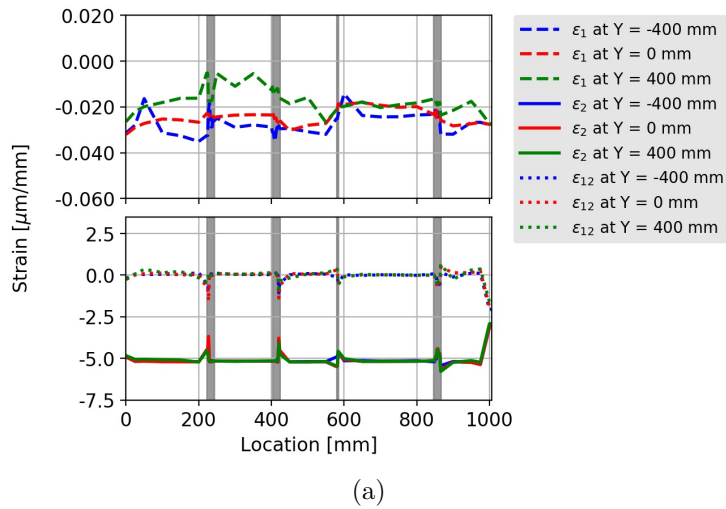
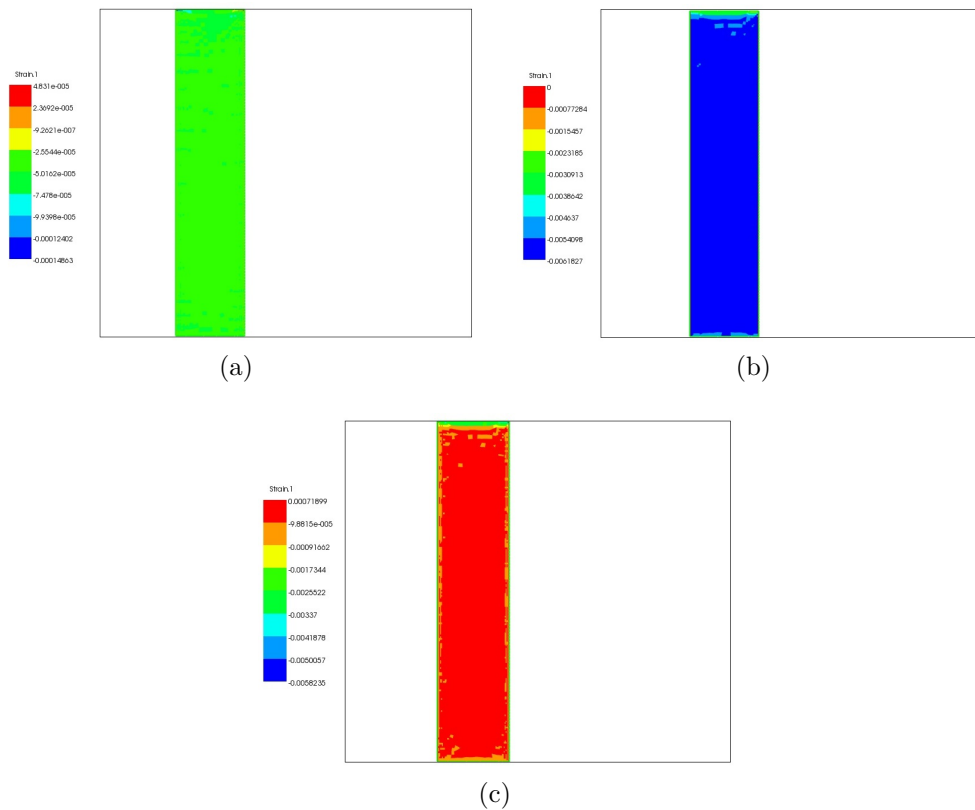


Figure B.38: Strains in ply 20 along ply length at various locations.

B.20 Ply 21 (Dropped)

Figure B.39: Strain distributions in ply 21, (a) ϵ_1 , (b) ϵ_2 , (c) ϵ_{12} .

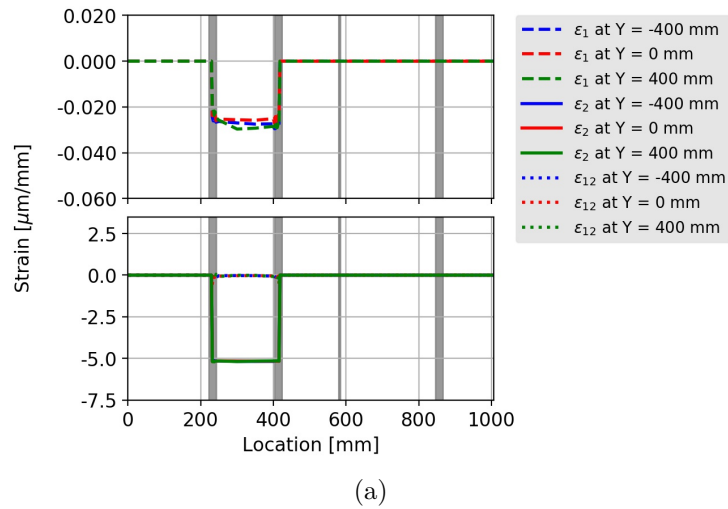
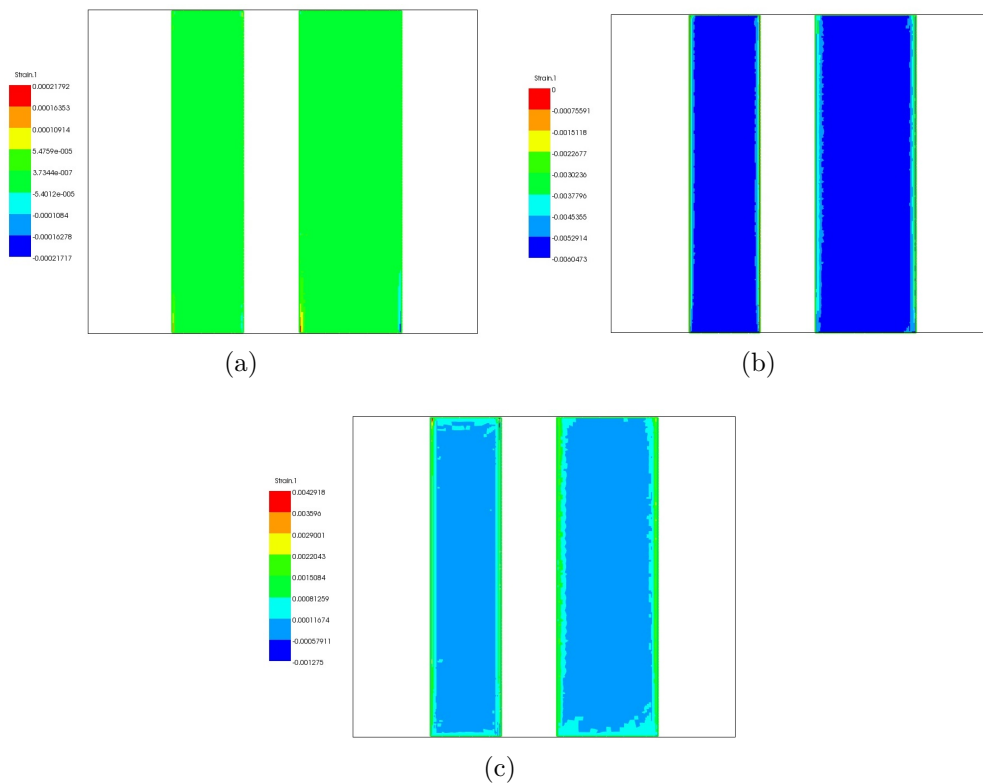


Figure B.40: Strains in ply 21 along ply length at various locations.

B.21 Ply 22 (Dropped)

Figure B.41: Strain distributions in ply 22, (a) ε_1 , (b) ε_2 , (c) ε_{12} .

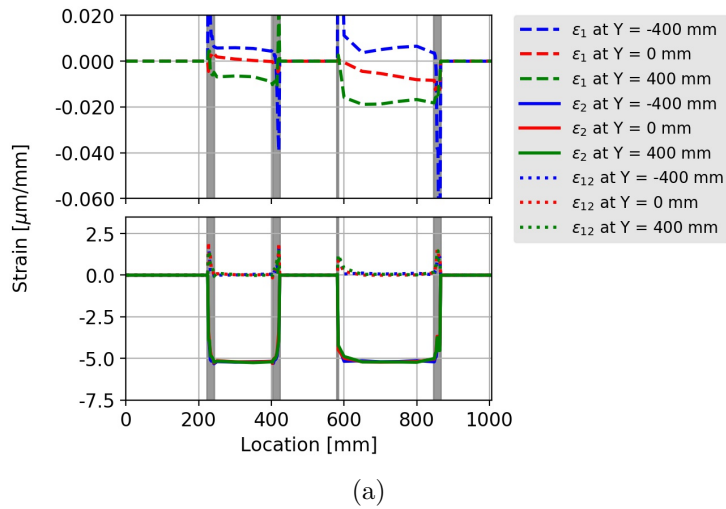
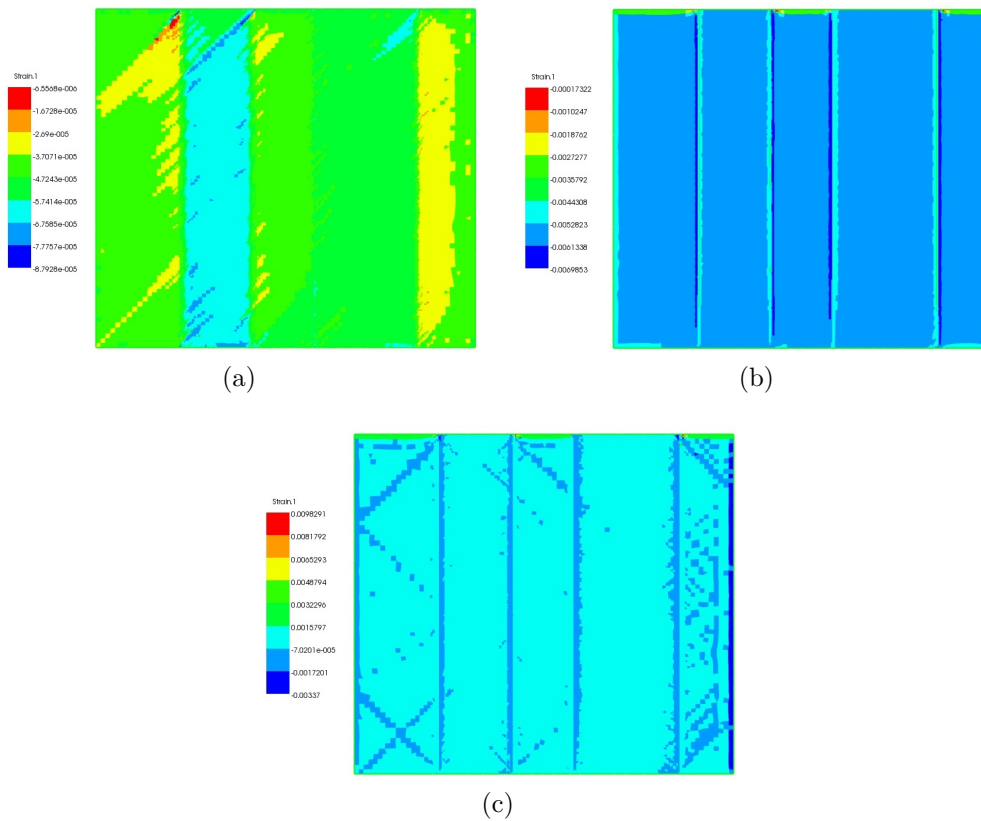


Figure B.42: Strains in ply 22 along ply length at various locations.

B.22 Ply 23

Figure B.43: Strain distributions in ply 23, (a) ε_1 , (b) ε_2 , (c) ε_{12} .

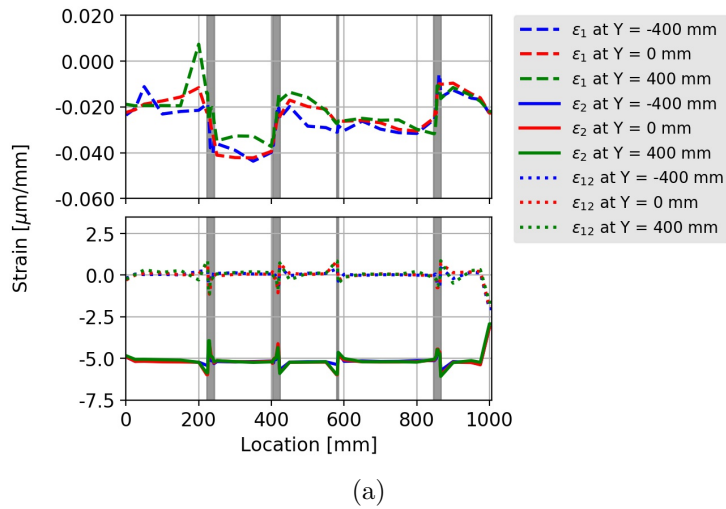


Figure B.44: Strains in ply 23 along ply length at various locations.